FUNDAMENTALS AND APPLICATIONS OF CHROMATOGRAPHIC ADSORPTION

A Dissertation Presented to

the Faculty of the Department of Biology and Biochemistry

University of Houston

In Partial Fulfillment

of the Requirements for the Degree

Doctor of Philosophy

By

Sagar Prabhakar Dhamane

May 2015

FUNDAMENTALS AND APPLICATIONS OF CHROMATOGRAPHIC ADSORPTION

Sagar Prabhakar Dhamane

Approved:

Dr. Richard C. Willson, Chairman

Dr. George E. Fox

Dr. Robert Fox

Dr. James Briggs

Dr. Navin Varadarajan

Dean, College of Natural Sciences and Mathematics

Acknowledgements

Finally the day has dawned - from now on; I will be addressed as Dr. Sagar Prabhakar Dhamane. The work presented in this dissertation is the fulfillment of one my dreams that I have chased in my life. The completion of my dissertation and subsequent Ph.D. is both painful and enjoyable experience. Achieving this would have been impossible without the support of many people that I would like to thank.

I would like to express my special appreciation and thanks to my guru, Dr. Richard C. Willson for providing me the opportunity to work in his group. His guidance, patience, flexibility, and faith in me enabled me to achieve this feat. I am also thankful to Dr. James Briggs, Dr. George E. Fox, Dr. Robert Fox, and Dr. Navin Varadarajan for agreeing to serve as my thesis committee members.

My Ph.D. work is a concerted effort and would have been incomplete without help from Dr. Katerina Kourentzi and Dr. Ulrich Strych. I owe my deepest gratitude for their valuable guidance. I am also highly grateful to our collaborator Dr. Christy Landes and her group members for carrying out the single molecule spectroscopy experiments. I deeply acknowledge my lab mates Dr. Anna Hagström, Dr. Meenu, Dr. Balakrishnan Raja, Dr. Mohan, Dr. Wen Chen, Gavin Garvey, Andrew Paterson, Hui Chen, Ujwal Patil and Dr. Julia Litvinov for keeping lively atmosphere in the lab. I am also thankful to my close friends Diwakar, Pramod, Amar, Kashinath, and Dr. Federico Augusto Ruiz Ruiz for all their motivating words and speeches.

I cannot express with words the love I feel for my parents, brother, sister and for my wife. None of this would have been possible without their support and love.

Thank you all!

FUNDAMENTALS AND APPLICATIONS OF CHROMATOGRAPHIC ADSORPTION

An Abstract of a Dissertation

Presented to

the Faculty of the Department of Biology and Biochemistry

University of Houston

In Partial Fulfillment

of the Requirements for the Degree

Doctor of Philosophy

By

Sagar Prabhakar Dhamane

May 2015

Abstract

The affinity and capacity of ion-exchange adsorbents of a given total-charge density are improved by immobilization of the charges in pre-ordered clusters, rather than individually in random locations. Here, we demonstrate that polyamine spermine can serve as an alternative to our previously described expensive peptide clustered ligands. Spermine Sepharose exhibited superior α-lactalbumin binding capacity (Q_{max} > 1.6 and 1.3-fold higher than those for Qiagen DEAE and GE DEAE Sepharose adsorbents of much greater charge density, respectively) and higher initial binding affinity (Q_{max}/K_D 2.4 and 2.1-fold higher, respectively). The new spermine-based matrix also exhibited a higher value of the salt-sensitivity Z parameter, suggesting an increased number of apparent interaction sites between the protein and the resin, and functioned well in column mode.

In another study, we developed an ultra-sensitive immunochromatographic lateral flow assay (LFA) for the detection of MS2 bacteriophage. LFAs are a well-established point-of-care diagnostic method, but the sensitivities of the standard gold and latex particle formats are not sufficient for many potential applications. Here we present a novel reporter, horseradish peroxidase (HRP)-labeled immuno-phage particles, for sensitivity-enhanced LFAs. Two different types of approaches were employed to manufacture antibody- and peroxidase-doubly-modified M13 bacteriophage, and these novel reporters were successfully integrated into an LFA. The sensitivity of the assay for a model viral pathogen, MS2, was 1000-fold greater than the traditional gold nanoparticle LFA with the same antibodies and results could easily be visually assessed, even without instruments.

In another study in collaboration with the group of C. Landes of Rice University, we employed a single-molecule, super-resolution imaging technique called motion-blur Points Accumulation for Imaging in Nanoscale Topography (mbPAINT) to study complex mechanistic details involved in protein adsorption. We demonstrated that clusters of charges are necessary to create detectable adsorption sites and that even chemically-identical ligands create adsorption sites of varying kinetic properties that depend on steric availability at the interface. Simulated elution profiles predicted from the molecular-scale data suggest that if it were possible to engineer uniform optimal interactions into ion-exchange systems, separation efficiencies could be improved by as much as a factor of five.

Table of Contents

Chapter I: Introduction

1.1 Liquid Chromatography

1.1.1 Basic principles of liquid chromatography

Liquid chromatography is one of the most-studied and commonly used technologies for separation of biomolecules such as proteins and nucleic acids. In liquid chromatography, separation of molecules is based on their differential partitioning in the solid and liquid phases. Molecules with higher affinity for the stationary phase will move with a lower velocity than the molecules with a lower affinity for the stationary phase (or higher affinity for the mobile phase). Typically a column packed with porous beads acts as a solid phase through which the mobile phase, the *eluent*, is pumped. Biomolecules that are to be separated are dissolved in an aqueous buffer (mobile phase) and are introduced into one end of the column. Biomolecules travel with different velocities through the column, thus forming a basis for separation. Biomolecules are then subsequently detected by measuring UV absorbance at specific wavelength and collected at the other end of the chromatographic column. Depending on the chemical and physical properties to be exploited, biomolecules can be separated using different modes of chromatography, differing mainly in the type of stationary phase used (**Table 1.1**).

1.1.2 Ion Exchange chromatography

Ion-exchange chromatography is commonly used for separation of proteins where adsorption occurs due to the ionic interactions between proteins in solution and charged

groups on the ion exchanger. Ion exchangers have either positively (anion exchangers) or negatively (cation exchangers) charged ligands that form electrostatic interactions with proteins. Proteins are separated based on their overall surface charge and charge distribution (1-3). The strength of interaction between an ion exchanger (ligand) and a protein depends on various factors like the number and distribution of charges on protein and ion exchanger at a given pH, dielectric constant of the medium, and ionic strength. In general, proteins are adsorbed at low ionic strength and desorbed by either increasing ionic strength (by increasing salt concentration) or by changing running buffer pH (**Figure 1.1)**. In a linear salt gradient elution biomolecules will elute roughly in order of increasing charge (4,5).

Table 1.1 Different types of biochromatography (6)

Separation Principle	Types of Chromatography
Size and shape	Gel filtration/ size exclusion chromatography
Net charge	Ion exchange chromatography
Isoelectric point	Chromatofocusing
Hydrophobicity	Hydrophobic interaction chromatography
	Reversed phase chromatography
Biological function	Affinity chromatography
Antigenicity	Immunoadsorption
Carbohydrate content	Lectin affinity chromatography
Metal binding	Immobilized metal affinity chromatography
Miscellaneous	Hydroxyapatite chromatography
	Dye affinity chromatography
	Mixed mode chromatography

A functional group on ion exchanger is either acid (cation exchanger) or base (anion exchanger). Depending on the pK_a values of their functional groups ion exchangers are classified as weak or strong (**Table 1.2**). Weak ion exchangers (anion and cation) have a functional pH limit set by ligand titration whereas mostly strong ion exchangers do not have a pH limit.

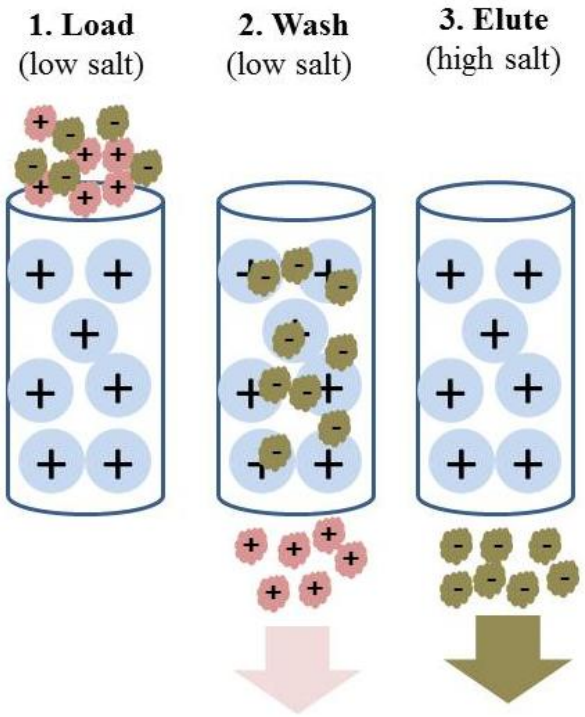

Figure 1.1: Working principle of anion-exchange chromatography

Table 1.2: Functional groups of ion exchangers (7)

Names	Designation	pK_a	Structure
	Anion Exchangers		
Diethylaminoethyl	DEAE	5.8 & 9.1	$-OCH_2NH(C_2H_5)_2$
Trimethylaminoethyl	TMAE	-	$-OCH_2CH_2N^+(CH_3)_3$
Dimethylaminoethyl	DMAE	~10	$-OCH_2CH_2NH(CH_3)_2$
Trimethylhydroxypropyl	QA		$-OCH_2CH(OH)NH(C_2H_5)_2$
Quaternary amino ethyl	QAE		$-OCH_2CH_2N^+(C_2H_5)_2$ $CH_2CH(OH)CH_3$
Quaternary amine	Q		$-OCH_2N^+(CH_3)_3$
Triethyl amine	TEAE	9.5	$-OCH_2N^+(C_2H_5)_3$
	Cation Exchangers		
Methacrylate		6.5	$-CH_2CH(CH_3)COOH$
Carboxymethyl	CM	3.5-4	$-OCH_2COOH$
Orthophosphate	P	3 & 6	$-OPO_3H_2$
Sulfoxyethyl	SE	2	$-OCH_2CH_2SO_3H$
Sulfopropyl	SP	2-2.5	$-OCH_2CH_2CH_2SO_3H$
Sulfonate	S	2	$-OCH_2SO_3H$

1.1.3 Methods to study protein interactions with a chromatographic surface

Various methods have been employed to study adsorption of protein on chromatographic surfaces including adsorption isotherm measurements (8-11), chromatographic dynamics (12,13), isothermal titration calorimetry (14,15), NMR (16,17), refractive-index based optical microscopy (18,19) and microscopic observation of fluorescent dye labeled proteins (20,21). To construct the adsorption isotherm, the equilibrium concentration of

biomolecule (protein or nucleic acid) bound on the surface (stationary phase) is plotted against the concentration of free molecules in the solution or supernatant (mobile phase). An adsorption isotherm provides the maximum binding capacity and affinity of protein for the adsorbent, and some indication of heterogeneity. Confocal laser scanning microscopy (CLSM) allows directly to monitor the transport of protein on chromatographic adsorbents (22-25). However, the information obtained from these methods is ensemble-averaged over a large number of molecules. This strategy averages out the fundamental processes of individual protein molecule's interactions with individual ligands when applied to complex systems. Efforts have been made to study dynamics of single protein molecule adsorption using techniques like atomic force microscopy (26) and lateral force microscopy (27).

In recent years single-molecule methods have greatly advanced many fields. Single-molecule spectroscopy has substantially advanced our ability to measure dynamic processes in complex materials. Single-molecule imaging by Total Internal Reflectance Fluorescence (TIRF) microscopy and fluorescence resonance energy transfer (FRET) are promising techniques to measure association and dissociation kinetics of single biomolecules in bulk phases and at interfaces without ensemble averaging that occurs in classical methods of chromatographic research (28-32). Combining actual chromatographic experiments with single-molecule imaging would provide us mechanistic insights of separation processes and will aid us in designing new separation media and modes (33-36).

1.2 Immunochromatography

1.2.1 Introduction

In the past, chromatographic methods have been developed for the analysis of biomolecules. Gas chromatography (GC) and high-performance liquid chromatography (HPLC) are the two most-commonly employed standard chromatographic techniques in diagnostics (37-40). The advantages of chromatographic techniques include the following: 1) Separation of analytes from a complex biological sample. 2) Good reproducibility and high performance of accurate quantitative analysis (e.g. HPLC and GC). Disadvantages of chromatographic methods include: 1) In general chromatographic methods require expensive instruments. Hence, the cost per assay is relatively high compare to other assay methods. 2) These assay methods often require prior enrichment of a target analyte (41).

Immunoassay is the most popular format in the molecular diagnostics. In an immunoassay, a target analyte is captured using a capturing reagent (often an antibody) immobilized on a solid support. The captured analyte is then detected using a reporter conjugated antibody. Commonly employed reporters in immunoassays are enzymes (Enzyme Linked ImmunoSorbent Assay), radioactive isotopes (Radioimmunoassay), DNA (immunoPCR), fluorescent tags (Fluoroimmunoassay), and electrochemiluminescent tags (Electrochemical immunoassay). Among these immunoassay formats ELISA is the most popular format, as it offers various advantages: 1) ELISAs are sensitive enough to detect picomolar concentrations of analytes (42). 2)

Compared to other assay methods like chromatographic methods, maintenance cost of ELISA is low. 3) Handling related errors are greatly reduced because of the commercially available automated plate washing and reader systems. 4) Assay time per sample is less and cost is reduced when performed in 96-well plates. Disadvantages of ELISA include: 1) Plasma constituents may interfere in the enzymatic reaction. 2) Dynamic linear range is small especially for smaller molecules (43). Combining these two orthogonal detection techniques (chromatography and immunoassay), in what is called immunochromatography overcomes the individual drawbacks. Immunochromatographic methods provide more information about the target analyte than either chromatography or immunoassays alone. Immunochromatographic techniques are mainly divided into two types, the pre-column techniques and the post-column techniques. In the pre-column mode, antibodies are used as the sample clean-up and enrichment reagent, e.g., as in immunoaffinity chromatography (detection of albumin and immunoglobulin G in serum (44)). In post-column mode, antibodies are used in an immunoassay mode, e.g., as detection molecules (immunochemical detection of methionyl granulocyte colony stimulating factor (45)). As with the immunoassays and chromatographic methods, immunoaffinity chromatographic techniques also require expensive instruments, trained technicians and large laboratories. Thus, these drawbacks have constrained their use to hospitals and diagnostics laboratories, e.g., immunoaffinity chromatographic test developed for detection of *Clostridium botulinum* neurotoxin (46). On the other hand, point-of-care (POC) techniques have been developed to allow diagnosis at patient's home

or in the physician's office. These are rapid, easy to use and affordable analytical techniques (47). Several POC techniques are successfully commercialized including blood glucose meters, rapid pregnancy tests, occult blood slide test, dipsticks (urine test strip, liver function test strip), and nucleic acid based testing (NABT). The immunochromatographic lateral flow assay (LFA) is one such POC method which has become enormously popular because of its great simplicity.

1.2.2 Lateral Flow Assays (LFAs)

LFAs are a well-established, inexpensive POC technology. The first big application of LFA was developed for the home pregnancy test by detecting human chorionic gonadotropin (HCG) in urine samples (48).

The LFA test strip is composed of four basic compartments – a sample pad, a conjugate pad, the membrane and an adsorbent pad. When a test is performed, sample is added on the sample pad. The sample pad holds the sample and makes it compatible with the test, e.g., removal of blood cells. From the sample pad sample fluid migrates towards the conjugate pad. In the conjugate pad the sample fluid interacts with the infused particulate conjugates. The particulate conjugates are the reporter particles (typically colloidal gold) conjugated with the specific recognition elements. Target analyte from the sample fluid interacts with the particulate conjugate and forms a complex that migrates into the membrane. The membrane is a porous structure in which another biological component of the assay is immobilized as the test line. The test line captures analyte-particulate

conjugate complexes. The appearance of color at the test line indicates a positive result. Further downstream to the test line is a control. Presence of a color at the control line confirms that the reporter conjugates moved successfully through the strip and indicates the proper functioning of the test. The excess reagents move past the control line towards the adsorbent pad.

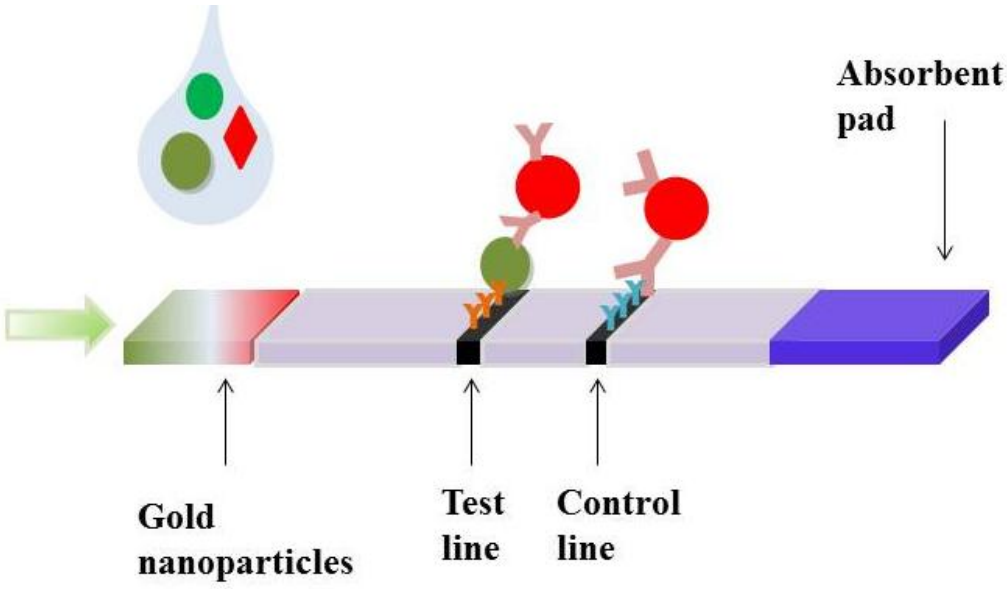

Figure 1.2: Principle of a lateral flow assay

Membranes in LFA

The membrane is a vital part of the lateral flow assay because it provides the surface for the formation of the immunocomplexes and on this surface signal is generated and

detected (49). Various membranes have been used in the lateral flow assays including polyether sulfone, cellulose, glass fibers, nitrocellulose, and polyesters. However, nitrocellulose membranes have been the most popular choice.

Nitrocellulose has been used as a substrate for formation of biochemical complexes well over 50 years (50-55). Attributes like high protein-binding capacity, large pore size, established protocols to make it wettable with aqueous solutions and good capillary flow characteristics make nitrocellulose useful in a lateral flow assay. Protein binding is essential to make test and control lines on the membrane. Due to the hydrophobic nature of nitrocellulose, proteins bind mainly through hydrophobic interactions (56). Blocking of nitrocellulose membrane is essential to avoid non-specific binding of reporter. Blocking agents' type and concentration are selected based on the compatibility with the assay system. Sensitivity to humidity and shelf life issues are the major limitations of nitrocellulose membranes.

FUSION 5 is a glass-fiber based material developed by GE healthcare (57). It can serve multiple roles in a LFA: blood separator, sample pad, conjugate release material, membrane or adsorbent pad. It can also replace all of these components and hence allow an entire lateral flow assay test to be run on a single material. FUSION 5 overcomes some of the limitations of nitrocellulose. FUSION 5 is a hydrophilic in nature and hence does not require extensive blocking. Unlike nitrocellulose FUSION 5 is not sensitive to humidity and does not significantly age on storage. It has high wicking speed and typically takes 4 minutes to complete a test without significant loss of sensitivity or

specificity (57). FUSION 5 has a permanent negative charge which can be exploited to adsorb proteins. When a protein is sprayed at pH < pI (typically at pH 3.0) it binds to FUSION 5 through electrostatic interactions. If the protein is not stable at low pH then carrier beads can be used to make test and control lines (57). Proteins are applied on the surface of carrier beads of an appropriate size (typically 2 – 4 μm). When these beads are applied on the FUSION 5 surface they get trapped within the membrane due to their size and form a good test/control line. FUSION 5 due to its highly porous nature provides an alternative platform for lateral flow assay development, especially where large size reporters are used. Low cost, fast wicking rate, hydrophilic nature, easy protein adsorption, and low background are the best advantages of using FUSION 5.

Labels for lateral flow assays

Colloidal gold is a highly popular label for LFAs because it is inexpensive and gives an intense color (58). It is easy to prepare and is stable in water. Relatively easy conjugation protocols are available in the literature. Use of colored latex (59), selenium (60) or paramagnetic particles (61) as labels in LFAs have been also reported. Several other labels such as liposomes, quantum dots, polymers (dextrans and polylysine chains), fluorescent and luminescent labels, were explored to improve the sensitivity of lateral flow assays (62,63). Enzyme labels are popular in immunoassays like ELISA but not very common in lateral flow assays primarily because of their instability at room temperature, and rapid diffusion of enzymatic reaction end product on the membrane. However a main advantage of enzyme labels is the potential signal amplification. This

particular property of enzyme labels has been exploited to enhance the sensitivity of LFA by using enzyme conjugated gold nanoparticles as the reporters (64-66). In general, labels for lateral flow assays should possess some characteristics such as easy to conjugate with proteins, show low non-specific binding, and be stable under various conditions.

1.3 M13 Bacteriophage

M13 (or F1) is a bacteriophage that infects *E.coli*. It is a non-lytic phage and belongs to the *Inoviridae* family. It infects *E.coli* through F pili and inserts its viral genome into the host cell. Once the viral genome is inserted, it exploits host's metabolic machinery for the production of new progeny phage (67). M13 bacteriophages particle (**Figure 1.3**) has a filamentous shape (~930 nm long and a diameter of 6.5 nm). The phage particle contains a single stranded DNA (ssDNA, 6,407 nt), enclosed within five coat proteins (pVIII, pIII, pVI, pVII and pIX). Minor coat proteins are present at the end of the phage: five copies of pVII and pIX at the proximal end and five copies of pIII and pVI at the distal end. The major coat protein pVIII (~2700 copies) is a 50- amino acid protein which warps phage DNA in helical symmetry (68) and forms short rod like structure (67). This rod like structure has three regions: a negatively charged N-terminal acidic amino acid of major coat protein forms a hydrophilic outer layer, a positively charged C-terminal form interior, and a hydrophobic region for formation of a phage particle.

Figure 1.3: The M13 phage structure (69).

Phage display: The minor coat proteins of M13 have been used for displaying foreign peptides on the surface of the phage virion. George Smith from the University of Missouri was the first to show that M13 phage can tolerate the insertion of a foreign DNA fragment (70) and yielded a phage particle displaying a foreign polypeptide. Following this discovery by Smith, a variety of molecules were displayed on phage, such as antibody fragments (71,72), cytokines (73), enzymes (74,75), DNA binding proteins (76) and more.

***AviTag phage*:** The prominent feature of phage display technique is the genotypic-phenotypic relationship which requires both peptide and DNA fragments to be of known

sequence. Typically single chain variables (scFVs) of an antibody against target are displayed on the phage surface and the phage particles can be used as the detection reagent in an assay. However, scFVs generally have lower affinity and avidity than the parent antibody. However, displaying full antibodies is difficult. SAM-AviTag is a derivative of M13 phage in which few copies of the minor coat protein pIII contain a biotinylable AviTag peptide (77-79). The AviTag is a 15 amino-acid peptide (GLNDIFEAQKIEWHE) which is displayed on N terminal of pIII protein. The lysine (K) residue of AviTag is a substrate for biotinylation by biotin ligase enzyme (*birA*). Thus any biotinylated protein or full antibody can be linked to these enzymatically biotinylated phage particles using an avidin-biotin linkage (79,80) which has a dissociation constant of 10^{-15}M (81).

Chapter 2: Spermine Sepharose as a Clustered-Charge Anion Exchange Adsorbent

*Portions of this chapter are published in Dhamane, S., Ruiz-Ruiz, F., Chen, W. H., Kourentzi, K., Benavides, J., Rito-Palomares, M., and Willson, R. C. (2014) Spermine Sepharose as a clustered-charge anion exchange adsorbent. Journal of Chromatography A **1324**, 135-140. The text has been amended to include unpublished data.*

2.1 Introduction

The steady increase in titers and sales of recombinant pharmaceutical proteins have increased interest in high-efficiency, high-capacity downstream processes for the recovery and purification of biologics (82-84), particularly since estimates of the fraction of bioprocess costs devoted to purification range as high as 80% (85-87). Moreover, the continuing need for selective, scalable and economical unit operations has driven the design of novel bioengineering strategies (88,89).

Chromatographic purification remains the most costly element of biopharmaceutical downstream processing (90,91), and development of optimal chromatographic processes is a central issue in bioprocess engineering. Because it offers strong and easily reversible protein adsorption, ion-exchange chromatography is widely used for the selective purification of biomolecules (1,92). Traditional ion-exchange adsorbents present a

random charge distribution over the particle surface that creates a heterogeneous field of adsorption sites (93). It might be anticipated that the regions of high charge density would play a dominant role in the protein adsorption and the regions with low charge density will not be included in the process under the typical operating conditions. In order to improve this random charge distribution for protein capture, adsorbents have been modified in the past to present improved characteristics by either increasing ligand density through the use of tentacular adsorbents (94,95) or by attaching polyions such as polyethyleneimine or polylysine in order to enhance product selectivity and recovery (96).

Many proteins present a characteristic high charge-density patch (acidic, basic or mixed charge cluster). Negative charge clusters in protein often coordinate with metals, e.g., thermolysin, mannose binding protein, and aminopeptidase. Mixed charge clusters are often found in proteins where protein-protein interactions are crucial, e.g., S-transferase, catalase, and fructose-1,6-bisphosphate aldolase (97). High charge-density patches can play a dominant role in the ion-exchange adsorption of these molecules (1-3,98). We have previously found that an adsorbent displaying uniform clusters of positive charges shows a higher affinity and capacity for negatively charged biomolecules than an adsorbent with the same total charge density displayed as dispersed charges (1,99). More specifically, clustered pentaargininamide (**Figure 2.1**) adsorbents of relatively low ligand density show higher affinity for negatively charged biomolecules (e.g., nucleic acids) than conventional adsorbents like GE DEAE, Q Sepharose of much higher ligand density

(1,99). The use of "improved" ligands such as pentaargininamide in research or for process scale purification, however, must contend with the cost and base-lability of the ligand which hampers efficient resin cleaning.

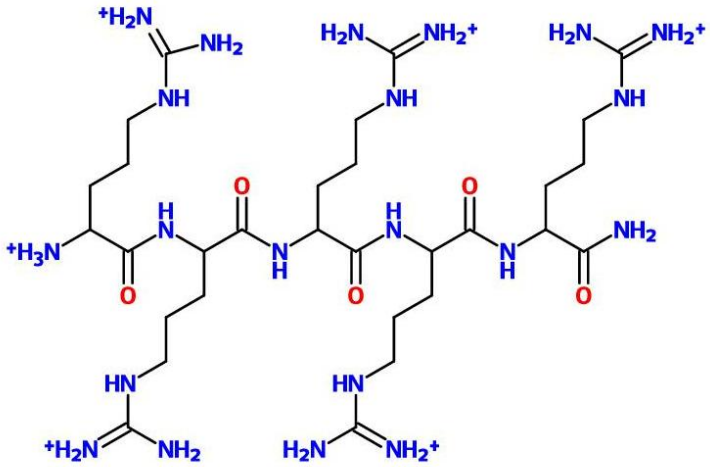

Figure 2.1: Structure of penta-argininamide ligand.

In this work we describe spermine as an inexpensive, stable ligand for the development of clustered adsorbents (100). Spermine is a polycationic polyamine involved in DNA packaging whose four amines (see **Figure 2.2**) can form a cluster of four positive charges (101), and whose low cost and alkali stability make it potentially suitable as a ligand for clustered-charge anion exchange chromatography.

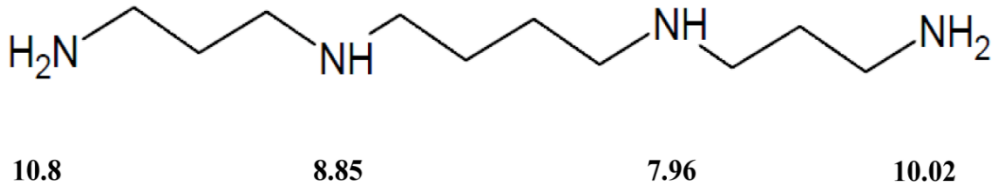

Figure 2.2. Spermine molecule with corresponding pK_a values for titratable atoms. Note that pK_a values for symmetry-related atoms differ because of the sequential addition of protons to the molecule.

We demonstrate the superior affinity and capacity of a spermine Sepharose clustered-charge anion exchanger for the anionic protein α-lactalbumin, which presents a modifiable charge cluster. The clustered-charge adsorbent presents enhanced initial binding affinity (Q_{max}/K_D) and maximum binding capacity (Q_{max}) when compared to dispersed-charge commercial adsorbents, even when the latter have higher ligand density.

2.2 Materials and Methods

2.2.1 Methods

Sepharose CL-6B, Q Sepharose Fast Flow and DEAE Sepharose were from GE Healthcare (Piscataway, NJ). DEAE Plasmid Plus resin was from Qiagen (Valencia, CA). All other reagents were from Sigma Aldrich (St. Louis, MO) including salmon sperm DNA (Cat. number: D1626), Baker's yeast RNA (Cat. number: R6750) and Ca^{2+} depleted α-lactalbumin from bovine milk (Cat. number: L6010). α-lactalbumin was

prepared from unpasteurized bovine milk and was purified by ion exchange chromatography on DEAE-agarose. Its purity is ≥ 85% as was determined by PAGE. The molar mass for the protein used was 14,100 g/mol and the extinction coefficient $\varepsilon^{1\%}$ = 20.1 (102).

2.2.2 Adsorbent preparation

Aldehyde activation of Sepharose was based on the method of Miron and Wilchek (103). For activation, DI water-washed Sepharose CL-6B (400 µl in 1.6 mL water) was treated with 0.2 M sodium periodate for 3 h at room temperature, then washed with DI water and resuspended in 50 mM borate buffer pH 9.5 ± 0.2. To 400 µl of activated Sepharose CL-6B settled resin, 1.6 mL of spermine tetrahydrochloride (45 mg/mL) solution in 50 mM borate buffer, pH 9.5 was added and incubated on a gyratory rotator at room temperature for 2 h and centrifuged 2 min at 16,000 *x g*. The gel with the bound spermine was treated for 3 h with 2 mL of 2 mM sodium borohydride in 50 mM borate buffer, pH 9.5 to reduce the initially formed Schiff base into a stable secondary amine linkage. Spermine modified Sepharose was washed with 20 mM phosphate buffer, pH 7.0 and stored at 4 ˚C.

2.2.3 Ligand density determination

The ligand density of spermine Sepharose was determined by titration with 5 mM NaOH in column mode using an AKTA purifier FPLC equipped with a post-column pH monitor. Spermine Sepharose was packed in a column (5x20 mm) and equilibrated with 5 column volumes of 0.1 M HCl, and then 5 mM NaOH was run through a bypass in order to equilibrate the extra-column volume. After the equilibration, 5 mM NaOH was passed

through the column to determine the moles of base required to titrate the acidified adsorbent. The amount of 5 mM NaOH required for titration of unmodified Sepharose (typically about 1.2 mL) was subtracted from that required to titrate the spermine Sepharose (typically about 6.8 mL) to obtain the millimoles of NaOH used to titrate spermine.

2.2.4 Adsorption isotherm measurements

Aliquots (25 µl) of 60 % v/v spermine Sepharose suspension in binding buffer (10 mM Tris, 10 mM NaCl, pH 8) were placed in 1.5 mL Eppendorf tubes. To these tubes different amounts of protein stock solution (10-180 µl of 5 mg/mL Ca^{2+}-depleted bovine α-lactalbumin (or RNA) in binding buffer) were added, followed by binding buffer up to 1 ml. Tubes were placed on a gyratory rotator at room temperature for 1 h, then centrifuged for 10 min at 16,000 *x* g. Protein concentration in the supernatant was quantified by 280 nm absorbance using a Tecan Infinite M200 Pro microplate reader (Tecan, USA). The adsorbent pellets were washed with 1 mL of binding buffer followed by recentrifugation (the wash contained only a small fraction, 3.1% ± 1.7%, of the added protein). Bound protein was eluted with 1 mL of elution buffer (binding buffer + 1 M NaCl) and adsorbed protein content was determined. In order to determine the completeness of protein recovery, mass balances were performed by dividing the sum of the protein remaining in the supernatant after adsorption equilibration + protein recovered in the wash + protein in the elution fraction, by the original amount of protein added. The ionic strength of the 10 mM Tris buffer, 10 mM NaCl, pH 8 is estimated at 0.015 M.

2.2.5 Data analysis

The mass balance recoveries for all points in all experiments closed in the range of 86-111%. Protein adsorption data were fit to the Langmuir (Eq. 1), Langmuir-Freundlich (Eq. 2) isotherms and the steric mass action (SMA) model of Cramer et al. (Eq. 3) (104).

$$y = \frac{Q_{max}X}{K_D + X} \qquad \text{(Eq. 1)}$$

$$y = \frac{Q_{\max} X^{n_H}}{K^{n_H} + X^{n_H}} \qquad \text{(Eq. 2)}$$

$$y = \left(\frac{Q_\alpha}{K}\right)\left(\frac{X}{\Lambda - [\nu+\sigma]Q_\alpha}\right)^\nu \qquad \text{(Eq. 3)}$$

In these equations, y is the bound protein concentration, X is the free protein concentration, Q_{max} is the maximum binding capacity (in μmol/ml of settled bed adsorbent), and K_D is the dissociation constant. In Eq. 2, n_H is the Langmuir-Freundlich heterogeneity parameter. In Eq. 3, Q_a is the equilibrium adsorbent-bound protein concentration, K is the equilibrium constant, Λ is the total ionic capacity of the adsorbent in μmol/ml of settled bed adsorbent, σ is the dimensionless steric factor that reflects the number of sites on the surface that are shielded by the adsorbate and prevented from exchange with salt counter-ions in solution and ν is the dimensionless characteristic charge that reflects the number of sites that the protein interacts with on the surface. Fitting used Igor Pro (WaveMetrics, Lake Oswego, OR; version 6.05) which uses the Levenberg-Marquardt algorithm to search for parameters which minimize the X^2 values,

as described previously (1,99). The initial guess vectors for the parameters were varied manually to ensure that a true global optimum was found.

Boardman and Partridge (105) and Regnier (106) have described the stoichiometric displacement model which emphasizes the importance of electrostatic interactions between proteins and adsorbents in terms of ionic equilibria. If an electrolyte such as NaCl is used, the equilibrium of Na^+ ions and target proteins (a polyion represented by P^{n+}) between the mobile phase (m) and the adsorbent (ad) can be represented by: ZNa_{ad} + $P_m \leftrightarrow P_{ad}$ + $ZNa_{m.}$ Beginning with this equilibrium an expression was derived which relates the binding affinity of the adsorbent to the molarity of the displacing salt in the mobile phase which was then linearized to the form (1,105,106): $\log [K'] = Z \log[NaCl] + \log [I]$ where *K*' is the initial binding affinity of the adsorbent, I is a constant and *Z* represents the number of counter ions displaced when a target protein is adsorbed on the resin surface. This also has been interpreted as the number of chemical interactions between the adsorbate and the adsorbent (1,107), though we have shown that *Z* can be fractional and can vary with temperature (108). When the initial binding affinities of the proposed adsorbents at different NaCl concentrations are plotted, a *Z*-plot can be generated and the negative value of the slope of this graph gives the respective *Z* value. Finally, the *Z* values for adsorption of α-lactalbumin on the proposed clustered adsorbent and a commercial non-clustered adsorbent (Qiagen DEAE) were calculated.

2.2.6 Column chromatography

Column chromatography experiments were performed using a glass column (21 mm H X 5 mm ID) packed with the anion exchange adsorbent. The column was initially equilibrated with 5 column volumes (CV) of buffer A (10 mM Tris, 10 mM NaCl, pH 8.0). 1 ml of a protein mixture containing equal amounts of Ca^{2+} depleted α-lactalbumin (0.2 mg) and bovine serum albumin (BSA; 0.2 mg) were loaded on the column. The column was washed with 5 CV of Buffer A (10 mM Tris, 10 mM NaCl, pH 8.0), then sample was eluted over 25 CV with a linear gradient from Buffer A to Buffer A + 250 mM NaCl. All experiments were carried out at 4 °C on an ÄKTA purifier 10 (GE Healthcare, Uppsala, Sweden). The proteins were identified based on their retention times when run separately on the same column.

2.3 Results and Discussion

2.3.1 Adsorbent preparation

The four pK_a values of spermine are 7.96, 8.85, 10.02, and 10.80, with the higher pK_as corresponding to the terminal amines (101,109). We used SPARC to estimate that in the linkage created by conjugation of spermine to Sepharose by the periodate method [OH-CH_2-CH_2-CH(OH)-O-CH_2-CH_2-H_2N-CH_2-…] the pK_a of the coupled nitrogen is near 9.39; this implies that all four groups should be significantly protonated at the working pH of this investigation, pH 8.0. According to the Henderson-Hasselbalch equation, at pH 8.0, the spermine molecule conjugated to Sepharose has 3.3 charges/molecule.

In this initial work, we chose to prepare spermine Sepharose with a relatively low ligand density (typically 17 mM, 68 mM protonatable nitrogens) in order to avoid a heterogeneous landscape of interacting adsorption sites as found in traditional ion exchange adsorbents (**Figure 2.3**). As mentioned above (1), clustered-charge adsorbents such as the spermine Sepharose used in this work, differ from the tentacular ion exchange adsorbent matrix (1,94).

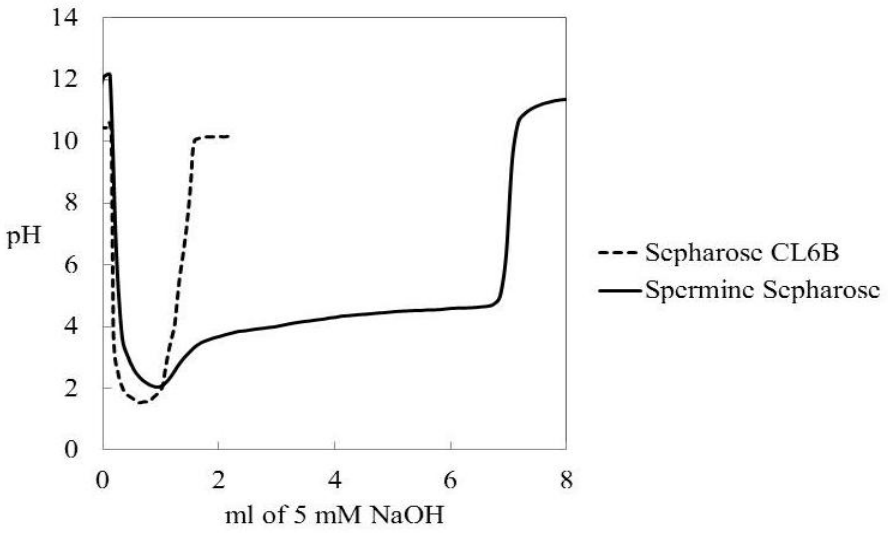

Figure 2.3: Titration curve of spermine Sepharose and Sepharose CL-6B. Titration curves were obtained using an AKTA purifier FPLC equipped with a post-column pH monitor. Sepharose (modified/unmodified) was packed in a column (5x20 mm) and equilibrated with 5 column volumes of 0.1 M HCl, and then 5 mM NaOH was run through a bypass in order to equilibrate the extra-column volume. After the equilibration, 5 mM NaOH was passed through the column to determine the moles of base required to titrate the acidified Sepharose adsorbent (modified/unmodified). Milimoles of NaOH required to titrate spermine on Sepharose was determined by subtracting the amount of 5 mM NaOH required for titration of unmodified Sepharose from that required to titrate the spermine Sepharose. All experiments were carried out at 4 °C on an ÄKTA purifier 10 (GE Healthcare, Uppsala, Sweden)(100).

In a tentacular ion exchange adsorbent, accessibility of the ligand is improved by using long linear polymer chains, which carry the functional ligands. In the case of clustered-charge adsorbents like spermine Sepharose, the ligand itself is a small charged polymer which forms a cluster of positive charges.

Sepharose CL-6B was chosen as a base matrix since it offers a hydrophilic surface and can be easily activated with sodium periodate to a controlled degree, as reported elsewhere (103). The terminal amines of spermine have pK_as of 10.02 and 10.8, and the internal amines have pK_as 7.96 and 8.85 (109). In order to achieve low ligand density by rendering some potentially-reactive amines charged and unreactive, spermine was coupled at pH 9.5 ± 0.2.

2.3.2 Adsorption isotherm measurements

α-lactalbumin is a popular model system for study of protein adsorption and chromatography (110-112). Like at least 30% of eukaryotic proteins (113), it is a molten globule under physiological conditions, but it is compact and not hydrophobic (114-117). α -lactalbumin has a conserved Ca^{2+} binding domain (dissociation constant of 10^{-7} M) (118), rich in aspartate residues located at the interface between the two subdomains of the protein (**Figure 2.4**) (119). In the Ca^{2+}-depleted form of α -lactalbumin, repulsion among these residues increases the solvent accessibility of this anionic charge patch.

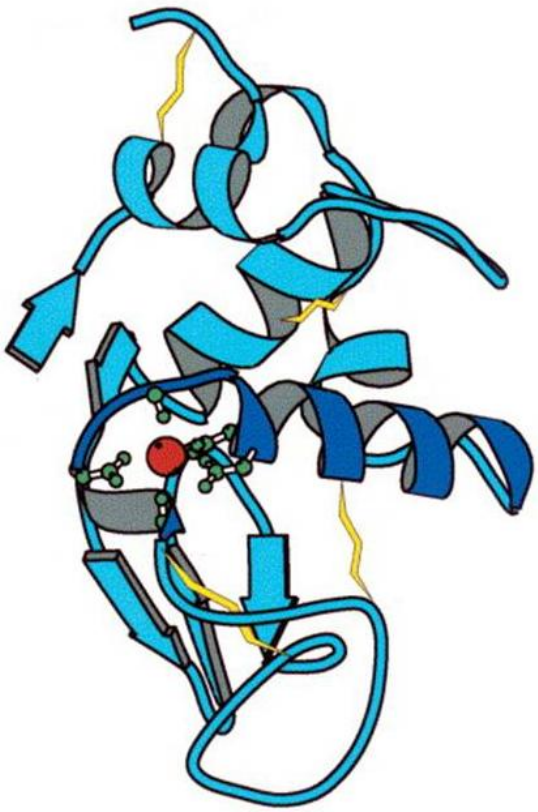

Figure 2.4: Structure of α-lactalbumin with the calcium binding region highlighted. The calcium binding residues shown in a ball-and-stick representation (Lys79, Asp82, Asp84, Asp87 and Asp88) form a cluster of negative charge (120).

The maximum binding capacity (Q_{max}) and initial binding affinity (Q_{max}/K_D) were compared for the spermine Sepharose adsorbent and for conventional commercial adsorbents. As shown in **Figure 2.5** and **Table 2.1**, the lower-ligand-density (17 mM ligand) charge-clustered spermine Sepharose adsorbent gave a higher protein binding capacity (Q_{max} = 0.8 ± 0.1 mM) and initial binding affinity (Q_{max}/K_D = 0.17) than DEAE Qiagen adsorbent (with 125 mM charge density (99); Q_{max} = 0.5 ± 0.04 mM; Q_{max}/K_D =

0.07) and the GE DEAE Sepharose (with 135 mM charge density; Q_{max} = 0.6 ± 0.08 mM; Q_{max}/K_D = 0.08).

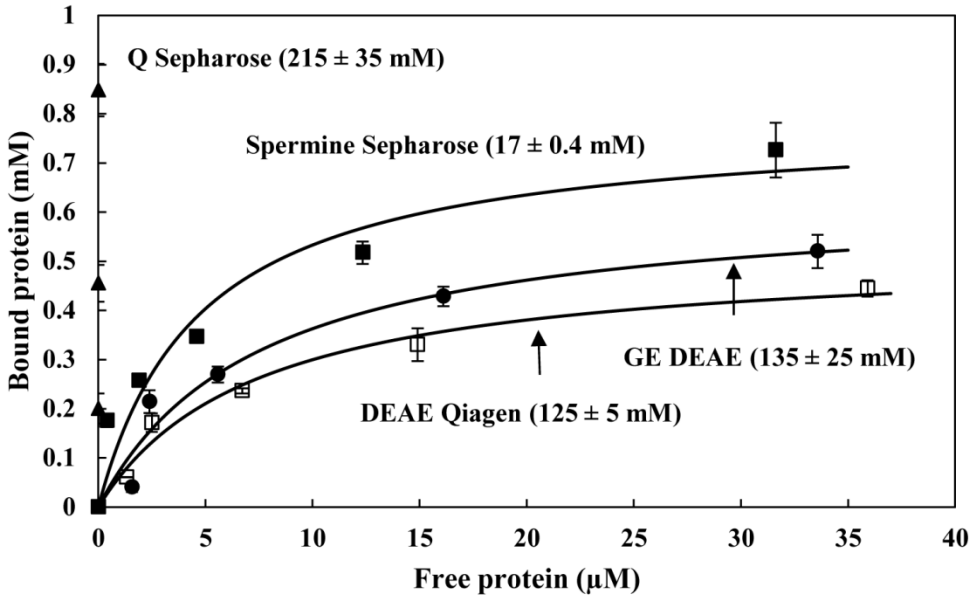

Figure 2.5. Adsorption isotherms of α-lactalbumin (Ca^{2+} depleted) on Q Sepharose resin (▲), spermine Sepharose resin (■), GE DEAE Sepharose resin (●) and DEAE Qiagen resin (□), 25 ^{o}C in 10 mM Tris, 10 mM NaCl, pH 8. Numbers in parenthesis refer to the reported ligand density of each resin according to provider specifications or our measurements. Error bars reported refer to the mean ± 1 SD.

The much-lower ligand and charge density of the spermine adsorbent should be emphasized in these comparisons, as it strongly affects protein adsorption (121). Wu and Walters (122) established that increased ligand density increased lysozyme adsorption in carboxylate-based cation-exchange supports. This behavior has also been discussed for large-molecular-weight molecules such as monoclonal antibodies (123). For the GE DEAE Sepharose adsorbent tested, the average through-space distance (which probably

slightly over-estimates the actual distance because ligands often are somewhat confined to a specific surface area) between ligands is 23 Å vs. 46 Å for the spermine Sepharose adsorbent. The equivalent spherical diameter for α-lactalbumin is 32 Å (124), which could imply that the commercial adsorbent forms an increased number of interactions with the target molecule as compared to spermine Sepharose. Nevertheless, the more widely separated ligands of the spermine Sepharose resin show higher affinity and binding capacity than the GE DEAE resin, supporting the idea that the clustered-charge approach provides enhanced protein adsorption. It is worthy of note that if the ligand density of the clustered spermine adsorbent were increased to densities typical of commercial adsorbents, interactions between ligands would create a more complicated landscape of adsorption sites. Every charge, however, would be located in a cluster energetically competent to serve as a functional adsorption site.

Table 2.1. Values of Langmuir Isotherm Parameters Q_{max} and K_D and Langmuir-Freundlich Q_{max} and K_D parameters and heterogeneity parameter n_H, for adsorption of α-lactalbumin (Ca^{2+} depleted) on spermine-Sepharose, DEAE Qiagen and GE DEAE Sepharose adsorbents.

	Langmuir Isotherm Parameters			Langmuir Freundlich Parameters		
Resin	Q_{max} (mM)	K_D (μM)	Q_{max}/K_D	n_H	K_D (μM)	Q_{max} (mM)
Spermine Sepharose						
10 mM NaCl	0.8 ± 0.1	4.7 ± 2.0	0.17	0.5 ± 0.1	121 ± 4	2.0 ± 0.6
26 mM NaCl	0.6 ± 0.1	13.3 ± 2.7	0.045	0.6 ± 0.01	94 ± 8	1.2 ± 0.0
40 mM NaCl	0.9 ± 0.4	73.4 ± 40	0.012	0.8 ± 0.02	292 ± 2	1.9 ± 0.1
60 mM NaCl	0.5 ± 0.2	71.2 ± 47	0.007	0.8 ± 0.1	225 ± 4.7	0.94 ± 0.0
DEAE Qiagen						
10 mM NaCl	0.5 ± 0.1	7.4 ± 1.7	0.07	0.8 ± 0.2	12 ± 2	0.63 ± 0.2
26 mM NaCl	0.5 ± 0.04	14.0 ± 2.7	0.035	0.9 ± 0.3	20 ± 4	0.55 ± 0.2
40 mM NaCl	0.4 ± 0.03	12.9 ± 2.4	0.031	1.4 ± 0.3	10 ± 2	0.3 ± 0.03
60 mM NaCl	0.3 ± 0.01	9.6 ± 1	0.031	1.0 ± 0.1	8 ± 2	0.27 ± 0.03
DEAE GE Healthcare						
10 mM NaCl	0.6 ± 0.1	7.5 ± 2.6	0.08	1.2 ± 0.1	6 ± 3	0.6 ± 0.1

The low ligand density used raises the possibility that the ligands may be localized to the outer layers of the agarose particles. We do not, however, expect the formation of ligand clusters which significantly modify adsorption behavior, based on the following calculation: Assuming that the spermine ligand is only localized in the outer 3% of the radius of the beads (mean bead diameter is 90 μm) the average inter-ligand distance would be 20.4 Å, whereas assuming uniform ligand distribution the average inter-ligand distance would be 46.1 Å. Given that the equivalent spherical diameter of α-lactalbumin protein is 32 Å (124), in either case at a given spot there would be no more than two ligands that could interact with the protein, except at rare statistical clusters which would not support the observed protein capacity.

We also analyzed the adsorption data by the steric mass action (SMA) model of Cramer et al. (104), which is based on the stoichiometric displacement model of Regnier et al. (125) (**Table 2.2**). Fitting of the 4-parameter SMA model to the data set gave inconsistent convergence. To resolve this issue, we set as initial guesses in the SMA fitting, the Langmuir Q_{max} and K_d parameters as SMA Q_a and K, respectively and estimated values of v and σ values. The SMA steric factor (σ), which reflects the number of sites on the surface shielded by an adsorbed protein, is 10-fold lower for spermine Sepharose than for the GE and Qiagen DEAE adsorbents, which have 7.9 and 7.4-fold higher ligand densities, respectively. We ascribe most or all of this difference to the difference in ligand density, any effect of clustering would best be determined using a spermine adsorbent of much higher ligand density, at which inter-ligand interactions might, however, become important.

Table 2.2. Steric mass action model parameters Q_a, K, L, σ (steric factor) and ν for adsorption of α-lactalbumin (Ca^{2+} depleted) on spermine-Sepharose, DEAE Qiagen and GE DEAE Sepharose adsorbents.

Resin	Q_a (mM)	K (μM)	Λ (mM)	σ	ν
Spermine Sepharose					
10 mM NaCl	0.8 ± 0.1	4.7 ± 2.0	17 ± 0.4	21 ± 0.1	0.4 ± 0.6
26 mM NaCl	0.6 ± 0.1	13.3 ± 2.7	17 ± 0.4	28 ± 0.1	0.5 ± 0.1
40 mM NaCl	0.9 ± 0.4	73.4 ± 40.1	17 ± 0.4	17 ± 0.8	0.7 ± 0.1
60 mM NaCl	0.5 ± 0.2	71.2 ± 46.9	17 ± 0.4	31 ± 0.5	0.7 ± 0.1
DEAE Qiagen					
10 mM NaCl	0.5 ± 0.1	7.4 ± 1.7	125 ± 5	239 ± 0.6	0.4 ± 0.1
26 mM NaCl	0.5 ± 0.04	14 ± 2.7	125 ± 5	261 ± 0.3	0.5 ± 0.1
40 mM NaCl	0.4 ± 0.03	12.9 ± 2.4	125 ± 5	338 ± 0.6	0.5 ± 0.1
60 mM NaCl	0.3 ± 0.01	9.6 ± 1	125 ± 5	430 ± 0.2	0.4 ± 0.1
DEAE GE Healthcare					
10 mM NaCl	0.6 ± 0.1	7.5 ± 2.6	135 ± 25	211 ± 0.7	0.5 ± 0.1

Salt effects upon protein binding also were studied. **Figures 2.6a** and **2.6b** present α-lactalbumin adsorption isotherms at four different NaCl concentrations (10 – 60 mM). At the lower salt concentrations tested (10 and 26 mM NaCl), both the initial binding affinity (Q_{max}/K_D) and maximum binding capacity (Q_{max}) were higher for the spermine adsorbent when compared to the Qiagen DEAE: 2.4 and 1.3 fold higher in Q_{max}/K_D at 10 and 26 mM and 1.6 and 1.2 fold higher in the maximum binding capacity. For the 40 and 60 mM NaCl concentrations, the initial binding affinity was higher for the DEAE adsorbent; clustered spermine adsorbent exhibits an increased sensitivity to salt concentration. This characteristic is important in elution-based chromatography since a

stronger dependence of adsorption affinity on salt concentration may imply higher resolution capabilities in column mode chromatographic operations.

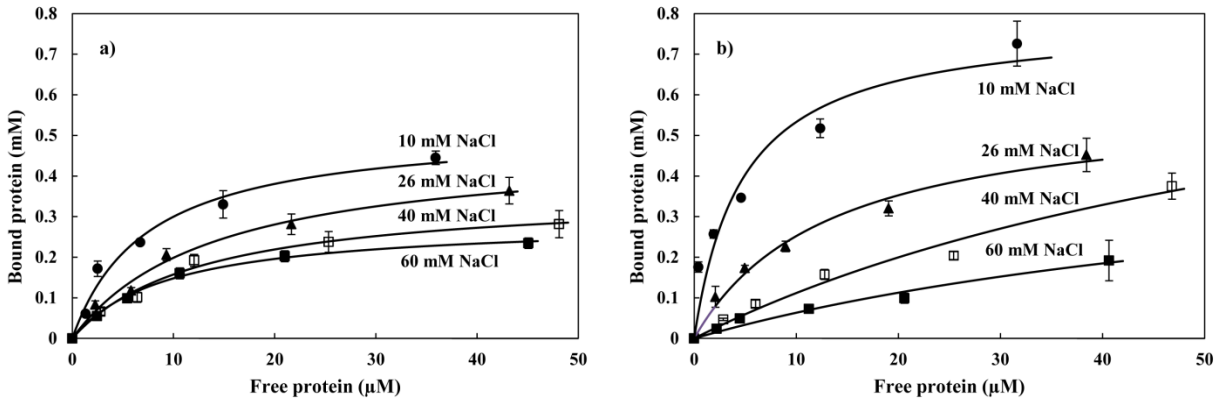

Figure 2.6. Adsorption isotherms of α-lactalbumin (Ca^{2+} depleted) on (a) DEAE Qiagen resin and (b) spermine Sepharose at 25 ^{o}C in 10 mM Tris, pH 8 at 10 mM NaCl (●), 26 mM NaCl (▲), 40 mM NaCl (□) and 60 mM NaCl (■). Error bars reported refer to the mean ± 1 SD.

Salt concentration effects can also be described by the *Z* plot derived from the stoichiometric displacement model (122,126), as presented in **Figure 2.7**. This graphical representation often exhibits a linear relationship between the logarithm of the initial binding affinity (Q_{max}/K_D) of an adsorbent and the logarithm of the salt concentration employed. The slope for this plot gives the apparent numbers of interaction sites, *Z*, of the protein surface with the stationary phase. In our original investigation of clustered adsorbents, the α-lactalbumin *Z* value for pentalysinamide was 1.4 ± 0.2 (vs. 1.2 ± 0.2 for the unclustered monolysinamide adsorbent of the same total charge) and that for pentaargininamide was 1.0 ± 0.1 (vs. 0.3 ± 0.1 for the non-clustered monoargininamide

of the same total charge) (1). In the present investigation, the *Z* value for the spermine-based adsorbent was 2.2 ± 0.3, compared to 0.3 ± 0.02 for the DEAE Qiagen adsorbent. Each of these observations is consistent with the idea that clustered-charge adsorbents form a larger number of intermolecular interactions with the adsorbate, thus presenting a higher *Z* value and increased protein adsorption.

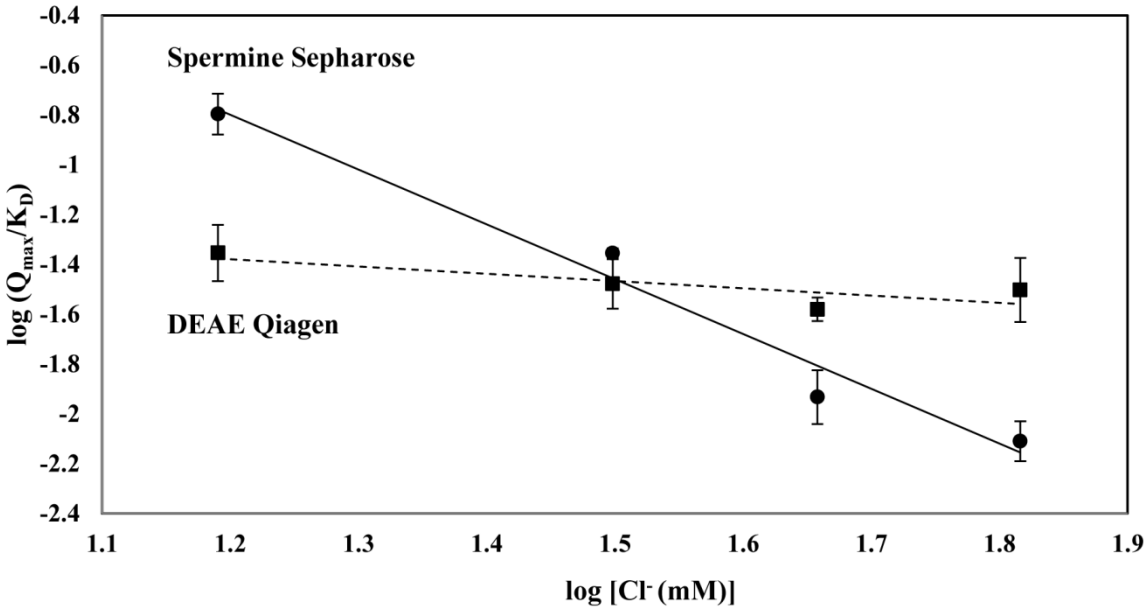

Figure 2.7. *Z* plots for determining the value of the stoichiometric displacement parameter *Z* for adsorption of α-lactalbumin (Ca^{2+} depleted) on spermine Sepharose (●) and DEAE Qiagen (■) in 10 mM Tris, pH 8 at 10, 26, 40 and 60 mM NaCl. $Z_{spermine}$: 2.2 ± 0.3 and Z_{DEAE}: 0.3 ± 0.02.

The Langmuir-Freundlich heterogeneity index for spermine Sepharose in 10 mM NaCl (0.5 ± 0.1) was substantially lower than those for the dispersed-charge adsorbents, DEAE Qiagen and DEAE Sepharose (0.8 ± 0.2 and 1.2 ± 0.1, respectively). In our previous

work (1), we also observed a lower heterogeneity index for the clustered charged adsorbent as compared to the dispersed-charge. This behavior is striking in view of the chemical uniformity of the charge clusters in the clustered adsorbent, and likely reflects local variations in steric accessibility, surface entropy, etc. It is also observed that increases in salt concentration favor an increase in the heterogeneity index towards unity of the spermine Sepharose adsorbent. One possible explanation is that salt-mediated shielding of low affinity interactions eliminate them from the functional population (127).

As clustered adsorbents show selectivity toward proteins displaying clusters of charge, it might be expected that they also would show high affinity toward nucleic acids, and indeed we found that pentaargininamide clustered ligands exhibit high affinity for nucleic acids (99). The biological function of spermine involves pseudospecific packing interactions with DNA (128), and it has been used in purification of DNA, and spermine agarose has been previously shown to have high affinity for DNA (129-131).

We confirmed the high affinity of spermine agarose for (total baker's yeast) RNA. As shown in **Figure 2.8** and **Table 2.3**, spermine Sepharose showed a higher RNA binding capacity (Q_{max} = 9.2 ± 0.9 mg/mL adsorbent) and a higher binding affinity (Q_{max}/K_d = 642 mL/mL adsorbent) than a 1.2 mM pentaargininamide adsorbent previously developed (Q_{max} = 2.1 ± 0.1 mg/mL adsorbent; $Qmax/K_d$ = 395 mL/mL adsorbent) (99). Finally, in terms of economic comparison, spermine represents a much more economical approach to synthesis of clustered-charge adsorbents than pentaargininamide.

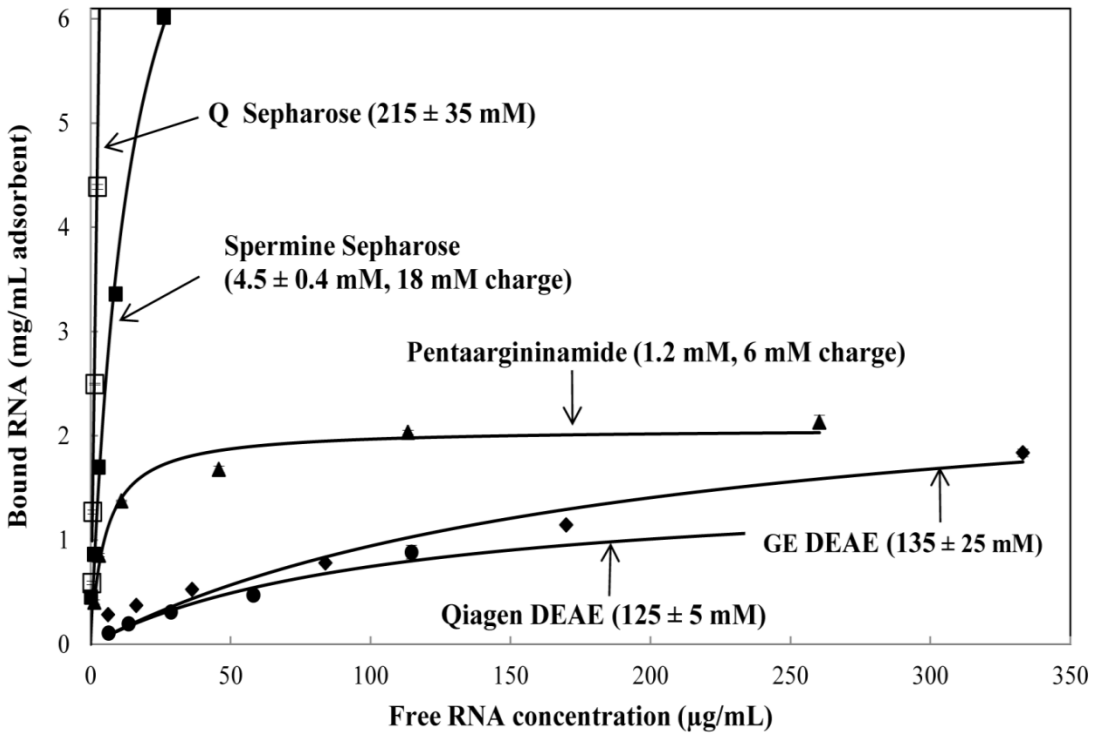

Figure 2.8. Adsorption isotherms of Baker's yeast RNA. Langmuir fits for Q Sepharose resin (□), Spermine Sepharose (■), Pentaargininamide adsorbent (▲), GE DEAE (♦), and Qiagen DEAE resin (●) at 25 ^{o}C in 10 mM Tris, 10 mM NaCl at pH 8.0. (Results other than spermine Sepharose from Reference (99)).

Table 2.3. Values of Langmuir isotherm parameters Q_{max} and K_d for adsorption of Baker's yeast RNA on Qiagen DEAE resin, GE DEAE Sepharose, pentaargininamide adsorbents (Arg5; 1.2 mM ligand density), spermine Sepharose and Q Sepharose at 25 ˚C in 10 mM Tris, 10 mM NaCl at pH 8.0.

Adsorbent	Q_{max} (mg/mL adsorbent)	K_d (µg/mL)
Qiagen DEAE (125 ±5 mM)	1.6 ± 0.2	109 ± 27
GE DEAE Sepharose (135 ±25 mM)	2.8 ± 0.7	192 ± 92
Pentaargininamide adsorbent (1.2 mM, 6 mM charge)	2.1 ± 0.1	5.3 ± 0.1
Spermine Sepharose (4.5±0.4 mM, 18 mM charge)	9.2 ± 0.9	14.3 ± 3.2

2.3.3 Column Chromatography

To show the applicability of spermine Sepharose in column mode we demonstrated the separation of two anionic proteins using spermine Sepharose (ligand density 13.2 ±0.4 mM or charge density 52.8 mM) and compared its separation efficiency with GE DEAE (ligand density 135 ± 25 mM) (**Figure 2.9**). 1 ml of a mixture of α-lactalbumin (0.2 mg; pI: 4.5, with a surface charge cluster) and BSA (0.2 mg; pI 4.7 without any surface charge cluster) was loaded on the column and eluted with a salt gradient. On the spermine Sepharose column, α-lactalbumin elutes at 127 mM NaCl and BSA elutes at 184 mM NaCl whereas on GE DEAE α-lactalbumin elutes at 125 mM NaCl and BSA elutes at 175 mM NaCl. This confirms that spermine Sepharose performs well in column chromatography, even at low ligand densities.

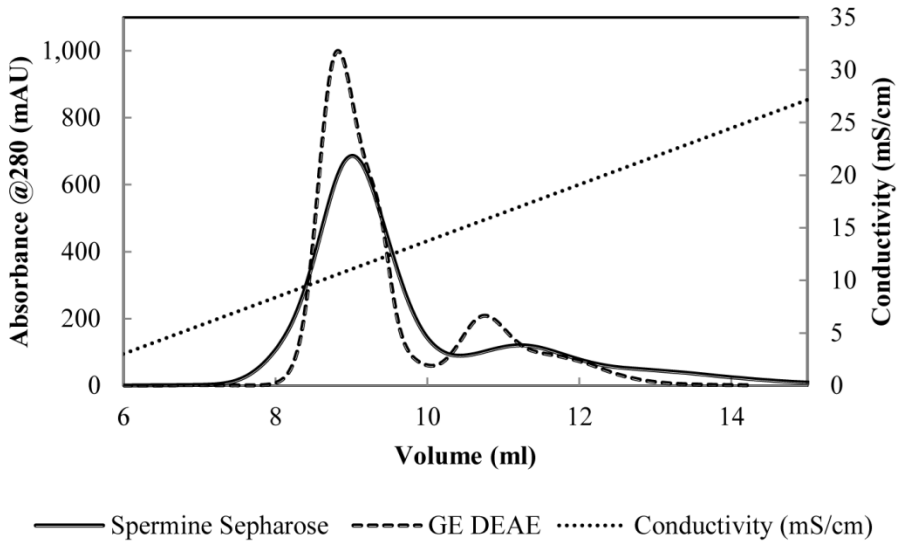

Figure 2.9. Linear gradient elution chromatography on spermine Sepharose (13.2 ± 0.4 mM ligand or 52.8 mM charge) and GE DEAE (135 ± 25 mM) of Ca^{2+} depleted α-lactalbumin and BSA. 0.4 mg (1 ml) of protein containing equal amounts of Ca^{2+} depleted α-lactalbumin and BSA were loaded onto a 21 mm H X 5 mm ID column on an ÄKTA purifier 10 (GE Healthcare, Uppsala, Sweden). The columns were washed with 5 CV of Buffer A (10 mM Tris, 10 mM NaCl pH 8.0), then eluted over 25 CV with a linear gradient from Buffer A to Buffer A + 250 mM NaCl. On spermine Sepharose α-lactalbumin elutes at 127 mM NaCl whereas BSA elutes at 184 mM NaCl. The proteins were identified based on their retention times when run separately on the same column; absorbance during regeneration with 1 M NaCl was negligible.

2.4 Conclusions

A clustered-charge spermine Sepharose adsorbent exhibited enhanced α-lactalbumin binding capacity (Q_{max} >1.6 and 1.3-fold higher than those for Qiagen DEAE and GE DEAE Sepharose adsorbents of much greater charge density) and higher initial binding affinity (Q_{max}/K_D 2.4 and 2.1-fold higher, respectively), and performs well in a column chromatographic separation. The spermine Sepharose adsorbent exhibits higher salt

dependency for protein adsorption than conventional DEAE Qiagen adsorbents, raising the possibility of improved resolution of closely related proteins employed in a column mode. Spermine also is more attractive than previously reported clustered adsorbents in terms of alkali stability and ligand cost. Finally, the high affinity and selectivity of spermine Sepharose support the idea that charge clusters play an important role in ion-exchange adsorption, even on conventional adsorbents.

Chapter 3: Functionalized Viral Nanoparticles As Ultrasensitive Reporters In Lateral-Flow Assays

*Portions of this chapter are published in Adhikari, M., Dhamane, S., Hagstrom, A. E., Garvey, G., Chen, W. H., Kourentzi, K., Strych, U., and Willson, R. C. (2013) Functionalized viral nanoparticles as ultrasensitive reporters in lateral-flow assays. The Analyst **138**, 5584-5587. The text has been amended to include unpublished data.*

3.1. Introduction

Immunochromatographic lateral flow assays (LFAs) are a well-established, inexpensive point-of-need diagnostic analytical method with proven utility for the primary testing of diverse samples. LFAs quickly provide a qualitative or semi-quantitative result without the need for elaborate sample preparation or capital investment. In conventional LFAs colloidal gold (**Figure 3.1**), selenium, blue latex or carbon nanoparticles bearing antibodies to the target are used as the reporter. If the test sample contains the analyte (target molecule), then the latter will bind to the reporter particles. The reporter-analyte immunocomplex will flow through the membrane and bind to a capture antibody or antigen attached to the surface of a nitrocellulose strip at the test line. The appearance of a color at the test line indicates a positive result and presence of the analyte, whilst a color at a control line further downstream confirms that the test has performed correctly.

LFAs have been used to detect a wide range of biomolecules, including nucleic acids, proteins, toxins, and hormones, as well as bacterial and viral pathogens (58). However, the sensitivity of LFAs, particularly for detecting viruses, lags behind more elaborate laboratory methods, such as plaque counting or PCR (132,133). For example, colloidal gold LFA detection of Japanese encephalitis virus in swine are reported to require at least 2.5 x 10^6 pfu mL^{-1}(134). A comparable assay for filamentous *Escherichia coli* M13 phage was able to detect 5 x 10^7 pfu mL^{-1}(135).

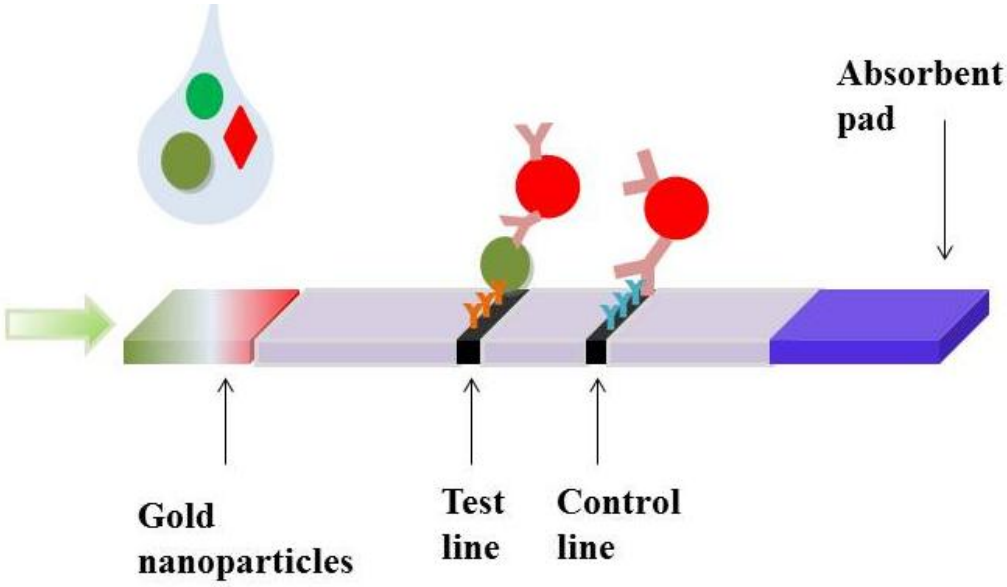

Figure 3.1: Principle of a lateral flow assay

M13 phage is a filamentous virus composed of a circular single stranded DNA encapsulated by major coat protein (approximately 2700 copies) and capped by four different minor proteins (**Figure 1.3**)(136,137). The coat protein can be engineered to display peptides on the surface of phage during phage display. Peptides and antibodies

displayed on the phage surface often have a good specificity and affinity for the analyte (138). Using phage display technology, many interesting M13 phage applications ware developed such as high power phage batteries (137,139,140), gene transfer vectors (141,142), targeted drug delivery (143), and biological sensors (144-147). However, the phage display technology is mainly limited to the peptide and protein evolution.

A variety of research efforts have been presented to label directly phage capsid proteins. The abundant pVIII sites are the most rewarding sites for the covalent attachment of other molecules. Methods for labeling on the reactive amino acids of M13 coat proteins such as lysine, aspartic acid, glutamic acid, and tyrosine are reported in (148). Other strategies include modification of the N-terminus of the coat proteins such as sortase-mediated chemo-enzymatic reaction for attaching molecules to pIII, pIX, and pVIII proteins (149), conjugation via diazotization reaction on the engineered M13 phage (150). M13 bacteriophage can be chemically decorated with drugs (151-154), fluorescent dyes (155,156), and enzymes (157) for various applications. The decorated viral nanoparticles have previously been reported to be suitable as affinity reagents in enzyme-linked immunosorbent assays (ELISAs) (158-160). Here, we present two different approaches to the manufacture of antibody- and peroxidase-doubly-modified M13 bacteriophage, and their use in LFAs (to detect bacteriophage MS2) (161). In the first approach, horseradish peroxidase (HRP) and target specific antibodies are chemically attached to the abundant coat protein (pVIII) of M13 (**Figure 3.3**). In an alternative approach, SAM-AviTag phage, derivatives of phage M13 where the N-terminus of the few-copy phage coat

protein pIII contains the enzymatically biotinylatable AviTag peptide (GLNDIFEAQKIEWHE), are employed. The lysine residue (K) in the AviTag is a substrate for biotinylation by *E. coli* biotin ligase (birA). Using streptavidin or neutravidin, any biotinylated affinity agent can then easily be linked to these enzymatically biotinylated phage particles (77-79).

MS2 bacteriophage: MS2 bacteriophage is the F-specific RNA phage belongs to the family *Leviviridae*. The MS2 phage has a single-stranded RNA genome of 3,569 nucleotides enclosed in an icosahedral capsid protein (162). The protein capsid is 27 nm in diameter and consists of 180 copies of the coat protein (**Figure 3.2**).

Figure 3.2: Schematic drawing of the MS2 protein shell (163).

MS2 virus is a harmless virus to human and other higher animals. It is used as a model for viral pathogens, including Ebola virus, and Marburg virus (164). MS2 has been used in various studies such as developing methods to study removal of viruses from water

(165-168), pathogens studies in ground water (169-173) and for the development technologies for detection of biological warfare agents (174-178). LFAs for bacteriophage MS2 have previously been commercialized as a tool for the detection of *E. coli* (MicroPhage Inc., Golden, CO) after phage expansion, but no limit of detection has been published.

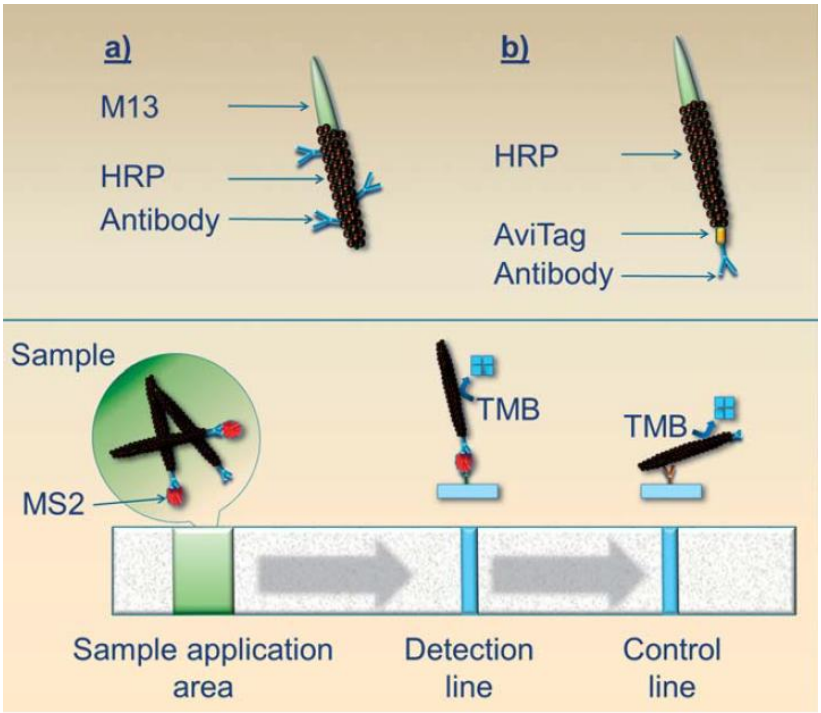

Figure 3.3: Viral nanoparticles as lateral-flow reporters: (Top panel) two types of nanoparticles were used. (a) The M13 coat proteins were functionalized with horseradish peroxidase (HRP) and analyte-specific antibodies. (b) The SAM-AviTag protein, pIII, was specifically biotinylated and functionalized with analyte-specific antibodies, and the coat proteins were functionalized with HRP. (Bottom panel) lateral flow assay for MS2 bacteriophage. The detection line contains MS2-specific antibodies, and the control line has anti-M13 antibodies. HRP-labeled phage were detected using the chromogenic substrate, 3,30,5,50-tetramethylbenzidine (TMB).

3.2. Materials and methods

3.2.1. Materials

E.coli strain (# 15597) and MS2 bacteriophage were from ATCC (Mannsas, VA). Rabbit-anti-MS2 polyclonal antibody was Tetracore, Inc. (Gaithersburg, MD). Rabbit-Anti-M13 antibody was from Novus Biologicals (Littleton, CO). Neutravidin, EZ-Link Sulfo-NHSLC-Biotin, Traut's reagent, and sulfo-SMCC were from Thermo Fisher Scientific (Waltham, MA). All other reagents were from Sigma Aldrich (St. Louis, MO).

3.2.2. Culture and titration of MS2 bacteriophage

Bacteriophage MS2 (#15597-B1) and its *E. coli* host strain (#15597) were obtained from the American Type Culture Collection (Manassas, VA). For MS2 propagation, the *E. coli* host was propagated in tryptic soy broth (TSB) at 37 ºC with shaking until log phase. For phage enrichment, 75 mL of bacterial host culture and 100 mL of MS2 stock (~10^9 pfu mL^{-1}) were added to a sterile tube containing 5 mL 0.7% tryptic soy agar (TSA), kept at 48 ºC. The contents of the tube were gently mixed, and then carefully poured onto a pre-warmed 1.5% TSA plate. After overnight incubation at 37 ºC, phage were harvested by gently scraping the top layer of soft agar into a 50 mL tube. Equal volumes (~20 mL) PBS and chloroform were added and the mixture was vortexed for 5 min. After 30 min centrifugation at 4000 x g the MS2-containing aqueous phase was carefully removed and filtered through sequentially smaller low protein-binding filters (0.45/0.22 mm). Aliquots of the MS2 stocks were stored at -80 ºC. For phage titering, dilutions of the phage stock were mixed with the *E. coli* host and the TSA, and poured onto 1.5% TSA plates.

Individual plaques were counted after overnight incubation (179). MS2 concentration was also estimated spectrophotometrically (specific absorbance at A_{260} = 7.81; molecular weight = 3.6 x 10^6 g/mol) as described in (180).

3.2.3. Culture and titration of M13 bacteriophage

SAM-Avitag M13 phage were a gift from Dr. Brian Kay, UIC (Chicago, IL). For phage enumeration, *E. coli* TG1 was grown to mid-log phase in LB at 37 ºC with shaking. The bacterial culture (5 mL) was then infected with 5 µL of phage stock (~10^{12} pfu mL^{-1}) and grown for 2 h at 37 ºC with shaking. This pre-culture was then transferred to 500 mL 2 x TY medium and incubated overnight at 37 ºC on a shaker. Bacteria were separated from phage in the supernatant by centrifugation (30 min, 3200 x g) and filtration through 0.45 µm filters. Phage were then precipitated using PEG/NaCl as previously described (181). The concentrated phage were stored at 4 ºC with 0.02% sodium azide. Phage titers were determined on X-Gal/IPTG plates as described (182).

3.2.4. Biotinylation of bacteriophage M13

SAM-AviTag phage were enzymatically biotinylated using *E. coli* biotin ligase (Avidity, Aurora, CO, or prepared in-house) according to the manufacturer's instructions. Briefly, 10^{10} phage particles were mixed with 14.3 µL Biomix-A (0.5 M biocin buffer, pH 8.3), 14.3 µL of Biomix-B (100 mM ATP, 100 mM Magnesium acetate), 10 µL d-biotin (500 µM), 1 µL of biotin ligase (2 mg/mL) in 10 mM Tris pH 8.0 buffer. Reaction volume was maintained to 1 mL. Sample was incubated for 1 h at 25 ºC. After 1 h, biotinylated phage was precipitated using PEG/NaCl as described in (181).

3.2.5. **Biotinylation of anti-MS2 antibody**

Rabbit-Anti- MS2 polyclonal antibody was biotinylated using EZ-Link Sulfo-NHS-LC-Biotin (Thermo Fisher Scientific) reagent. Anti-MS2 antibody was mixed with a 20-fold molar excess of EZ-Link Sulfo-NHS-LC- Biotin reagent in PBS, pH 7.4 for 1h at room temperature. After 1 h, excess biotin reagent was removed using Zeba^{TM} spin desalting column (7 kDa, MWCO). Number of biotin/antibody was estimated using the HABA reagent (Thermo Scientific).

3.2.6. **Phage-enzyme conjugation**

The biotinylated phage were then covalently coupled to horseradish peroxidase (HRP, Sigma-Aldrich, St. Louis, MO) using Traut's reagent (2- iminothiolane-HCl, Thermo Fisher Scientific, Waltham, MA) and sulfo-SMCC (succinimidyl- 4-(N-maleimidomethyl) cyclohexane-1-carboxylate; Thermo Fisher Scientific).

Phage activation using Traut's reagent: Briefly, 100 µL (~10^{11}) phage were suspended in 800 mL PBS, 3 mM EDTA. Traut's reagent was added to a final concentration of 7 µM and the reaction was allowed to continue for 90 min at 25 ºC. Excess Traut's reagent was removed using 10 kDa filters (Cat. no. UFC901024, Millipore, Billerica, MA) (**Figure 3.4**).

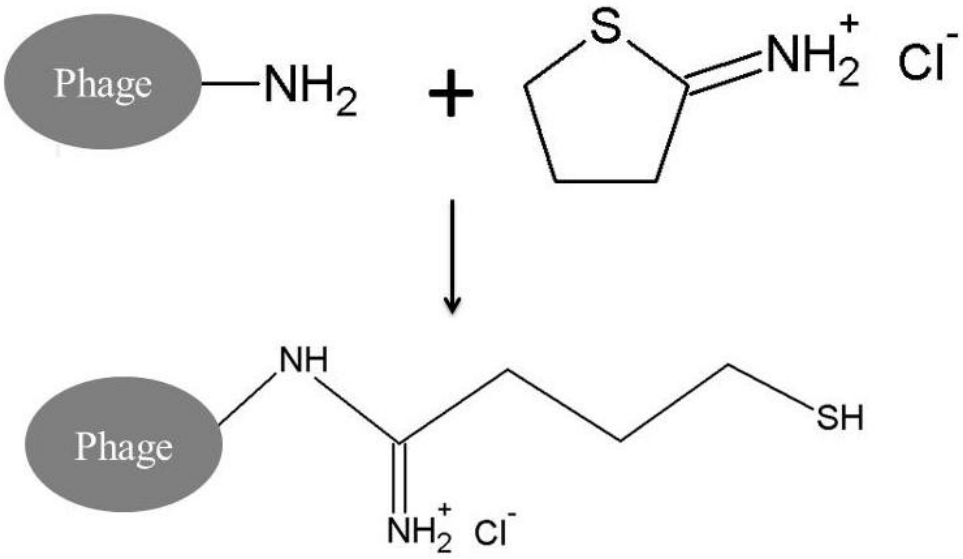

Figure 3.4: Reaction scheme of Traut's reagent. Traut's reagent reacts with primary amines of M13 phage to add small spacer arm with a free sulfhydryl group.

HRP activation using sulfo-SMCC: Maleimide-HRP was prepared by mixing HRP and sulfo-SMCC (succinimidyl- 4-(N-maleimidomethyl) cyclohexane-1-carboxylate) for 30 min to achieve final concentrations of 22 µM and 1.14 mM, respectively, in 1 mL PBS (**Figure 3.5**). Excess sulfo-SMCC was removed using a 10 kDa filter.

Traut's reagent-modified phage and sulfo-SMCC-modified HRP were then mixed in PBS for 90 min at 25 ºC. Maleimide group from the sulfo-SMCC-modified HRP reacts with sulfhydryl group from the Traut's reagent-modified phage and forms a stable covalent bond (**Figure 3.6**). Free HRP from the HRP-labelled phage was removed using 100 kDa filters (Millipore). Neutravidin (Thermo Fisher Scientific) was bound to the HRP-labelled phage through the biotinylated AviTag displayed on phage protein III.

Neutravidin-functionalized phage and biotinylated anti-MS2 antibody (at a 10-fold molar excess) were incubated for 1 h at 37 ºC. Uncoupled antibodies were removed using a 300 kDa spin dialyzer (Harvard Apparatus, Holliston, MA).

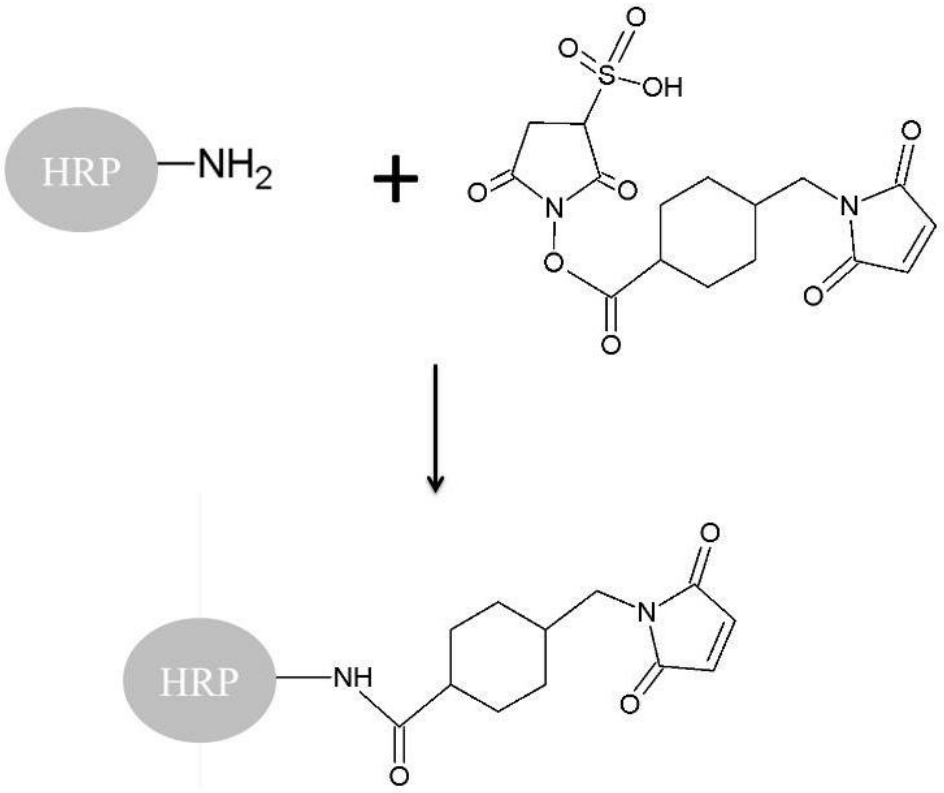

Figure 3.5: Reaction scheme for maleimide activation of enzyme (HRP).

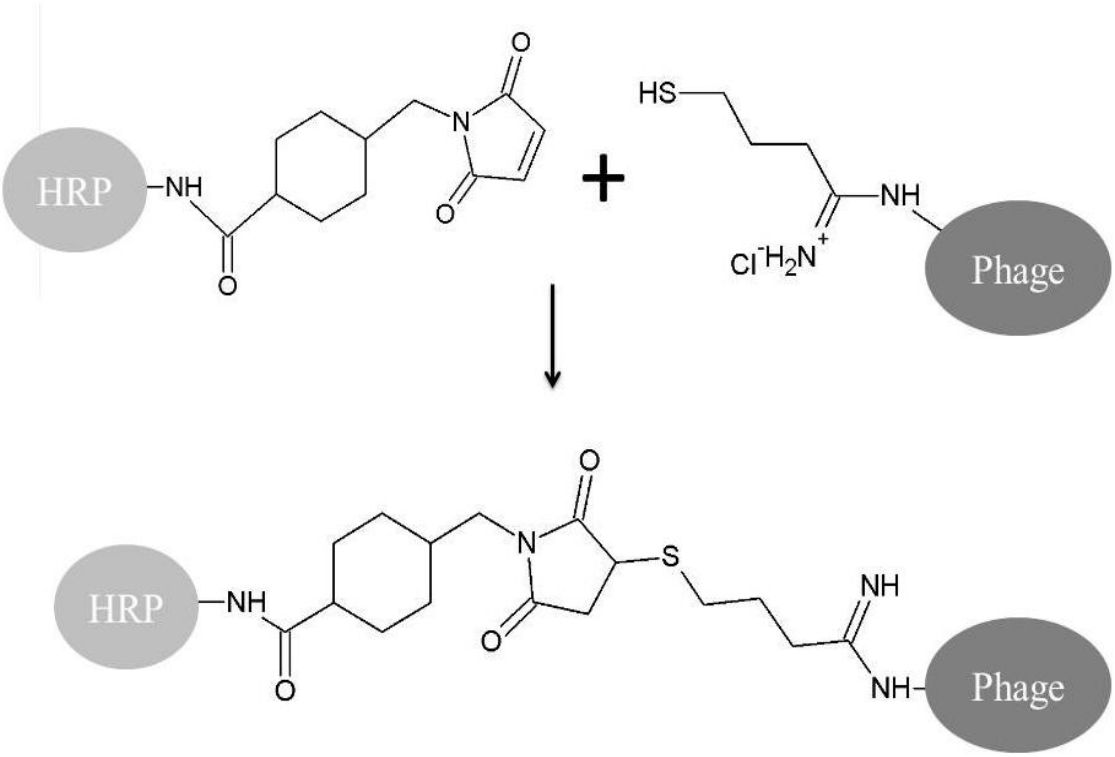

Figure 3.6: Reaction scheme for conjugation of M13 phage and HRP.

3.2.7. Bacteriophage M13 functionalization through covalent coupling of antibody and reporter enzyme

In this approach, HRP and anti-MS2 antibody were both covalently attached to M13 phage. M13 phage were activated using Traut's reagent as described above. Maleimide-HRP and maleimide anti-MS2 antibodies were separately prepared as described above for HRP activation, and combined with Traut's reagent-activated M13 phage particles at a molar ratio (HRP : Antibody : Phage) of 270 000 : 10 : 1. After 90 min at 25 ºC, the

complex was dialyzed using a 300 kDa spin dialyzer (Harvard Apparatus) to remove free enzyme and antibody.

3.2.8. Characterization of functionalized HRP labeled phage reporter

Concentration of the phage constructs were estimated using real-time PCR. The AviTag-targeted PCR primers were as follows: Forward: 5'-GTTGTTTCTTTCTATTCTCACTCC-3', and Reverse: 5'-CAGACGTTAGTAAATGAATTTTCTG-3'. For the PCR amplification reaction 15 µl of master mix (0.1 µl of 10 µM forward primer and, 0.1 µL of 10 µM reverse primer, 10 µL of 2xPCR mix and 4.8 µL of RNase- and DNase-free DI water) were mixed with 5 µl of each phage sample. The PCR were performed in a MX3005P QPCR System (Agilent Technologies) with PCR conditions: 10 min at 95 °C, 40 cycles of 30 sec at 90 ^{o}C, 30 s at 62 °C and 30 s at 72 °C, followed by dissociation step (1 min at 95 °C, 30 s at 55 °C, and 30 s at 95 °C). A standard curve (Ct values vs phage number) was obtained from a 10-fold dilution series of unmodified phage (its concentration obtained by tittering on X-Gal/IPTG plates). The concentration of modified phage were obtained using that standard curve.

To confirm the successful attachment of antibody on the phage, phage constructs were evaluated in ELISAs. 100 µL anti-MS2 antibodies (2 µg/ml in PBS) were incubated overnight on Nunc MediSorp^{TM} plates at RT. After incubation, the wells were blocked with 3% BSA solution in PBS for 1h at RT. Then, different concentrations of MS2 bacteriophage were offered for 2 h at RT. After 2 h, wells were washed three times with

PBS, 0.1 % Tween 20 and M13 phage construct (~10^8) were offered for 2 h at RT. The unbound phage construct were removed by washing three times with PBS, 0.1 % Tween 20. 100 µL of 1-Step Ultra TMB ELISA solution was added to the wells. After 30 min, enzymatic reaction was stopped using 50 µL of H_2SO_4 and absorbance was measured at 450 nm using a Tecan Infinite M200 Pro Plate reader.

3.2.9. Preparation of LFA strips

To form MS2-detection and M13 control lines, 5 µL anti-MS2 antibodies (0.4 µg μL^{-1}) and 5 µL anti-M13 antibodies (0.1 µg μL^{-1}), (GE Healthcare, Piscataway, NJ), both in 50 mM sodium acetate buffer (pH 3.6), were spotted on Fusion 5 membranes (GE Healthcare Biosciences, Piscataway, NJ) using a Lateral Flow Reagent Dispenser (Claremont BioSolutions, Upland, CA) equipped with an external syringe pump (Chemyx, Stafford, TX). The strips were allowed to dry for 1 h at 25 ºC. We also explored the use of nitrocellulose, commonly used in conventional immunochromatographic assays, with similar results as for Fusion 5, though a noticeably higher background was observed.

3.2.10. Lateral flow assay

The bacteriophage MS2 test analyte was diluted in LFA buffer (135) (100 mM Tris–HCl, pH 8; 0.3% Tween-20; 0.2% BSA; 0.1% PEG-3350). 100 µL samples were pipetted onto the sample application area of a prepared 7 x 50 mm Fusion 5 strip with anti-MS2 antibodies on the detection line and anti-M13 antibodies on the control line. The strips were first washed with 200 µL test buffer before 10 µL of the respective phage construct

(~10^8) were dispensed onto the distal end of the LFA strip. The strips were washed again with 500 µL LFA buffer, before signals were obtained by spotting 25 µL TMB Liquid Substrate System for Membranes (Sigma-Aldrich) on each line. After 15 min strips were scanned in a Perfection V600 flatbed color scanner (Epson, Long Beach, CA) and analyzed by ImageJ density analysis function.

3.2.11. Classical gold nanoparticles LFA for MS2

Our novel phage LFA was compared with the classical gold nanoparticle based LFA.

3.2.11.1. Functionalization of gold nanoparticles

100 µL of 4 mM K_2CO_3 was added to 1 mL of 40 nm gold nanoparticles (10^{11}/ml, OD_{520}=1, DCN, Carlsbad, CA). Then 10 µg rabbit anti-MS2 antibodies (Tetracore Inc., Gaithersburg, MD) were adsorbed, for 20 min at 25°C on a rotator. BSA, 100 µL (10 % (w/v)) was added to block the nanoparticles. After 20 min, the functionalized nanoparticles were collected by centrifugation (5 min, 10000 x g). The particles were washed once with 1 mL of storage solution (PBS, pH 7.4; 1% (w/v) BSA; 10% (w/v) sucrose), thereafter suspended in 100 µL and stored at 4°C. To estimate the concentration of gold nanoparticles their absorbance at 520 nm was measured.

3.2.11.2. Gold nanoparticle lateral flow assay

Nitrocellulose membrane, Prima 60 (GE Healthcare Biosciences, Piscataway, NJ) was used. The detection line with anti-MS2 antibodies (1 µg/cm) and control line with anti-rabbit antibodies (0.25 µg/cm) were spotted using a Lateral Flow Reagent Dispenser

(Claremont BioSolutions, Upland, CA) equipped with an external syringe pump (Chemyx, Stafford, TX). The strips were allowed to dry for 1 h at 37°C.

Assay strips (5 mm x 40 mm) were cut and 20 µL LFA buffer (100 mM Tris-HCl, pH 8; 0.3% (v/v) Tween-20; 0.2% (w/v) BSA; 0.1% (w/v) PEG 3350) was added at the bottom of the strip. Thereafter dilutions of MS2 viral particles in LFA buffer were added followed by 60 µL LFA buffer. Functionalized gold nanoparticle reporters ($2x10^9$) were added in 20 µL of LFA buffer, followed by another 60 µL LFA buffer. The strips were left to dry and thereafter scanned in a Perfection V600 flatbed color scanner (Epson, Long Beach, CA).

3.3. Results and discussion

3.3.1. Characterization of phage construct

The presence of functional anti-MS2 antibody and HRP on the phage construct was confirmed via MS2 bacteriophage ELISA. Anti-MS2 antibodies were adsorbed on the plate to which 10^7 and 10^8 MS2 phage in PBS was offered. After washing unbound MS2 phage thrice with PBS, 10^8 reporter M13 phage construct was offered and incubated for 2 h at RT. The plate was washed thrice to remove unbound phage constructs and color was developed using TMB ELISA substrate. The enzymatic reaction was stopped using 50 µL H_2SO_4 and the absorbance was measured at 450 nm. As shown in **Figure 3.7** phage constructs were retained in the MS2 captured wells indicating the presence of functional anti-MS2 antibody on the phage construct. Similar results were obtained with phage

construct prepared by attaching HRP and anti-MS2 antibody on coat protein of M13 phage.

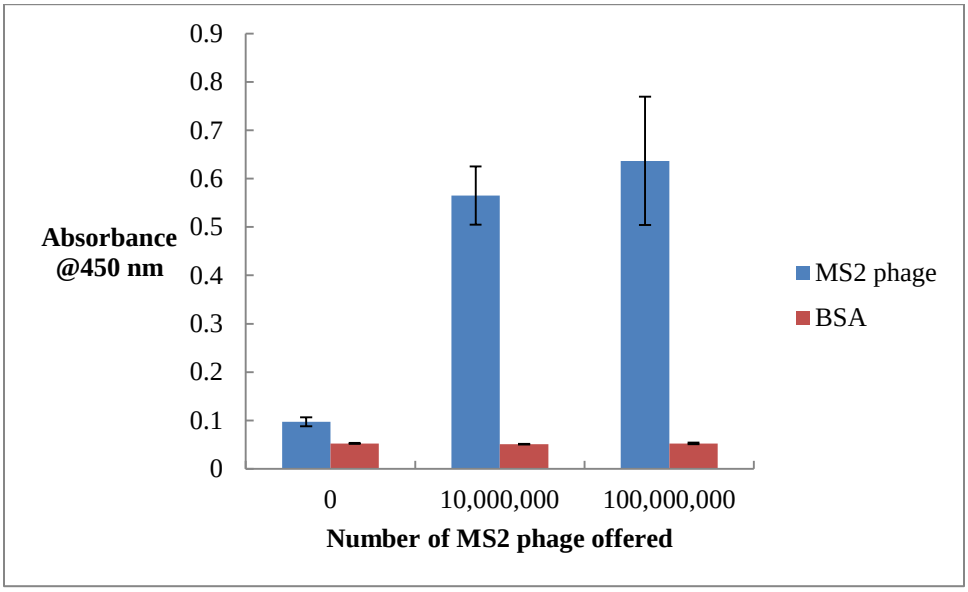

Figure 3.7: Characterization of M13 bacteriophage construct (functionalized through avidin-biotin) using a sandwich MS2 ELISA.

3.3.2. **Lateral flow assay using HRP labeled phage construct**

While immunochromatographic assays are a widely useful method for point-of-care diagnostics, there is a felt need for improved LFA analytical sensitivity. This can be addressed by pre-concentrating the target analyte, (135,183) or, as described in this work, by developing improved reporter particles. In order to obtain a stronger signal per individual affinity agent, we employed viral nanoparticles as the scaffold to which we chemically attached multiple reporter enzymes. Even considering mutual steric exclusion, the 2700 pVIII coat proteins of phage M13 likely offer hundreds of binding sites for reporters such as horseradish peroxidase, as well as for antibodies specific for the target

of interest. For the addition of antibodies to these phage affinity agents, we compared two approaches, the covalent linkage of the antibodies to the phage coat proteins and the avidin-mediated coupling of biotinylated antibodies to enzymatically biotinylated AviTag peptides displayed on the phage tail proteins.

3.3.2.1. **Lateral flow assay using HRP labeled phage construct functionalized with antibody through avidin-biotin linkage**

The model analyte used in our study, the *E. coli* bacteriophage MS2, has been widely used as a model for viral pathogens, and is used as an indicator of water quality by the United States Environmental Protection Agency. Serial dilutions of the phage were prepared from a stock whose titer had been determined using the double agar overlay plaque assay, the standard for the enumeration of MS2 (179), and independently confirmed spectrophotometrically (180). Anti-MS2 antibodies were spotted at the detection line to capture any MS2 phage and subsequently viral nanoparticles with anti-MS2 antibodies (**Figure 3.8A**). After adding the enzyme substrate, the LFA strips were scanned and the data were evaluated using Image J's density analysis function (184) (**Figure 3.8B**).

A signal was obtained at the anti-M13 control line for all samples, indicating that the viral nanoparticle reporters successfully moved through the membrane. At the test line, the signal obtained for 10^3 pfu of MS2 was clearly distinguishable from the control containing no phage (**Figure 3.8C**). In addition, we have shown that without anti-MS2 antibodies the M13 phage is not non-specifically retained by the anti-MS2 antibodies.

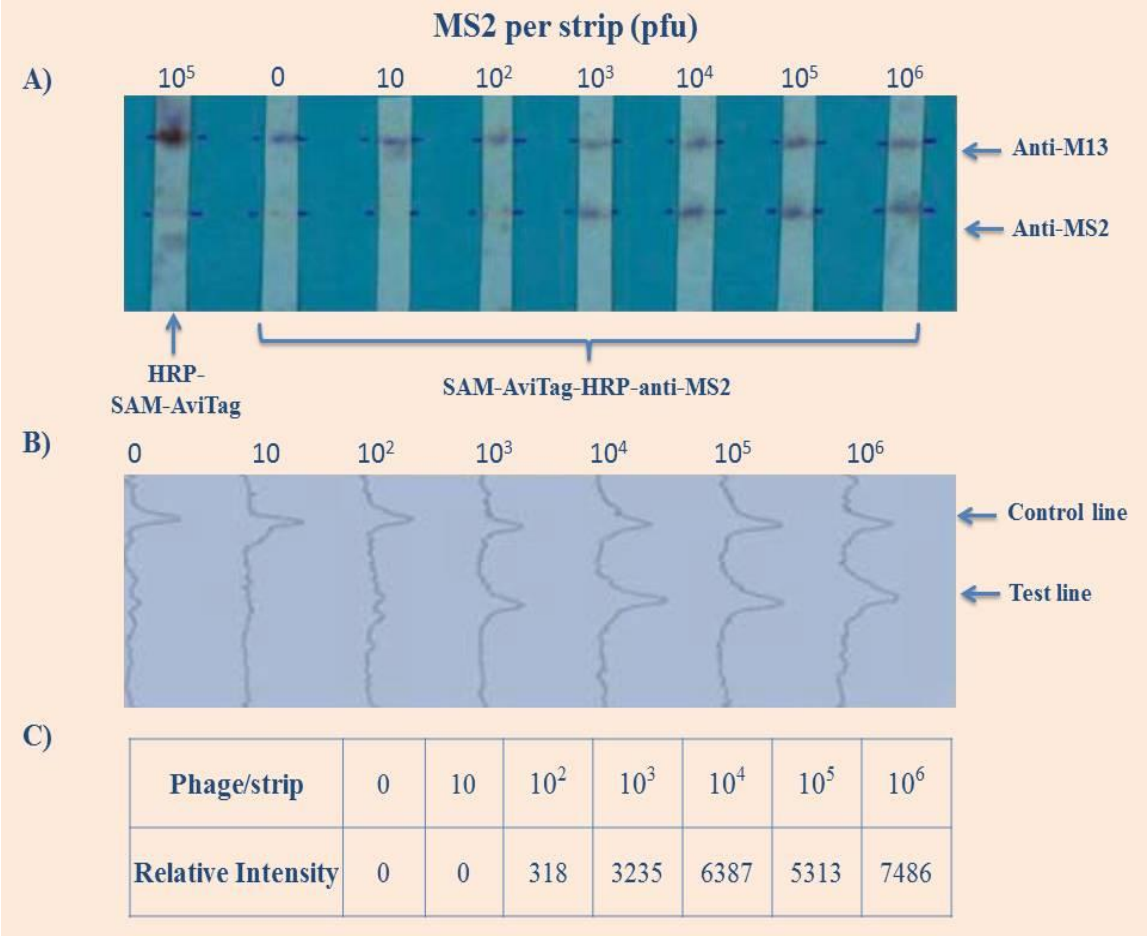

Phage/strip	0	10	10^2	10^3	10^4	10^5	10^6
Relative Intensity	0	0	318	3235	6387	5313	7486

Figure 3.8: Immunochromatographic detection of bacteriophage MS2. (**A**) Various numbers of MS2 phage were added to a Fusion 5 strip containing anti-MS2 and anti-M13 antibodies. Anti-MS2 antibodies were added to a biotin on the tail protein (pIII) of the M13 derivative, SAM-AviTag via avidin–biotin conjugation. Horseradish peroxidase (HRP) was chemically linked to the coat proteins, pVIII. SAM-AviTag phage carrying just the HRP reporter (HRP-M13) enzyme were used as a control. (**B**) Image J density analysis of the LFA strips in (A). (**C**) Relative intensities of the test lines shown in (A).

3.3.2.2. **Lateral flow assay using antibody-HRP labeled phage construct functionalized via covalent coupling**

In an alternative approach, anti-MS2 antibody and HRP were covalently coupled M13 phage's major coat protein. LFA was performed with these constructs as described in the previous section.

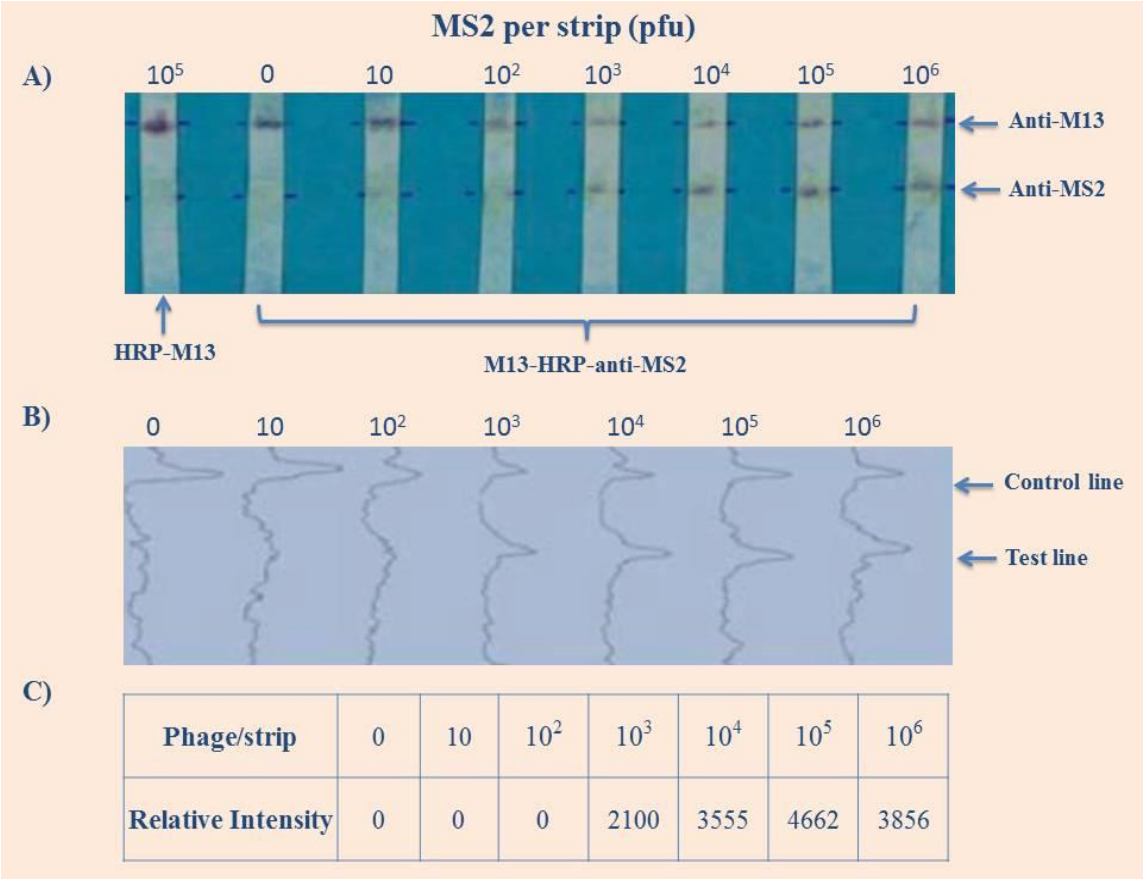

Phage/strip	0	10	10^2	10^3	10^4	10^5	10^6
Relative Intensity	0	0	0	2100	3555	4662	3856

Figure 3.9: Immunochromatographic detection of bacteriophage MS2. (**A**) Various numbers of MS2 phage were added to a Fusion 5 strip containing anti-MS2 and anti-M13 antibodies. M13 phage, chemically functionalized with anti-MS2 antibodies and horseradish peroxidase were added to bind to both the detection (anti-MS2; in the presence of analyte) and control (anti-M13) lines. M13 phage carrying just the HRP reporter enzyme (HRP-M13) were used as a control (leftmost strip). (**B**) Image J density analysis of the LFA strips in (A). (**C**) Relative intensities of the test lines shown in (A).

As shown in **Figure 3.9,** we did not observe any significant difference in sensitivity between M13 phage containing anti-MS2 antibodies attached to the pIII tail protein, and

those with the antibodies attached to the phage coat. Assuming that the number of pIII molecules is between three and five per phage, and the number of pVIII coat proteins is 2700, we would have expected a significantly larger number of antibodies per phage in the latter approach.

Given a sample volume of 100 µL, this corresponds to a titer of 10^4 pfu mL^{-1}, which represents almost one thousand-fold increased sensitivity compared to gold nanoparticle LFA with the same antibodies (**Figure 3.10**), and at least a one hundred-fold improvement in sensitivity over previously reported LFAs for viral detection (134,135).

3.3.2.3. Reproducibility test of the phage lateral flow assay

Reproducibility of the assay was tested by performing later flow assays with reporter phage constructs from three different batches. The LFA strips were then scanned and were evaluated using Image J's density analysis function. Relative intensity data of six independent experiments are given in **Table 3.1**. These experiments confirm the limit of detection of 10^4 pfu mL^{-1}.

Number of phage /strip	Covalent attachment			Avidin-biotin linkage		
	CC-I	CC-II	CC-III	AV-I	AV-II	AV-III
0	0	0	0	319	0	0
10^1	0	0	0	180	0	0
10^2	0	0	0	325	233	318
10^3	4613	5374	2100	2470	1541	3235
10^4	7723	6944	3555	5498	3859	6387
10^5	7679	9397	4662	5661	4514	5313
10^6	10441	9004	3856	7818	4341	7486

Table 3.1: Relative intensity of the test line for six independent lateral flow assays using functionalized M13 bacteriophage to detect MS2 virus. CC1-3: Reporter enzyme and antibody were covalently attached to M13. AV1-3: The antibody was attached through avidin:biotin linkage; the reporter enzyme was attached covalently.

The success of M13 reporters with low antibody loadings is consistent with the successful practice of phage-display library screening in the "monovalent phage display" format, in which a helper phage technique is used to display only a single genetically encoded candidate antibody on the M13 tail protein, eliminating the confounding effects of multivalent binding by multiple copies of the displayed antibody (185,186). The success of this method implies that phage are retained at significant efficiency by affinity

of a single displayed antibody, and argues that M13 LFA reporters should display small numbers of antibodies and a maximal number of enzyme reporters.

3.3.3. Gold nanoparticle based lateral flow assay for MS2 virus

To compare our novel ultra-sensitive LFA with the traditional LFA, we also developed gold nanoparticle based LFA for detection of MS2 virus. This assay was developed on nitrocellulose membrane. The results of gold nanoparticle LFA detecting MS2 viral particles are shown in **Figure 3.10**. The limit of detection of gold nanoparticle LFA is 10^7 pfu of MS2 i.e. 10^8 pfu/mL.

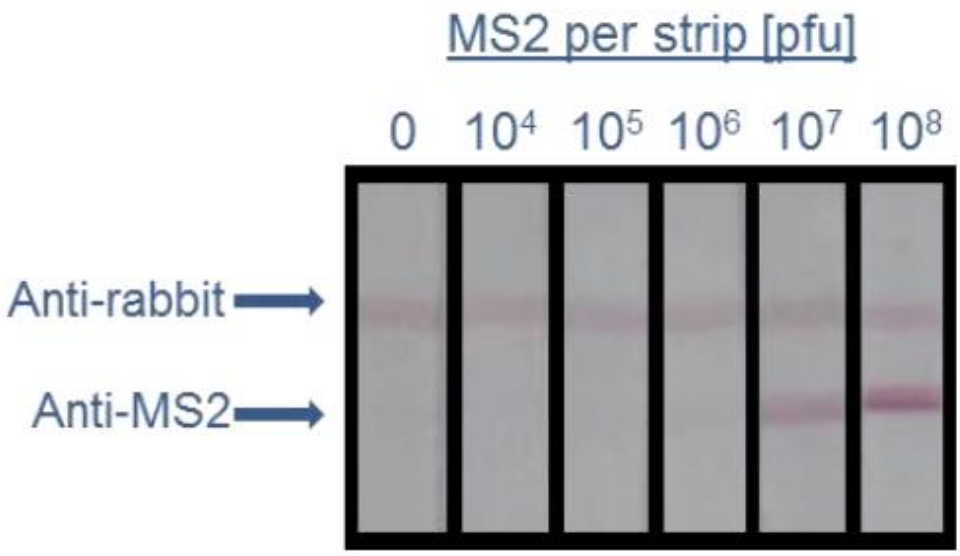

Figure 3.10: Immunochromatographic detection of bacteriophage MS2. Various numbers of MS2 phage were added to a nitrocellulose strip containing anti-MS2 and anti-rabbit antibodies. Gold nanoparticles with adsorbed rabbit anti-MS2 antibodies were captured on the test line by MS2, and on the control line by anti-rabbit antibodies.

3.4. Conclusions

Analytical sensitivity of LFAs can be mainly improved by preconcentrating target analyte (135) or by developing improved reporters. Enzyme labels, because of their potential signal amplification property, have been used to obtain stronger signal in LFAs (65,66). Here we used antibody- and peroxidase-doubly-modified M13 bacteriophage as a reporter in LFAs. The 2700 copies of the major coat protein of M13 bacteriophage bear several sites for enzyme labels and target specific antibodies bioconjugation. We compared HRP labeled phage constructs manufactured using two different approaches, the covalent coupling of antibodies to HRP labeled phage and the coupling of biotinylated antibodies to enzymatically biotinylated AviTag peptides displayed on pIII minor coat protein through avidin-biotin linkage. These constructs were able to detect MS2 virus in LFA with a sensitivity of 10^4 pfu/mL. When compared with the traditional gold nanoparticle LFA this novel LFA shows almost one thousand fold higher sensitivity. Thus we have successfully shown that M13 phage decorated with enzymes and analyte specific antibodies can serve as reporters in immunochromatographic assays of greatly enhanced sensitivity.

Chapter 4. Mechanistic Insight into Protein Ion-exchange Adsorptive Separations using Unified Super-resolution Imaging

*Portions of this chapter are published in Kisley, L., Chen, J., Mansur, A. P., Shuang, B., Kourentzi, K., Poongavanam, M.-V., Chen, W.-H., Dhamane, S., Willson, R. C., and Landes, C. F. (2014) Unified superresolution experiments and stochastic theory provide mechanistic insight into protein ion-exchange adsorptive separations. Proceedings of the National Academy of Sciences **111**, 2075-2080. The text has been amended to include unpublished data.*

4.1. Introduction

The biopharmaceutical industry is increasingly dependent on chromatographic separation techniques for purification of biotherapeutics (187). Among the various modes of chromatography, ion-exchange chromatography is extensively used for protein purification because it offers strong and easily reversible protein adsorption (1,188). Typically ion-exchange adsorbents are prepared by random chemical derivatization which creates a heterogeneous charge distribution over a particle's surface. To improve the heterogenous charge distribution over the ion-exchange adsorbent's surface efforts are mainly focused on improving mass transfer kinetics through the use of tentacular adsorbents (189,190) or by attaching polyion ligands such as polyethyleneimine or polylysine to improve selectivity (191). We have found that intentionally engineered

clustered-charge, pentaargininamide agarose adsorbents show higher affinity for negatively charged proteins than singly-charged monoargininamide adsorbents of same charge density (1). It can be anticipated that the stochastic coupling of ligands in the preparation of the monoargininamide adsorbent leads to areas with high ligand density, and areas of low density. We speculate that under typical operating conditions areas of low ligand density do not offer adequate interaction energy to retain biomolecules, and that adsorption is dominated by stochastically-created areas of high density. Current ensemble-averaged methods of investigating these issues are promising but they lack molecular-scale mechanistic resolution of the interfacial dynamics that control adsorptive separation processes (192).

Recent advances in single-molecule techniques can provide a deeper level of understanding. A combination of single molecule spectroscopy and statistical theory can provide the ability to acquire detail information about protein interactions with the ligand that are blurred by ensemble averaging of bulk measurements. Recently developed superresolution methods (193-206) offer the potential to considerably improve our understanding of adsorptive separations at spatial resolutions far below the optical diffraction limit (down to ~20 nm). Pioneering diffraction-limited single-molecule studies of separations on relatively simple supports (36,207-213) and adsorption at interfaces (214,215) provide incentive for applying higher-resolution spectroscopic analyses to a more realistic stationary phase.

The single molecule microscopy studies presented here were done with our collaborator Dr. Christy Landes (Rice University). Here in this work we apply superresolution single-molecule spectroscopic technique (*motion-blur Points Accumulation for Imaging in Nanoscale Topography*) to study adsorption and desorption kinetics of α-lactalbumin on a realistic support (216). We observe functional protein adsorption sites directly and demonstrate not only that clustered-charge ligands provide detectable, functional adsorption, but also show that even chemically homogeneous clusters of charge give rise to sites of varying kinetic properties due to steric factors. We observe that detectable localized adsorption of α-lactalbumin occurs only at clusters of charges whereas adsorption of proteins on individual singly charged ligands for longer than 3 ms is unobservable under our experimental conditions, unless the ligands are intentionally but randomly clustered at high ligand densities. The onset of clustered-ligand behavior and specific adsorption is shown to occur at lower total charge density with engineered multi-charge oligomers compared with random (stochastic) clustering of single charges. By extracting single-protein adsorption and desorption kinetics at individual ligands, direct experimental evidence in support of the stochastic theory is obtained. A mechanistic relationship between on- and off-rates is observed, due to the varying steric availability of the peptides. Finally, by extending the stochastic theory (33) to model macroscale observables, the single-molecule kinetics are used to simulate ensemble chromatographic elution profiles. The elution profiles establish that, if feasible, the engineering of ligand

clustering could improve elution plate heights by a factor of five compared with randomly arranged single charges.

4.2. Materials and methods

4.2.1. Agarose surface preparation

Agarose surface preparation and protein labeling have been originally reported in Daniels *et al.* (217). Glass coverslips (No. 1; VWR, 22 x 22 mm) were cleaned at 80 °C for 90 s in a solution of 4% (v/v) H_2O_2 (Fisher Scientific, Radnor, PA) and 13% (v/v) NH_4OH, then cleaned with an oxygen plasma for 2 min (PDC-32G; Harrick Plasma, Ithaca, NY; medium power). Silicon templates (Grace BioLabs, Bend, OR) were attached to the cover slips, and 1 mL of hot 1% (w/w) agarose solution (US Biological, Swampscott, MA) was spun onto each cover slip at 2000–3000 rpm using a Brewer Science Cee 200CBX precision coat-bake system. A custom flow chamber (Grace BioLabs) was then placed over the agarose thin film.

Charged peptide ligands were attached to the agarose surfaces using aldehyde functionalities introduced by 30 min treatment with 20 mM $NaIO_4$, as described by Afanassiev *et al.* (218). After washing with DI water and drying under a stream of helium, the activated surfaces were treated with a 42 nM solution of the pentaargininamide peptide (NH2-GGRRRRRamide, Biomatik, Wilmington, DE); the amide form of the peptide was used to eliminate the negative charge on the C-terminus to avoid creating a zwitterionic ligand, as previously described (1,99) in coupling buffer (100 mM Na_2HPO_4/NaH_2PO_4 [EM Science, Gibbstown, NJ] and 150 mM NaCl

[Mallinckrodt Chemical, St. Louis, MO], pH 7.2). The guanidinium side group of arginine (pK_a=12.5) is protonated at this pH, thus we expect it to be unreactive towards the agarose aldehyde reactive groups, and coupling through the N-terminal primary amine to be strongly favored. The grafting density was controlled by varying the offered concentration of the respective peptide, as further discussed below (219). The peptides were immobilized on the surface with several drops of 20 mM $CNBH_4$ (Pierce, Rockford, IL) at 4 °C for 30 min. Excess uncoupled peptide was removed by rinsing with coupling buffer, and unreacted aldehyde sites were reduced with 66 mM of $NaBH_4$ (in 25% EtOH/75% phosphate-buffered saline) at 4 °C for 5 min. The surfaces were finally rinsed gently with deionized water and stored at 4 °C, if not used immediately. Control agarose surfaces were prepared following the procedure outlined above, but omitting the peptide from the coupling buffer. To investigate the effect of the ligand charge on protein adsorption, the peptide length was varied. Di-, tri- and tetra-argininamide peptides (NH_2-GGRRamide, NH_2-GGRRRamide and NH_2-GGRRRR respectively, Biomatik) were attached on agarose supports. The concentration of the peptides used for support modification was 107.5 μM, 71.6 μM, 53.75 μM for the di-, tri- and tetra-argininamide respectively, resulting in an identical offered charge concentration (215 μM) in all samples.

4.2.2. **Fluorescent dye labeling of α-lactalbumin**

For protein labeling, Alexa 555 succinimidyl ester (Life Technologies; abs/em maxima 555/565 nm) was dissolved in dimethylformamide at a concentration of 10 mg/mL, and

0.1 mL of this dye solution was slowly added to 1 mL of 10 mg/mL Ca^{2+}-depleted α-lactalbumin dissolved in 0.1 M $NaHCO_3$ buffer, pH 7.4, to preferentially label the protein amino terminus rather than lysine ϵ-amino groups (220). The reaction was incubated at room temperature for 1 h with constant gentle mixing, and the reaction was then stopped by addition of 0.1 mL of freshly prepared 1.5 M hydroxylamine, pH 8.5. The labeled protein was dialyzed against water for 24 h and then against 10 mM Tris-HCl and 100 mM NaCl at pH 8.0 for 24 h. To ensure complete removal of the unincorporated fluorophore, PD-10 desalting columns and/or gel filtration chromatography were used. Gel filtration was carried out on an AKTA Purifier10 using Sephadex 75 10/300 GL (GE Healthcare, Buckinghamshire, UK) with 10 mM Tris-HCl and 100 mM NaCl at pH 8.0 as running buffer. Fractions with an estimated fluorophore-to-protein ratio of 1.0 ± 0.2 were pooled and used for adsorption studies.

4.2.3. **Total internal reflectance fluorescence (TIRF) wide field microscopy setup**

Data were collected on a home-built TIRF wide-field microscope, shown schematically in **Figure 4.1**. Either a 532 nm solid state laser (Coherent, Compass 315M-100SL) or a 633 nm HeNe laser (CVI Melles Griot, 25-LHP-925-249) were used for excitation. The beams were passed through separate acousto-optic modulators (IntraAction, 402AF1) controlled by frequency generators (Fluke, 271-U 115V) to synchronize excitation to the detection rate (221) before being combined onto the same path with a long-pass dichroic filter (Chroma, 565dcxt). The beams were expanded prior to focusing at the edge of a 1.45 NA, 100x, oil-immersion objective (Carl-Zeiss, alpha Plan-Fluar) for through-the-

objective TIRF microscopy. The TIRF excitation penetrated a 1/*e* depth of ~85 nm at an intensity of ~5 mW/cm^2. Emission was collected in an epi-fluorescence setup and was separated from excitation with a dichroic mirror (Chroma, z532/633rpc) and notch filters (CVI, 623.8-25.0M and Kaiser, HNPF-532.0-1.0). Two dichroics (Chroma, T640lpxr) separated the emission and cross talk was reduced with bandpass filters (Chroma, ET685/70m and ET585/65m). The signal was detected on an electron-multiplied charge coupled device (Andor, iXon 897) at an integration time of 30 ms, frame rate of 16.072 Hz, and electron multiplying gain of 300.

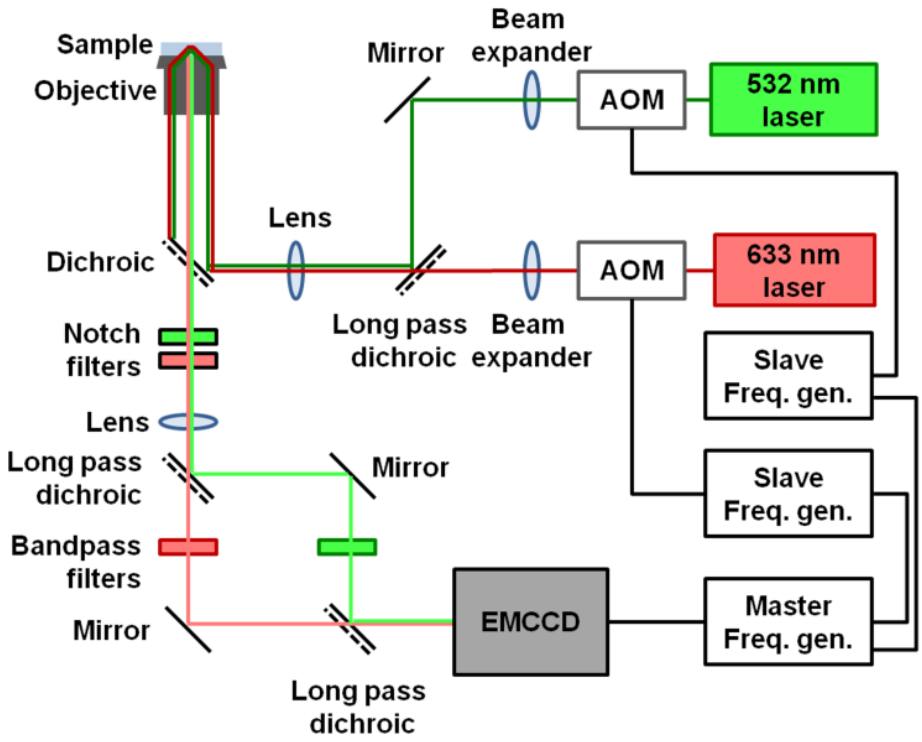

Figure 4.1 Schematic of wide field microscope, including acousto-optic modulator (AOM) controlled by frequency generators (Freq. gen.) and electron-multiplying charge coupled device (EMCCD) detector.

4.3. Results and Discussion

4.3.1. Superresolution image analysis of α-lactalbumin adsorption on ligand functionalized agarose support and bare agarose support.

Superresolution image analysis was performed on ligand-functionalized agarose supports spin-cast onto glass coverslips while flowing Alexa Fluor 555-labeled α-lactalbumin at 1μL/min in 10 mM Tris·HCl, pH 8.0; 10 mM NaCl buffer. When a protein stochastically adsorbed to the interface, each diffraction-limited single-molecule fluorescence emission pattern was fitted by a 2D Gaussian function, and the centroid location was recorded (**Figure 4.2A**). The interactions between the labeled protein and the stationary phase were tuned to be rare and reversible via low peptide loading on the agarose support, low protein concentration (500 pM), and use of a salt concentration chosen to make the average duration of adsorption events suitable for effective observation (10 mM Tris·HCl, pH 8.0; 10 mM NaCl; ionic strength 0.015 M; Debye length 24.5 Å). The fast diffusion of free α-lactalbumin (D ~150 $\mu m^2/s$) (217) in bulk solution compared to the detector temporal resolution (16 Hz) allowed the free α-lactalbumin to be unobservable in our experimental setup. Thus, stochastic on/off behavior of the fluorescently labeled protein at the stationary phase interface allows for superresolution imaging of adsorption/desorption events.

The centroid locations of all adsorption events in all frames were summed, with no assumptions about protein adsorption/ desorption history, resulting in a total centroid

event map (**Figure 4.2B**). We then renormalized data to distinguish events persisting over multiple frames at the same location from events occurring in only a single frame.

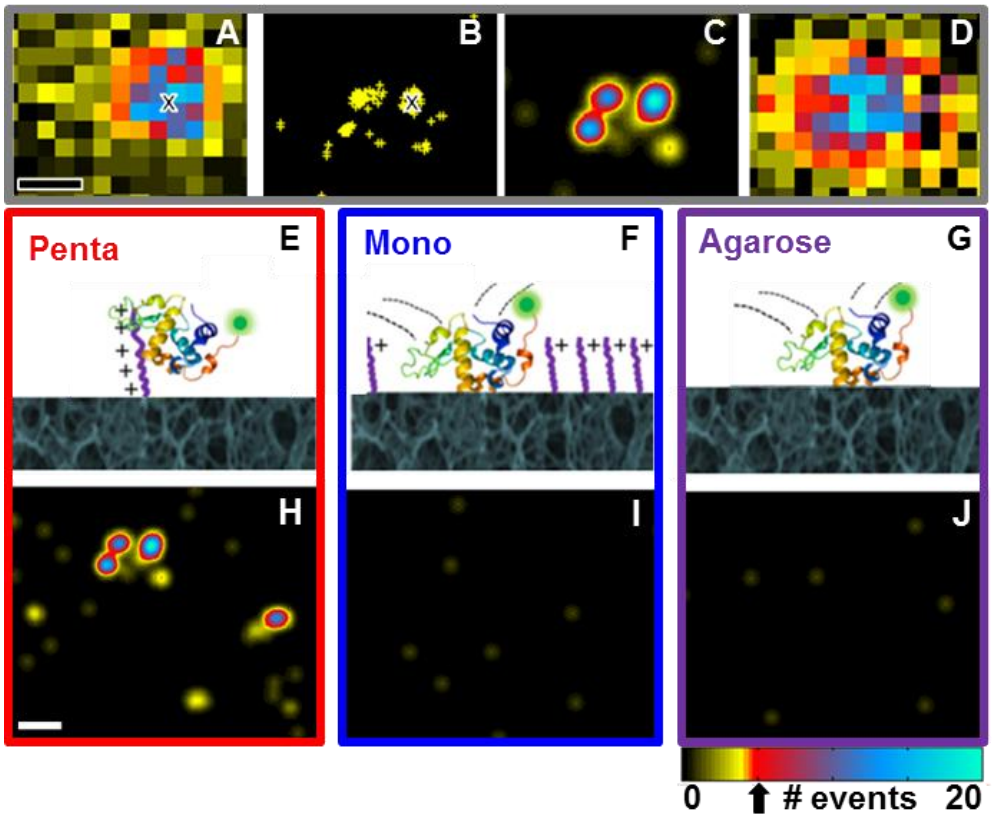

Figure 4.2. Superresolution imaging procedure and pseudo images at respective interfaces. (A–C) Steps to obtain superresolution pseudo images. (A) Single frame with an adsorbed α-lactalbumin protein. The centroid location obtained by a 2D Gaussian fit of the point spread function is noted by "x". (B) Centroid locations obtained from localizing 114 individual point-spread functions from 3,000 frames; location of centroid in A is indicated by "x". (C) Superresolution pseudo image from 3,000 frames depicting location and number of individual adsorption events. Specific adsorption sites were identified by the detection of more than five adsorption events (threshold indicated by arrow below color bar). (D) Summed diffraction-limited image from 3,000 frames for comparison with superresolved image. (E–G) Schemes and (H–J) superresolution pseudo images for α-lactalbumin at three stationary phase interfaces: (E and H) pentaargininamide, (F and I) monoargininamide, and (G and J) agarose, respectively. Data collected from 3,000 frames over 3.1 min are shown. Protein structure from PDB based on Chandra, et al. (222).(Scale bars: 200 nm.) Intensity scales range from (A) 50–1,800 and (D) 2–4 × 105 counts.

The resulting summed superresolution pseudo image in **Figure 4.2C** clearly identifies three distinct sites with multiple adsorption events whereas the summed diffraction-limited image (**Figure 4.2D**) cannot resolve these sites.

Superresolved event analysis distinguishes between specific protein adsorption at ligands and nonspecific steric interactions with the agarose support. Correlation analysis of the superresolution pseudo image selects Gaussian peaks that have maximum amplitude >5 adsorption events. The threshold of five adsorption events was selected to satisfy 99% confidence that the adsorption sites were not due to the nonspecific interactions observed on the bare agarose control samples.

4.3.2. Superresolution image analysis of α-lactalbumin adsorption at clustered and random charge peptides

Superresolution image analysis showed that (**Figure 4.2 H–J**) only the clustered-charge pentaargininamide stationary phase induced specific protein adsorption within the time resolution of the experiment. α-Lactalbumin interacted repeatedly at individual locations on the clustered charge stationary phase (**Figure 4.2H**), indicating specific adsorption sites where pentaargininamide was present. In control experiments at 1 M NaCl an insignificant number of distinct events were observed, demonstrating that the interactions were electrostatic, as expected for ion-exchange chromatography; this conclusion is further supported by the complete elution of α-lactalbumin from pentaargininamide adsorbents by 1 M NaCl in our previously reported ensemble studies of these systems (1).

Nonspecific interactions with the porous agarose interface (distinguishable by statistical analysis as mentioned above) were observed with all supports because, at the low ligand loading used to achieve single-molecule-appropriate conditions, the majority of the surface is bare agarose. Though singly charged ligands are commonly used (at higher ligand densities) in ion-exchange adsorbents, Super-resolution imaging of monoargininamide agarose samples (**Figure 4.2I**) show that all α-lactalbumin interactions at the sparse monoargininamide interface were indistinguishable within our instrumental capabilities. With the monoargininamide, only three out of 8,007 events were observed to have a single protein bound to a single location for longer than the five-frame threshold, similar to the frequency for the control agarose sample and unlike pentaargininamide surfaces there were no repeated adsorption events. Overall, the comparison of **Figure 4.2 H–J** shows the importance of charge clustering to adsorption via superresolution image analysis.

4.3.3. Comparison of specific protein adsorption with engineered oligomer clustered charges vs. stochastic clustering of single charges.

The onset of detectable specific α-lactalbumin adsorption was tested as a function of increasing oligomer length. As shown in **Figure 4.3**, in our experimental conditions specific adsorption events were observed to occur only with tri-argininamide and higher oligo-peptide lengths. No specific adsorption events were observed for mono- or diargininamide. The number of specific adsorption events increased with oligomer length

from tri-, tetra-, to penta-argininamide due to stronger electrostatic interaction energy with oligomer length (223).

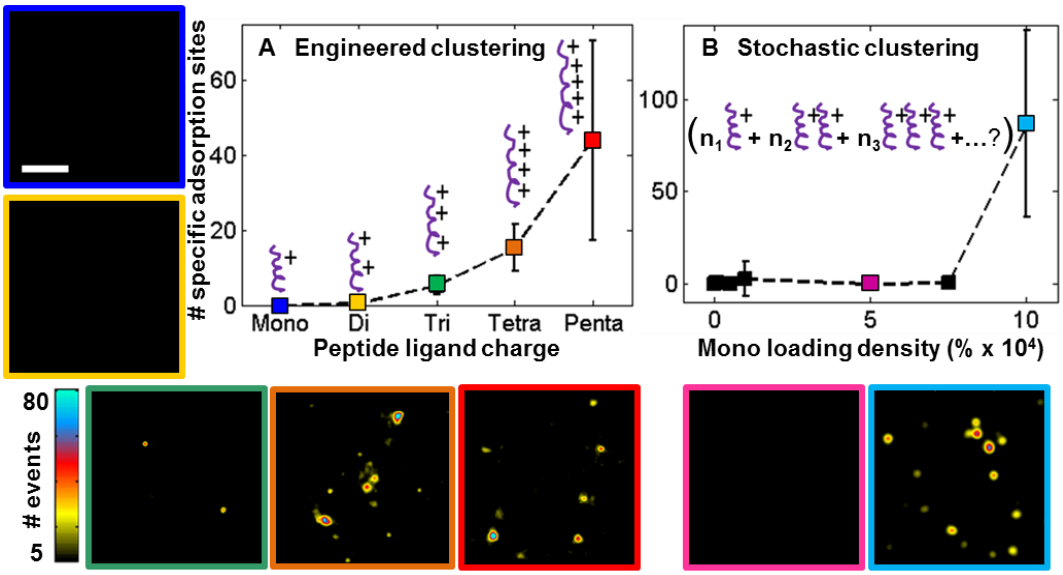

Figure 4.3. Onset of clustered-charge behavior, enabling specific adsorption of α-lactalbumin, via (A) synthetic peptide oligomer length and (B) increased grafting density of monoargininamide. The number of specific adsorption sites (per 160 μm^2, 60 s) is reported on each plot with graphic representations of the ligands overlaid. (A) Peptide oligomer length on the functionalized agarose was varied. The preparation charge concentration (215 μM) was the same for all samples during substrate modification. (B) Monoargininamide density as a percent increase from the benchmark 215 μM shown in Figure 4.2I was varied. Representative superresolution pseudo images are shown for each corresponding color-coded point. (Scale bar: 1 μm.) Dashed lines are shown as guide for the eye. Error bars represent the SD from five different 62-s trials taken from three different areas of the same sample.

If the hypothesis that clusters of charge are necessary for specific protein adsorption is correct, stochastic clustering of single charges must occur in commercial adsorbents bearing high concentrations of singly charged ligands. This hypothesis was tested by systematically increasing monoargininamide loading between factors of 2 and 1,000 times those used in the experiments described above. The numbers of specific adsorption

sites and superresolution pseudo images were recorded. As shown in **Figure 4.3** protein interactions became specific only at a ligand charge density three orders of magnitude higher than the level initially used. After the threshold was reached, many adsorption sites were observed, as shown in the superresolution pseudo image (**Figure 4.3**, light blue). The onset of clustering and adsorption is consistent with previous ensemble studies at and above this threshold by Wu and Walters (122). Because these sites were due to stochastic clustering, it remains unknown how many monoargininamide ligands were present at each site. The data shown in **Figure 4.3B** suggest that the formation of monoargininamide clusters is rare, likely due to electrostatic peptide–peptide repulsion, and explains the high ligand loading required for commercial stationary phases (~100 mM). By comparing intentionally clustered (**Figures 4.2H** and **4.3A**) and stochastically clustered (**Figure 4.3B**) peptide interactions, it can be concluded that the engineered clustering of peptide charges produces functional adsorption sites at much lower ligand concentrations than does stochastic arrangement of single charges.

4.3.4. **A kinetic analysis of single α-lactalbumin adsorption at clustered and random charged ligands**

A kinetic analysis of single α-lactalbumin adsorption at single pentaargininamide peptides (**Figure 4.4 A–C**) offers a direct experimental test of the physical model proposed in the stochastic theory (224-226): single analyte adsorption to a single ligand. For each identified adsorption site, the desorption time was defined as the dwell time from when a protein was first observed until it was not whereas the adsorption time was

the time between the end of one adsorption event and the beginning of the next adsorption event. Desorption and adsorption times for individual protein–ligand adsorption events at each specific adsorption site were extracted as reported in **Figure 4.4 A** and **B**. To maximize the resolution of each stochastic adsorption event, the frequency of events per site was controlled to be low by maintaining a low protein concentration in solution.

Each specific adsorption site exhibited single-exponential decay kinetics, and a least squares fit extracted the respective desorption (k_d) and adsorption (k_a) rate constants. This validates the second assumption of the stochastic theory, namely, that a non-varying rate constant describes each individual adsorption site (225). In addition, this result supports the stochastic model of a Poisson-distributed process for α-lactalbumin adsorption/desorption at each site, with each site corresponding to an individual pentaargininamide ligand (i.e., our distribution of pentaargininamide molecules is not ≥2 sites per 30 nm). Further, these results confirm that diffusion is not the rate-limiting step within the adsorption/desorption process.

Comparing the kinetics among distinct adsorption sites, however, reveals heterogeneity, as depicted in **Figure 4.4 A** and **B** by the distribution of decay kinetics at the four different sites. To understand the origin of this adsorption/desorption heterogeneity, the distribution of k_d and k_a for 53 individual pentaargininamide adsorption sites is shown in **Figure 4.4C** on a double logarithmic scale. If k_d and k_a were truly independent for a single type of adsorption site, as described by the pure stochastic theory (224), the

comparison depicted in **Figure 4.4C** would yield a 2D Gaussian with a spread indicative of the experimental noise and uncertainty in rate constant fitting (**Figure 4.4C**, gray oval). Instead, an inverse relationship is observed, indicated by the least squares fit shown as a dashed line in **Figure 4.4C**, which is inconsistent with the theory.

There are several possible explanations for the intersite adsorption/desorption heterogeneity. To investigate the cause of intersite adsorption/desorption heterogeneity, experiments performed by varying the agarose concentration from 1% to 3%, and thus the agarose pore size (227), suggest that steric availability of the peptides is the most likely source of the observed intersite heterogeneity. As pore size decreases, fewer adsorption events are observed, and the events last for shorter periods of time. Steric screening of peptides impairs protein interaction with the charged ligand, reducing interaction energy, leading to shorter desorption times and longer adsorption times, and the inverse relationship between k_a and k_d observed. The importance of agarose sterics in α-lactalbumin separations is consistent with our previously reported findings (217).

4.3.5. Prediction of elution profiles from Single-Molecule Kinetics

Direct measurement of kinetic rate constants for single proteins adsorbing to individual ligands allows us to relate the microscopic stochastic theory to a macroscopic observable, the chromatographic retention curve (**Figure 4.4 D** and **E**). By converting the Poisson distribution of the duration of protein adsorption/desorption events to the frequency domain (ω) and accounting for the discontinuous distribution of single-molecule desorption times using the Lévy representation, the distributions of protein desorption

times, ΔF(τs, i), were related to the characteristic function formalism of the distribution, ϕ(ts; ω|t_m) (34), by:

$$\phi(t_s;\omega \mid t_m) = \exp\left[r_m \sum_{i=1}^{i=k} \left(\left\{ \exp\left[i\omega\tau_{s,i} \right] - 1 \right\} \Delta F(\tau_{s,i}) \right) \right] \qquad \text{Equation 4.1}$$

where t_s and t_m are the times spent in the stationary phase and mobile phase, respectively, for an analyte that has adsorbed to the stationary phase r_m times during a given t_m, and k is the index of the discrete set of desorption times (33,34). By performing a Fourier transform of Eq. 4.1 to the time domain, the chromatographic peak for each adsorption site was simulated using the cumulative distributions of desorption times to directly relate experimental single molecule measurements to theory. A fixed value of r_m (the number of stochastic adsorption events for a given time in the mobile phase) based on experimental conditions was used to simulate relative elution curves. It is therefore valid to consider the resulting curves to be relative to one another but individually unique to the specific, low-concentration, single-molecule conditions used.

Desorption cumulative distributions for the four individual sites depicted in **Figure 4.4 A** and **B** were used to simulate the characteristic elution curves for hypothetical columns populated purely with one of the four adsorption sites (**Figure 4.4D**). The variability of the elution curves in **Figure 4.4D** demonstrates the macroscopic effects of the intersite heterogeneity due to the steric variation discussed earlier. Overall, however, the influence of intersite heterogeneity was drastically reduced when all 603 events for the pentaargininamide support are considered as an ensemble (**Figure 4.4E**, red curve). The

pentaargininamide curve is dominated by a Gaussian distribution, with only slight fronting due to the heterogeneity in adsorption/desorption kinetics depicted in **Figure 4.4D**.

In contrast, the simulated elution profile for high-density monoargininamide shown in the light blue curve in **Figure 4.4E** demonstrates that elution peak broadening and asymmetry result when stochastic clustering dominates the adsorption kinetics. The kinetics of events (n = 1,706) at all identified specific adsorption sites for the high loading density-induced stochastically clustered single-charge monoargininamide (**Figure 4.3B**) were used to extract the light blue elution curve in **Figure 4.4E**. This result is consistent with the notion that stochastic clustering is by definition heterogeneous in comparison with engineered clustering.

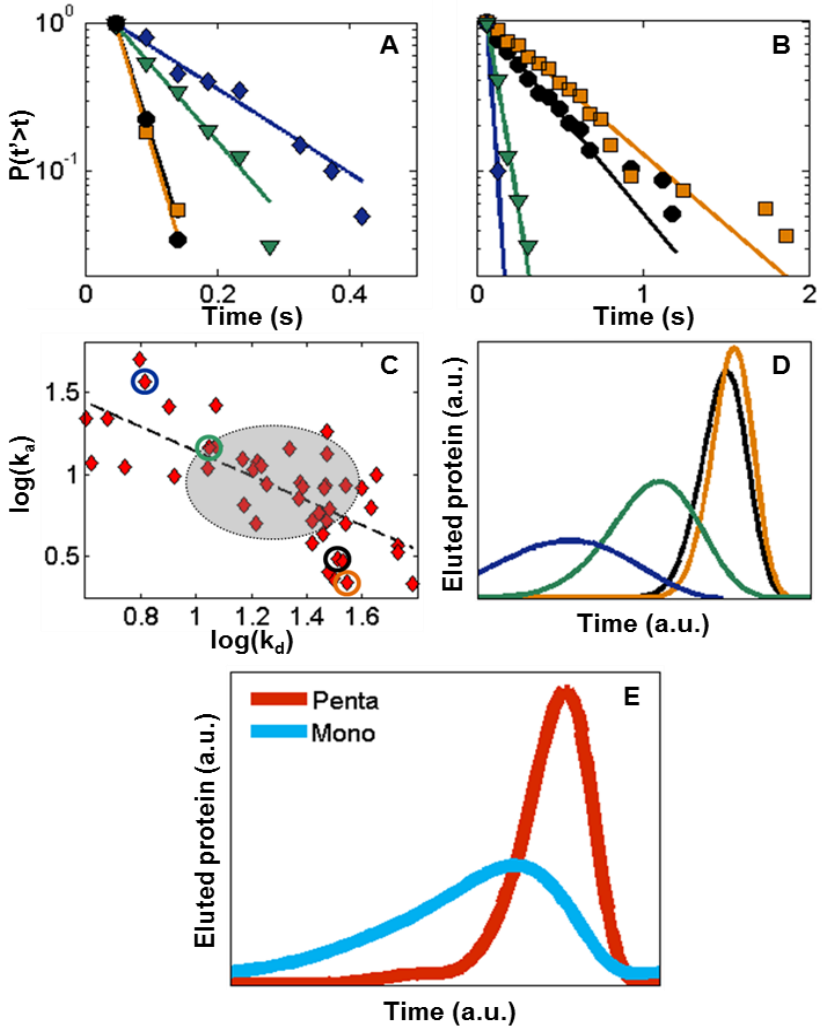

Figure 4.4. Kinetics and elution profiles obtained from single-molecule data. Cumulative distributions of (A) desorption and (B) adsorption times and respective fits (solid lines) for the four individual pentaargininamide adsorption sites shown in the superresolution pseudo image in (C) Relationship between k_d and k_a for 53 individual sites, with displayed locations in A noted by colored circles. A linear trend is observed indicated by the dashed line, as opposed to a 2D normal distribution represented by the gray circle (mean ± SD). (D and E) Relative ensemble isocratic chromatographic elution profiles obtained from single-molecule data using stochastic theory. (D) Elution curves for the four individual pentaargininamide adsorption sites. (E) Elution curves for ensemble of specific adsorption events for pentaargininamide (n = 603) and clustered monoargininamide (**Figure 4.3B**, light blue, 10×10^4%; n = 1,706). Data were obtained over 5.2 min.

The potential practical improvement in separations efficiency provided by engineered vs. stochastically clustered-charge ligands can be calculated by relating the elution curves shown in **Figure 4.4E** to the plate theory of chromatography (228). A relative comparison of the plate heights (H) between the two samples presented in **Figure 4.4E** can be made by taking the ratio of the square of the SDs of Gaussian fits to the peaks. The resulting H_{mono}/H_{penta} = 4.55, shows that plate heights potentially could be greatly reduced if it were possible to optimize the nature of the functional sites in ion exchange chromatographic matrices and also illustrates the potential for modeling macroscopic separations behavior from the fundamental properties of individual functional sites. Further improvements in this system also could be achieved by reducing the sterically induced heterogeneity in adsorption/desorption kinetics of functional adsorption sites. Although the very low ligand and protein concentrations used in the present study to prevent optical or functional overlaps are poorly compatible with standard column chromatography, the approach presented here is applicable to the characterization of higher-density conventional adsorbents usable in columns, as well as to other protein–surface interactions.

4.4. Conclusions

Here in this work we used single-molecule, super-resolution imaging technique termed '*motion blur' point accumulation for imaging in nanoscale topography* (mbPAINT) to measure the stochastic binding of single α-lactalbumin proteins to individual ligands on the agarose surface. This technique selectively sees only adsorbed proteins and the

unadsorbed proteins are not excited by the evanescent field. Adsorption/desorption kinetics of binding of proteins to individual ligands was estimated and elution curves were predicted using ensemble binding kinetics and stochastic theory. Several important conclusions can be drawn from this first molecular-scale investigation into protein ion-exchange chromatography by superresolution techniques and the stochastic theory. i) It is possible to apply the latest optical-imaging methodology to map functional adsorption sites in realistic agarose adsorbents with a resolution at least an order of magnitude smaller than the wavelength of light. ii) Clustering of charges is necessary for detectable ion-exchange adsorption under the conditions tested. iii) Engineering clusters is potentially more effective than relying on stochastic clustering. To create adsorption sites that specifically retain α-lactalbumin proteins on the agarose substrate, 215-μM preparation charge concentration is enough for the argininamide oligomers that have lengths of three or more monomers whereas 1,000 times as much, at least 200 mM, is required if monomers are used. iv) In a previously unidentified finding, the second assumption of the stochastic theory was confirmed to be valid by an experimental protein–ligand adsorption system: a nonvarying rate constant describes each individual adsorption site. v) Even chemically identical charged ligands give rise to kinetically heterogeneous single-protein adsorption/desorption kinetics, which we ascribe to steric effects. This heterogeneity between adsorption sites helps explain the unwanted fronting observed in bulk chromatographic protein separations. vi) The simulated elution profiles produced by combining the extracted single-molecule results and the stochastic theory

lead us to speculate that a fivefold improvement in separations efficiency, as defined by theoretical plate height, could result if it were possible to extend the single molecule results to a realistic separations medium. In summary, this work offers a fundamental understanding of the mechanisms of protein chromatography at the molecular scale, as well as other processes involving protein adsorption, such as immunoassays and biosensing.

Chapter 5 Conclusions and Future Work

5.1. **Spermine Sepharose as a Clustered-Charge Anion Exchange Adsorbent**

Peptide-based clustered charge anion exchange adsorbents (pentaargininamide and pentalysinamide) have shown higher initial binding affinity and capacity than dispersed charge adsorbents with similar charge density for biomolecules with inherent charge clusters. The peptide-based adsorbents, however, are too expensive for most practical applications. In order to create a more practical adsorbent, a novel clustered-charge adsorbent functionalized with spermine was prepared. Spermine Sepharose adsorbent exhibited enhanced α-lactalbumin binding capacity (Qmax > 1.6 and 1.3-fold higher than those for Qiagen DEAE and GE DEAE Sepharose adsorbents of much greater charge density) and higher initial binding affinity ($Qmax/K_D$ 2.4 and 2.1-fold higher, respectively) and functioned well in column mode. This establishes spermine as an economical and more practical ligand alternative to the pentaargininamide and pentalysinamide ligands. To extend the idea of clustered charge ion exchange adsorption, negatively charged ligands such as nitrilotriacetic acid can be used to make economical cation clustered charge adsorbents. Economical clustered charge adsorbents like spermine Sepharose can be used to study the effect of the nanostructured, clustered charge distribution on resolution of closely related proteins.

5.2. **Functionalized viral nanoparticles as ultrasensitive reporters in lateral-flow assays**

Viral nanoparticles have been demonstrated to be a robust scaffold that offer a number of sites for bioconjugation. Viral nanoparticles have previously been reported as affinity reagents in enzyme-linked immunosorbent assays (ELISAs). We have demonstrated that M13 particles decorated with enzyme labels and target specific antibodies can function as reporters in the immunochromatographic assays. We showed that M13 bacteriophage decorated with peroxidase enzyme and anti-MS2 antibodies can detect target MS2 virus particles in LFA with enhanced sensitivity compared to the conventional gold nanoparticle LFAs. The sensitivity of the assay could be improved by employing more sensitive HRP substrates, e.g., a chemiluminescent substrate. The number of steps in this assay can be reduced by integrating it into a paper microfluidics system. We also plan to explore the use of alternative viral nanoparticle reporters of different morphology such as TMV and T7 phages. Finally the novel LFA will be tested on real clinical samples.

5.3. **Mechanistic insight into protein ion-exchange adsorptive separations using unified super-resolution imaging**

In this work we demonstrated a novel technique for monitoring of single protein molecules in realistic adsorbent matrices. We have shown that functional adsorption sites can be mapped with a resolution of 30 nm. We have shown that clusters of charges are necessary to create detectable functional adsorption sites, and that chemically-identical

charged ligands give rise to kinetically-heterogeneous single-protein adsorption/desorption kinetics, which we ascribe to steric availability. Simulated elution profiles predicted by combining single-protein adsorption/desorption kinetics and stochastic theory suggest that separation efficiency of chromatographic adsorbents can be improved by using engineered cluster charging. In future studies we would like to apply this technique to comprehend the adsorption and desorption kinetics of proteins on varying charge density adsorbents. We would also like to compare predicted simulated elution profiles from the molecular scale data with the actual column chromatography data. This molecular scale method can be employed to study other processes which involve protein adsorption, such as immunoassay.

6. References

1. Fu, J. Y., Balan, S., Potty, A., Nguyen, V., and Willson, R. C. (2007) Enhanced protein affinity and selectivity of clustered-charge anion-exchange adsorbents. *Analytical Chemistry* **79**, 9060-9065

2. Gill, D. S., Roush, D. J., and Willson, R. C. (1994) Presence of a preferred anion-exchange binding site on cytochrome b5: structural and thermodynamic considerations. *Journal of Chromatography A* **684**, 55-63

3. Roush, D. J., Gill, D. S., and Willson, R. C. (1993) Anion-exchange chromatographic behavior of recombinant rat cytochrome b5. Thermodynamic driving forces and temperature dependence of the stoichiometric displacement parameter Z. *Journal of Chromatography A* **653**, 207-218

4. Prazeres, D. M. F., Schluep, T., and Cooney, C. (1998) Preparative purification of supercoiled plasmid DNA using anion-exchange chromatography. *Journal of Chromatography A* **806**, 31-45

5. Ramsden, J. J., Roush, D. J., Gill, D. S., Kurrat, R., and Willson, R. C. (1995) Protein Adsorption Kinetics Drastically Altered by Repositioning a Single Charge. *Journal of the American Chemical Society* **117**, 8511-8516

6. Janson, J.-C., and Jönsson, J. Å. (2011) Introduction to Chromatography. in *Protein Purification*, John Wiley & Sons, Inc. pp 23-50

7. Karlsson, E., and Hirsh, I. (2011) Ion Exchange Chromatography. in *Protein Purification*, John Wiley & Sons, Inc. pp 93-133

8. Lan, Q., Bassi, A. S., Zhu, J.-X., and Margaritis, A. (2001) A modified Langmuir model for the prediction of the effects of ionic strength on the equilibrium characteristics of protein adsorption onto ion exchange/affinity adsorbents. *Chemical Engineering Journal* **81**, 179-186

9. Asthagiri, D., and Lenhoff, A. M. (1997) Influence of Structural Details in Modeling Electrostatically Driven Protein Adsorption. *Langmuir* **13**, 6761-6768

10. Cano, T., Offringa, N. D., and Willson, R. C. (2005) Competitive ion-exchange adsorption of proteins: competitive isotherms with controlled competitor concentration. *Journal of Chromatography A* **1079**, 116-126

11. Chang, C., and Lenhoff, A. M. (1998) Comparison of protein adsorption isotherms and uptake rates in preparative cation-exchange materials. *Journal of Chromatography A* **827**, 281-293
12. Osberghaus, A., Hepbildikler, S., Nath, S., Haindl, M., von Lieres, E., and Hubbuch, J. (2012) Optimizing a chromatographic three component separation: a comparison of mechanistic and empiric modeling approaches. *Journal of Chromatography A* **1237**, 86-95

13. Bowes, B. D., and Lenhoff, A. M. (2011) Protein adsorption and transport in dextran-modified ion-exchange media. II. Intraparticle uptake and column breakthrough. *Journal of Chromatography A* **1218**, 4698-4708

14. Bowen, W. R., and Hughes, D. T. (1993) Ion Exchange of Proteins: A Microcalorimetric Study of the Adsorption of Bovine Serum Albumin on Anion-Exchange Materials. *Journal of Colloid and Interface Science* **158**, 395-402

15. Blaschke, T., Varon, J., Werner, A., and Hasse, H. (2011) Microcalorimetric study of the adsorption of PEGylated lysozyme on a strong cation exchange resin. *Journal of Chromatography A* **1218**, 4720-4726

16. Chung, W. K., Freed, A. S., Holstein, M. A., McCallum, S. A., and Cramer, S. M. (2010) Evaluation of protein adsorption and preferred binding regions in multimodal chromatography using NMR. *Proceedings of the National Academy of Sciences of the United States of America* **107**, 16811-16816

17. Holstein, M. A., Chung, W. K., Parimal, S., Freed, A. S., Barquera, B., McCallum, S. A., and Cramer, S. M. (2012) Probing multimodal ligand binding regions on ubiquitin using nuclear magnetic resonance, chromatography, and molecular dynamics simulations. *Journal of Chromatography A* **1229**, 113-120

18. Bankston, T. E., Stone, M. C., and Carta, G. (2008) Theory and applications of refractive index-based optical microscopy to measure protein mass transfer in spherical adsorbent particles. *Journal of Chromatography A* **1188**, 242-254

19. Stone, M. C., and Carta, G. (2007) Patterns of protein adsorption in chromatographic particles visualized by optical microscopy. *Journal of Chromatography A* **1160**, 206-214

20. Lewus, R. K., and Carta, G. (2001) Protein Transport in Constrained Anionic Hydrogels: Diffusion and Boundary-Layer Mass Transfer. *Industrial & Engineering Chemistry Research* **40**, 1548-1558

21. Russell, S. M., Belcher, E. B., and Carta, G. (2003) Protein partitioning and transport in supported cationic acrylamide-based hydrogels. *AIChE Journal* **49**, 1168-1177

22. Harinarayan, C., Mueller, J., Ljunglof, A., Fahrner, R., Van Alstine, J., and van Reis, R. (2006) An exclusion mechanism in ion exchange chromatography. *Biotechnology and bioengineering* **95**, 775-787

23. Hubbuch, J., Linden, T., Knieps, E., Thommes, J., and Kula, M. R. (2002) Dynamics of protein uptake within the adsorbent particle during packed bed chromatography. *Biotechnology and bioengineering* **80**, 359-368

24. Hubbuch, J., Linden, T., Knieps, E., Ljunglof, A., Thommes, J., and Kula, M. R. (2003) Mechanism and kinetics of protein transport in chromatographic media studied by confocal laser scanning microscopy. Part I. The interplay of sorbent structure and fluid phase conditions. *Journal of Chromatography A* **1021**, 93-104

25. Linden, T., Ljunglof, A., Kula, M. R., and Thommes, J. (1999) Visualizing two-component protein diffusion in porous adsorbents by confocal scanning laser microscopy. *Biotechnology and bioengineering* **65**, 622-630

26. Hinterdorfer, P., Baumgartner, W., Gruber, H. J., Schilcher, K., and Schindler, H. (1996) Detection and localization of individual antibody-antigen recognition events by atomic force microscopy. *Proceedings of the National Academy of Sciences of the United States of America* **93**, 3477-3481

27. Yuan, Y., and Lenhoff, A. M. (2003) Measurement of mobility of adsorbed colloids by lateral force microscopy. *Journal of Colloid and Interface Science* **267**, 352-359

28. Ha, T. (2001) Single-Molecule Fluorescence Resonance Energy Transfer. *Methods (San Diego, Calif.)* **25**, 78-86

29. Deniz, A. A., Laurence, T. A., Dahan, M., Chemla, D. S., Schultz, P. G., and Weiss, S. (2001) Ratiometric single-molecule studies of freely diffusing biomolecules. *Annual review of physical chemistry* **52**, 233-253

30. Kim, H. D., Nienhaus, G. U., Ha, T., Orr, J. W., Williamson, J. R., and Chu, S. (2002) Mg2+-dependent conformational change of RNA studied by fluorescence correlation and FRET on immobilized single molecules. *Proceedings of the National Academy of Sciences of the United States of America* **99**, 4284-4289

31. Liu, H. W., Cosa, G., Landes, C. F., Zeng, Y., Kovaleski, B. J., Mullen, D. G., Barany, G., Musier-Forsyth, K., and Barbara, P. F. (2005) Single-molecule FRET studies of important intermediates in the nucleocapsid-protein-chaperoned minus-strand transfer step in HIV-1 reverse transcription. *Biophysical Journal* **89**, 3470-3479

32. Kastantin, M., Langdon, B. B., Chang, E. L., and Schwartz, D. K. (2011) Single-Molecule Resolution of Interfacial Fibrinogen Behavior: Effects of Oligomer Populations and Surface Chemistry. *Journal of the American Chemical Society* **133**, 4975-4983

33. Pasti, L., Cavazzini, A., Felinger, A., Martin, M., and Dondi, F. (2005) Single-molecule observation and chromatography unified by Levy process representation. *Analytical Chemistry* **77**, 2524-2535

34. Dondi, F., Cavazzini, A., and Pasti, L. (2006) Chromatography as Levy stochastic process. *Journal of Chromatography A* **1126**, 257-267

35. Wirth, M. J., and Swinton, D. J. (2001) Single-Molecule Study of an Adsorbed Oligonucleotide Undergoing Both Lateral Diffusion and Strong Adsorption. *The Journal of Physical Chemistry B* **105**, 1472-1477

36. Kang, S. H., Shortreed, M. R., and Yeung, E. S. (2001) Real-time dynamics of single-DNA molecules undergoing adsorption and desorption at liquid-solid interfaces. *Analytical Chemistry 73*, 1091-1099

37. Maragos, C. M. (2009) Recent advances in the development of novel materials for mycotoxin analysis. *Analytical and Bioanalytical Chemistry* **395**, 1205-1213

38. Pikkemaat, M. G. (2009) Microbial screening methods for detection of antibiotic residues in slaughter animals. *Analytical and Bioanalytical Chemistry* **395**, 893-905

39. Pastor-Navarro, N., Maquieira, Á., and Puchades, R. (2009) Review on immunoanalytical determination of tetracycline and sulfonamide residues in edible products. *Analytical and Bioanalytical Chemistry* **395**, 907-920

40. Prieto-Simón, B., Noguer, T., and Campàs, M. (2007) Emerging biotools for assessment of mycotoxins in the past decade. *TrAC Trends in Analytical Chemistry* **26**, 689-702

41. Weller, M. G. (2000) Immunochromatographic techniques--a critical review. *Fresenius' journal of analytical chemistry* **366**, 635-645

42. Murdock, R. C., Shen, L., Griffin, D. K., Kelley-Loughnane, N., Papautsky, I., and Hagen, J. A. (2013) Optimization of a paper-based ELISA for a human performance biomarker. *Analytical Chemistry* **85**, 11634-11642

43. Baker, K. N., Rendall, M. H., Patel, A., Boyd, P., Hoare, M., Freedman, R. B., and James, D. C. (2002) Rapid monitoring of recombinant protein products: a comparison of current technologies. *Trends in biotechnology* **20**, 149-156

44. Hage, D. S., and Walters, R. R. (1987) Dual-column determination of albumin and immunoglobulin G in serum by high-performance affinity chromatography. *Journal of Chromatography* **386**, 37-49

45. Miller, K. J., and Herman, A. C. (1996) Affinity chromatography with immunochemical detection applied to the analysis of human methionyl granulocyte colony stimulating factor in serum. *Analytical Chemistry* **68**, 3077-3082

46. Gessler, F., Hampe, K., and Bohnel, H. (2005) Sensitive detection of botulinum neurotoxin types C and D with an immunoaffinity chromatographic column test. *Applied and Environmental Microbiology* **71**, 7897-7903

47. Chin, C. D., Linder, V., and Sia, S. K. (2012) Commercialization of microfluidic point-of-care diagnostic devices. *Lab on a Chip* **12**, 2118-2134

48. Gubala, V., Harris, L. F., Ricco, A. J., Tan, M. X., and Williams, D. E. (2012) Point of care diagnostics: status and future. *Analytical Chemistry* **84**, 487-515

49. Mansfield, M. (2005) The Use of Nitrocellulose Membranes in Lateral-Flow Assays. in *Drugs of Abuse* (Wong, R., and Tse, H. eds.), Humana Press. pp 71-85

50. Southern, E. M. (1975) Detection of specific sequences among DNA fragments separated by gel electrophoresis. *Journal of Molecular Biology* **98**, 503-517

51. Goldberg, D. A. (1980) Isolation and partial characterization of the Drosophila alcohol dehydrogenase gene. *Proceedings of the National Academy of Sciences of the United States of America* **77**, 5794-5798

52. Towbin, H., Staehelin, T., and Gordon, J. (1979) Electrophoretic transfer of proteins from polyacrylamide gels to nitrocellulose sheets: procedure and some

applications. *Proceedings of the National Academy of Sciences of the United States of America* **76**, 4350-4354

53. Zuk, R. F., and Litman, D. J. (1984) Immunochromatographic assay with support having bound "MIP" and second enzyme. Google Patents

54. Campbell, R. L., Wagner, D. B., and O'Connell, J. P. (1987) Solid phase assay with visual readout. Google Patents

55. Rosenstein, R. W., and Bloomster, T. G. (1989) Solid phase assay employing capillary flow. Google Patents

56. Oehler, S., Alex, R., and Barker, A. (1999) Is nitrocellulose filter binding really a universal assay for protein-DNA interactions? *Analytical biochemistry* **268**, 330-336

57. Jones, K. (2009) FUSION 5: A New Platform For Lateral Flow Immunoassay Tests. in *Lateral Flow Immunoassay* (Wong, R., and Tse, H. eds.), Humana Press. pp 1-15

58. Posthuma-Trumpie, G. A., Korf, J., and van Amerongen, A. (2009) Lateral flow (immuno)assay: its strengths, weaknesses, opportunities and threats. A literature survey. *Analytical and Bioanalytical Chemistry* **393**, 569-582

59. Danks, C., and Barker, I. (2000) On-site detection of plant pathogens using lateral-flow devices*. *EPPO Bulletin* **30**, 421-426

60. Lou, S. C., Patel, C., Ching, S., and Gordon, J. (1993) One-step competitive immunochromatographic assay for semiquantitative determination of lipoprotein(a) in plasma. *Clinical Chemistry* **39**, 619-624

61. Laborde, R. O. F., B. (2002) Paramagnetic particle detection in lateral flow assays. *IVD Technology*, 36

62. Song, X., and Knotts, M. (2008) Time-resolved luminescent lateral flow assay technology. *Analytica Chimica Acta* **626**, 186-192

63. Mirasoli, M., Buragina, A., Dolci, L. S., Guardigli, M., Simoni, P., Montoya, A., Maiolini, E., Girotti, S., and Roda, A. (2012) Development of a chemiluminescence-based quantitative lateral flow immunoassay for on-field detection of 2,4,6-trinitrotoluene. *Analytica Chimica Acta* **721**, 167-172

64. Mao, X., Ma, Y., Zhang, A., Zhang, L., Zeng, L., and Liu, G. (2009) Disposable nucleic acid biosensors based on gold nanoparticle probes and lateral flow strip. *Analytical Chemistry* **81**, 1660-1668

65. He, Y., Zhang, S., Zhang, X., Baloda, M., Gurung, A. S., Xu, H., Zhang, X., and Liu, G. (2011) Ultrasensitive nucleic acid biosensor based on enzyme-gold nanoparticle dual label and lateral flow strip biosensor. *Biosensors & Bioelectronics* **26**, 2018-2024

66. Parolo, C., de la Escosura-Muniz, A., and Merkoci, A. (2013) Enhanced lateral flow immunoassay using gold nanoparticles loaded with enzymes. *Biosensors & Bioelectronics* **40**, 412-416

67. Marvin, D. A., Welsh, L. C., Symmons, M. F., Scott, W. R., and Straus, S. K. (2006) Molecular structure of fd (f1, M13) filamentous bacteriophage refined with respect to X-ray fibre diffraction and solid-state NMR data supports specific models of phage assembly at the bacterial membrane. *Journal of Molecular Biology* **355**, 294-309

68. Day, L. A., Marzee, C. J., Reisberg, S. A., and Casadevall, A. (1988) DNA Packing in Filamentous Bacteriophages. *Annual Review of Biophysics and Biophysical Chemistry* **17**, 509-539

69. Arap, M. A. (2005) Phage display technology: applications and innovations. *Genetics and Molecular Biology* **28**, 1-9

70. Smith, G. P. (1985) Filamentous fusion phage: novel expression vectors that display cloned antigens on the virion surface. *Science (New York, N.Y.)* **228**, 1315-1317

71. Barbas, C. F., 3rd, Kang, A. S., Lerner, R. A., and Benkovic, S. J. (1991) Assembly of combinatorial antibody libraries on phage surfaces: the gene III site. *Proceedings of the National Academy of Sciences of the United States of America* **88**, 7978-7982

72. Nissim, A., Hoogenboom, H. R., Tomlinson, I. M., Flynn, G., Midgley, C., Lane, D., and Winter, G. (1994) Antibody fragments from a 'single pot' phage display library as immunochemical reagents. *The EMBO Journal* **13**, 692-698

73. Gram, H., Strittmatter, U., Lorenz, M., Glück, D., and Zenke, G. (1993) Phage display as a rapid gene expression system: production of bioactive cytokine-phage

and generation of neutralizing monoclonal antibodies. *Journal of Immunological Methods* **161**, 169-176

74. McCafferty, J., Jackson, R. H., and Chiswell, D. J. (1991) Phage-enzymes: expression and affinity chromatography of functional alkaline phosphatase on the surface of bacteriophage. *Protein Engineering* **4**, 955-961

75. R. Corey, D., Shiau, A. K., Qing, Y., Janowski, B. A., and Craik, C. S. (1993) Trypsin display on the surface of bacteriophage. *Gene* **128**, 129-134

76. Rebar, E. J., and Pabo, C. O. (1994) Zinc finger phage: affinity selection of fingers with new DNA-binding specificities. *Science (New York, N.Y.)* **263**, 671-673

77. Scholle, M. D., Collart, F. R., and Kay, B. K. (2004) In vivo biotinylated proteins as targets for phage-display selection experiments. *Protein Expression and Purification* **37**, 243-252

78. Scholle, M. D., Kehoe, J. W., and Kay, B. K. (2005) Efficient construction of a large collection of phage-displayed combinatorial peptide libraries. *Combinatorial Chemistry & High throughput Screening* **8**, 545-551

79. Scholle, M. D., Kriplani, U., Pabon, A., Sishtla, K., Glucksman, M. J., and Kay, B. K. (2006) Mapping protease substrates by using a biotinylated phage substrate library. *Chembiochem : a European Journal of Chemical Biology* **7**, 834-838

80. Predonzani, A., Arnoldi, F., Lopez-Requena, A., and Burrone, O. R. (2008) In vivo site-specific biotinylation of proteins within the secretory pathway using a single vector system. *BMC Biotechnology* **8**, 41

81. Green, N. M. (1990) Avidin and streptavidin. *Methods in Enzymology* **184**, 51-67

82. Asenjo, J. A., and Andrews, B. A. (2008) Challenges and trends in bioseparations. *Journal of Chemical Technology and Biotechnology.* **83**, 117-120

83. Rosa, P. A., Azevedo, A. M., Sommerfeld, S., Backer, W., and Aires-Barros, M. R. (2011) Aqueous two-phase extraction as a platform in the biomanufacturing industry: economical and environmental sustainability. *Biotechnology advances* **29**, 559-567

84. Birch, J. R., and Racher, A. J. (2006) Antibody production. *Advanced Drug Delivery Reviews* **58**, 671-685

85. Benavides, J., Aguilar, O., Lapizco-Encinas, B. H., and Rito-Palomares, M. (2008) Extraction and Purification of Bioproducts and Nanoparticles using Aqueous Two-Phase Systems Strategies. *Chem. Eng. Technol.* **31**, 838-845

86. Benavides, J., and Rito-Palomares, M. (2008) Practical experiences from the development of aqueous two-phase processes for the recovery of high value biological products. *Journal of Chemical Technology and Biotechnology*. **83**, 133-142

87. Langer, E. R., J. (2006) Capacity Bottleneck Squeezed By Downstream Processes. *Bioprocess International*. **4**, 14-17

88. Ruiz-Ruiz, F., Benavides, J., Aguilar, O., and Rito-Palomares, M. (2012) Aqueous two-phase affinity partitioning systems: current applications and trends. *Journal of Chromatography A* **1244**, 1-13

89. Low, D., O'Leary, R., and Pujar, N. S. (2007) Future of antibody purification. *Journal of Chromatography B, Analytical technologies in the biomedical and life sciences* **848**, 48-63

90. Jonathan Albanese, J. B., Hélène Chochois, Henri Colin, and Jean Guillerm. (2011) Industrial-Scale Biochromatography Columns Address Challenging Purification Needs. *Bioprocess International*. **9**, 60–63

91. Osberghaus, A., Hepbildikler, S., Nath, S., Haindl, M., von Lieres, E., and Hubbuch, J. (2012) Determination of parameters for the steric mass action model--a comparison between two approaches. *Journal of Chromatography A* **1233**, 54-65

92. Marichal-Gallardo, P. A., and Alvarez, M. M. (2012) State-of-the-art in downstream processing of monoclonal antibodies: process trends in design and validation. *Biotechnology Progress* **28**, 899-916

93. Subramonian, S., and Clifford, D. (1988) Monovalent/divalent selectivity and the charge separation concept. *Reactive Polymers*. **9**, 195-209

94. Xie, J., Aguilar, M.-I., and Hearn, M. T. W. (1995) Studies on the adsorption capacities of proteins with a tentacle-type ion exchanger and their relationship to the stoichiometric retention parameter Zc. *Journal of Chromatography A* **711**, 43-52

95. Heeboll-Nielsen, A., Dalkiaer, M., Hubbuch, J. J., and Thomas, O. R. (2004) Superparamagnetic adsorbents for high-gradient magnetic fishing of lectins out of legume extracts. *Biotechnology and Bioengineering* **87**, 311-323

96. Ethève, J., Déjardin, P., and Boissière, M. (2003) Adsorption of lysozyme on a hemodialysis sulfonated polyacrylonitrile membrane, with and without preadsorbed poly(ethyleneimine) on the external faces. *Colloids and surfaces. B, Biointerfaces* **28**, 285-293

97. Zhu, Z. Y., and Karlin, S. (1996) Clusters of charged residues in protein three-dimensional structures. *Proceedings of the National Academy of Sciences of the United States of America* **93**, 8350-8355

98. Bibak, N., Paul, R. M., Freymann, D. M., and Yaseen, N. R. (2004) Purification of RanGDP, RanGTP, and RanGMPPNP by ion exchange chromatography. *Analytical Biochemistry* **333**, 57-64

99. Chen, W. H., Fu, J. Y., Kourentzi, K., and Willson, R. C. (2011) Nucleic acid affinity of clustered-charge anion exchange adsorbents: effects of ionic strength and ligand density. *Journal of Chromatography A* **1218**, 258-262

100. Dhamane, S., Ruiz-Ruiz, F., Chen, W. H., Kourentzi, K., Benavides, J., Rito-Palomares, M., and Willson, R. C. (2014) Spermine Sepharose as a clustered-charge anion exchange adsorbent. *Journal of Chromatography A* **1324**, 135-140

101. Geall, A. J., Taylor, R. J., Earll, M. E., Eaton, M. A., and Blagbrough, I. S. (2000) Synthesis of cholesteryl polyamine carbamates: pK(a) studies and condensation of calf thymus DNA. *Bioconjugate Chemistry* **11**, 314-326

102. Gill, S. C., and von Hippel, P. H. (1989) Calculation of protein extinction coefficients from amino acid sequence data. *Analytical Biochemistry* **182**, 319-326

103. Miron, T., and Wilchek, M. (1981) Polyacrylhydrazido-agarose: Preparation via periodate oxidation and use for enzyme immobilization and affinity chromatography. *Journal of Chromatography A* **215**, 55-63

104. Brooks, C. A., and Cramer, S. M. (1992) Steric Mass-Action Ion Exchange: Displacement Profiles and Induced Salt Gradients. *AIChE Journal.* **38**, 1969-1978

105. Boardman, N. K., and Partridge, S. M. (1955) Separation of neutral proteins on ion-exchange resins. *The Biochemical Journal* **59**, 543-552

106. Kopaciewicz, W., Rounds, M. A., Fausnaugh, J., and Regnier, F. E. (1983) Retention model for high-performance ion-exchange chromatography. *Journal of Chromatography A* **266**, 3-21

107. Gill, D. S., Roush, D. J., and Willson, R. C. (1994) Adsorption Heterogeneity and Thermodynamic Driving Forces in Anion Exchange Equilibria of Cytochrome b5. *Journal of Colloid and Interface Science* **167**, 1-7

108. Roush, D. J., Gill, D. S., and Willson, R. C. (1993) Anion-exchange chromatographic behavior of recombinant rat cytochrome b5: Thermodynamic driving forces and temperature dependence of the stoichiometric displacement parameter Z. *Journal of Chromatography A* **653**, 207-218

109. Palmer, B. N., and Powell, H. K. J. (1974) Complex formation between 4,9-diazadodecane-1,12-diamine (spermine) and copper(II) ions and protons in aqueous solution. *Journal of the Chemical Society, Dalton Transactions* **0**, 2086-2089

110. Bolivar, J. M., Batalla, P., Mateo, C., Carrascosa, A. V., Pessela, B. C., and Guisan, J. M. (2010) Selective adsorption of small proteins on large-pore anion exchangers coated with medium size proteins. *Colloids and surfaces. B, Biointerfaces* **78**, 140-145

111. Lemque, R., Vidal-Madjar, C., Racine, M., Piquion, J., and Sebille, B. (1991) Anion-exchange chromatographic properties of alpha-lactalbumin eluted from quaternized polyvinylimidazole. Study of the role of the polymer coating. *Journal of Chromatography* **553**, 165-177

112. Machold, C., Schlegl, R., Buchinger, W., and Jungbauer, A. (2005) Continuous matrix assisted refolding of alpha-lactalbumin by ion exchange chromatography with recycling of aggregates combined with ultradiafiltration. *Journal of Chromatography A* **1080**, 29-42

113. Ward, J. J., Sodhi, J. S., McGuffin, L. J., Buxton, B. F., and Jones, D. T. (2004) Prediction and functional analysis of native disorder in proteins from the three kingdoms of life. *Journal of Molecular Biology* **337**, 635-645

114. Dolgikh, D. A., Abaturov, L. V., Bolotina, I. A., Brazhnikov, E. V., Bychkova, V. E., Gilmanshin, R. I., Lebedev Yu, O., Semisotnov, G. V., Tiktopulo, E. I., Ptitsyn, O. B., and et al. (1985) Compact state of a protein molecule with

pronounced small-scale mobility: bovine alpha-lactalbumin. *European Biophysics Journal : EBJ* **13**, 109-121

115. Dolgikh, D. A., Gilmanshin, R. I., Brazhnikov, E. V., Bychkova, V. E., Semisotnov, G. V., Venyaminov, S., and Ptitsyn, O. B. (1981) Alpha-Lactalbumin: compact state with fluctuating tertiary structure? *FEBS letters* **136**, 311-315

116. Ohgushi, M., and Wada, A. (1983) 'Molten-globule state': a compact form of globular proteins with mobile side-chains. *FEBS letters* **164**, 21-24

117. Redfield, C., Schulman, B. A., Milhollen, M. A., Kim, P. S., and Dobson, C. M. (1999) Alpha-lactalbumin forms a compact molten globule in the absence of disulfide bonds. *Nature Structural Biology* **6**, 948-952

118. Stuart, D. I., Acharya, K. R., Walker, N. P., Smith, S. G., Lewis, M., and Phillips, D. C. (1986) Alpha-lactalbumin possesses a novel calcium binding loop. *Nature* **324**, 84-87

119. Chrysina, E. D., Brew, K., and Acharya, K. R. (2000) Crystal structures of apo- and holo-bovine alpha-lactalbumin at 2. 2-A resolution reveal an effect of calcium on inter-lobe interactions. *The Journal of Biological Chemistry* **275**, 37021-37029

120. Wijesinha-Bettoni, R., Dobson, C. M., and Redfield, C. (2001) Comparison of the structural and dynamical properties of holo and apo bovine α-lactalbumin by NMR spectroscopy. *Journal of Molecular Biology* **307**, 885-898

121. Lu, H. L., Lin, D. Q., Zhu, M. M., and Yao, S. J. (2012) Effects of ligand density and pore size on the adsorption of bovine IgG with DEAE ion-exchange resins. *Journal of Separation Science* **35**, 2131-2137

122. Wu, D., and Walters, R. R. (1992) Effects of stationary phase ligand density on high-performance ion-exchange chromatography of proteins. *Journal of Chromatography A* **598**, 7-13

123. Wrzosek, K., Gramblicka, M., and Polakovic, M. (2009) Influence of ligand density on antibody binding capacity of cation-exchange adsorbents. *Journal of Chromatography A* **1216**, 5039-5044

124. Dumetz, A. C., Snellinger-O'brien A, M., Kaler, E. W., and Lenhoff, A. M. (2007) Patterns of protein protein interactions in salt solutions and implications for protein crystallization. *Protein science : a publication of the Protein Society* **16**, 1867-1877

125. Kopaciewicz, W., and Regnier, F. (1983) Mobile phase selection for the high-performance ion-exchange chromatography of proteins. *Analytical Biochemistry* **133**, 251-259

126. Whitley, R. D., Wachter, R., Liu, F., and Wang, N. H. L. (1989) Ion-exchange equilibria of lysozyme myoglobin and bovine serum albumin : Effective valence and exchanger capacity. *Journal of Chromatography A* **465**, 137-156

127. Kronman, M. J. (1989) Metal-ion binding and the molecular conformational properties of alpha lactalbumin. *Critical Reviews in Biochemistry and Molecular Biology* **24**, 565-667

128. Murphy, J. C., Wibbenmeyer, J. A., Fox, G. E., and Willson, R. C. (1999) Purification of plasmid DNA using selective precipitation by compaction agents. *Nature Biotechnology* **17**, 822-823

129. Harding, J. D., Bebee, R. L., and Gebeyehu, G. (1992) DNA isolation using methidium-spermine-sepharose. *Methods in Enzymology* **216**, 29-39

130. Joachimiak, A., Barciszewska, M., Barciszewski, J., and Wiewiorowski, M. (1979) Application of spermine-Sepharose column chromatography to the separation of plant-specific transfer ribonucleic acids and aminoacyl-tRNA synthetases. *Journal of Chromatography* **180**, 157-162

131. Harding, J. D., Gebeyehu, G., Bebee, R., Simms, D., and Klevan, L. (1989) Rapid isolation of DNA from complex biological samples using a novel capture reagent--methidium-spermine-sepharose. *Nucleic Acids Research* **17**, 6947-6958

132. Uyeki, T. M., Prasad, R., Vukotich, C., Stebbins, S., Rinaldo, C. R., Ferng, Y. H., Morse, S. S., Larson, E. L., Aiello, A. E., Davis, B., and Monto, A. S. (2009) Low sensitivity of rapid diagnostic test for influenza. *Clinical infectious diseases : an official publication of the Infectious Diseases Society of America* **48**, e89-92

133. Izzo, M. M., Kirkland, P. D., Gu, X., Lele, Y., Gunn, A. A., and House, J. K. (2012) Comparison of three diagnostic techniques for detection of rotavirus and coronavirus in calf faeces in Australia. *Australian Veterinary Journal* **90**, 122-129

134. Li, Y., Hou, L., Ye, J., Liu, X., Dan, H., Jin, M., Chen, H., and Cao, S. (2010) Development of a convenient immunochromatographic strip for the diagnosis of infection with Japanese encephalitis virus in swine. *Journal of Virological Methods* **168**, 51-56

135. Mashayekhi, F., Chiu, R. Y., Le, A. M., Chao, F. C., Wu, B. M., and Kamei, D. T. (2010) Enhancing the lateral-flow immunoassay for viral detection using an aqueous two-phase micellar system. *Analytical and Bioanalytical Chemistry* **398**, 2955-2961

136. Chiang, C. Y., Mello, C. M., Gu, J., Silva, E. C. C. M., Van Vliet, K. J., and Belcher, A. M. (2007) Weaving Genetically Engineered Functionality into Mechanically Robust Virus Fibers. *Advanced Materials* **19**, 826-832

137. Nam, K. T., Kim, D. W., Yoo, P. J., Chiang, C. Y., Meethong, N., Hammond, P. T., Chiang, Y. M., and Belcher, A. M. (2006) Virus-enabled synthesis and assembly of nanowires for lithium ion battery electrodes. *Science (New York, N.Y.)* **312**, 885-888

138. Smith, G. P., and Petrenko, V. A. (1997) Phage Display. *Chemical Reviews* **97**, 391-410

139. Nam, K. T., Wartena, R., Yoo, P. J., Liau, F. W., Lee, Y. J., Chiang, Y.-M., Hammond, P. T., and Belcher, A. M. (2008) Stamped microbattery electrodes based on self-assembled M13 viruses. *Proceedings of the National Academy of Sciences*

140. Lee, Y. J., Yi, H., Kim, W.-J., Kang, K., Yun, D. S., Strano, M. S., Ceder, G., and Belcher, A. M. (2009) Fabricating Genetically Engineered High-Power Lithium-Ion Batteries Using Multiple Virus Genes. *Science (New York, N.Y.)* **324**, 1051-1055

141. Kassner, P. D., Burg, M. A., Baird, A., and Larocca, D. (1999) Genetic selection of phage engineered for receptor-mediated gene transfer to mammalian cells. *Biochemical and Biophysical Research Communications* **264**, 921-928

142. Larocca, D., and Baird, A. (2001) Receptor-mediated gene transfer by phage-display vectors: applications in functional genomics and gene therapy. *Drug Discovery Today* **6**, 793-801

143. Nielsen, U. B., and Marks, J. D. (2000) Internalizing antibodies and targeted cancer therapy: direct selection from phage display libraries. *Pharmaceutical Science & Technology Today* **3**, 282-291

144. Yang, L. M., Diaz, J. E., McIntire, T. M., Weiss, G. A., and Penner, R. M. (2008) Covalent virus layer for mass-based biosensing. *Analytical Chemistry* **80**, 933-943

145. Yang, L.-M. C., Diaz, J. E., McIntire, T. M., Weiss, G. A., and Penner, R. M. (2008) Direct Electrical Transduction of Antibody Binding to a Covalent Virus Layer Using Electrochemical Impedance. *Analytical Chemistry* **80**, 5695-5705

146. Yang, L.-M. C., Tam, P. Y., Murray, B. J., McIntire, T. M., Overstreet, C. M., Weiss, G. A., and Penner, R. M. (2006) Virus Electrodes for Universal Biodetection. *Analytical Chemistry* **78**, 3265-3270

147. Souza, G. R., Christianson, D. R., Staquicini, F. I., Ozawa, M. G., Snyder, E. Y., Sidman, R. L., Miller, J. H., Arap, W., and Pasqualini, R. (2006) Networks of gold nanoparticles and bacteriophage as biological sensors and cell-targeting agents. *Proceedings of the National Academy of Sciences of the United States of America* **103**, 1215-1220

148. Li, K., Chen, Y., Li, S., Nguyen, H. G., Niu, Z., You, S., Mello, C. M., Lu, X., and Wang, Q. (2010) Chemical Modification of M13 Bacteriophage and Its Application in Cancer Cell Imaging. *Bioconjugate Chemistry* **21**, 1369-1377

149. Hess, G. T., Cragnolini, J. J., Popp, M. W., Allen, M. A., Dougan, S. K., Spooner, E., Ploegh, H. L., Belcher, A. M., and Guimaraes, C. P. (2012) M13 Bacteriophage Display Framework That Allows Sortase-Mediated Modification of Surface-Accessible Phage Proteins. *Bioconjugate Chemistry* **23**, 1478-1487

150. Murugesan, M., Abbineni, G., Nimmo, S. L., Cao, B., and Mao, C. (2013) Virus-based photo-responsive nanowires formed by linking site-directed mutagenesis and chemical reaction. *Scientific Reports* **3**, 1820

151. Yacoby, I., Bar, H., and Benhar, I. (2007) Targeted drug-carrying bacteriophages as antibacterial nanomedicines. *Antimicrobial Agents and Chemotherapy* **51**, 2156-2163

152. Yacoby, I., Shamis, M., Bar, H., Shabat, D., and Benhar, I. (2006) Targeting antibacterial agents by using drug-carrying filamentous bacteriophages. *Antimicrobial Agents and Chemotherapy* **50**, 2087-2097

153. Bar, H., Yacoby, I., and Benhar, I. (2008) Killing cancer cells by targeted drug-carrying phage nanomedicines. *BMC Biotechnology* **8**, 37

154. Yacoby, I., and Benhar, I. (2008) Targeted filamentous bacteriophages as therapeutic agents. *Expert Opinion on Drug Delivery* **5**, 321-329

155. Hilderbrand, S. A., Kelly, K. A., Weissleder, R., and Tung, C. H. (2005) Monofunctional near-infrared fluorochromes for imaging applications. *Bioconjugate Chemistry* **16**, 1275-1281

156. Hilderbrand, S. A., Kelly, K. A., Niedre, M., and Weissleder, R. (2008) Near Infrared Fluorescence-Based Bacteriophage Particles for Ratiometric pH Imaging. *Bioconjugate Chemistry* **19**, 1635-1639

157. Willford, J. D., Bisha, B., Bolenbaugh, K. E., and Goodridge, L. D. (2011) Luminescence based enzyme-labeled phage (Phazyme) assays for rapid detection of Shiga toxin producing Escherichia coli serogroups. *Bacteriophage* **1**, 101-110

158. Kim, H. J., Rossotti, M. A., Ahn, K. C., Gonzalez-Sapienza, G. G., Gee, S. J., Musker, R., and Hammock, B. D. (2010) Development of a noncompetitive phage anti-immunocomplex assay for brominated diphenyl ether 47. *Analytical Biochemistry* **401**, 38-46

159. Kim, H. J., Ahn, K. C., Gonzalez-Techera, A., Gonzalez-Sapienza, G. G., Gee, S. J., and Hammock, B. D. (2009) Magnetic bead-based phage anti-immunocomplex assay (PHAIA) for the detection of the urinary biomarker 3-phenoxybenzoic acid to assess human exposure to pyrethroid insecticides. *Analytical Biochemistry* **386**, 45-52

160. Kim, H. J., McCoy, M., Gee, S. J., Gonzalez-Sapienza, G. G., and Hammock, B. D. (2011) Noncompetitive phage anti-immunocomplex real-time polymerase chain reaction for sensitive detection of small molecules. *Analytical Chemistry* **83**, 246-253

161. Adhikari, M., Dhamane, S., Hagstrom, A. E., Garvey, G., Chen, W. H., Kourentzi, K., Strych, U., and Willson, R. C. (2013) Functionalized viral nanoparticles as ultrasensitive reporters in lateral-flow assays. *The Analyst* **138**, 5584-5587

162. Bollback, J. P., and Huelsenbeck, J. P. (2001) Phylogeny, genome evolution, and host specificity of single-stranded RNA bacteriophage (family Leviviridae). *Journal of Molecular Evolution* **52**, 117-128

163. Golmohammadi, R., Valegard, K., Fridborg, K., and Liljas, L. (1993) The refined structure of bacteriophage MS2 at 2.8 A resolution. *Journal of Molecular Biology* **234**, 620-639

164. O'Connell, K. P., Bucher, J. R., Anderson, P. E., Cao, C. J., Khan, A. S., Gostomski, M. V., and Valdes, J. J. (2006) Real-time fluorogenic reverse transcription-PCR assays for detection of bacteriophage MS2. *Applied and Environmental Microbiology* **72**, 478-483

165. Brion, G. M., and Silverstein, J. (2001) Selecting a sensitive bacteriophage assay for evaluation of a prototype water recycling system. *Life Support & Biosphere Science : International Journal of Earth Space* **8**, 9-14

166. Casteel, M. J., Jayaraj, K., Gold, A., Ball, L. M., and Sobsey, M. D. (2004) Photoinactivation of hepatitis A virus by synthetic porphyrins. *Photochemistry and Photobiology* **80**, 294-300

167. Chaidez, C., Moreno, M., Rubio, W., Angulo, M., and Valdez, B. (2003) Comparison of the disinfection efficacy of chlorine-based products for inactivation of viral indicators and pathogenic bacteria in produce wash water. *International Journal of Environmental Health Research* **13**, 295-302

168. De Roda Husman, A. M., Bijkerk, P., Lodder, W., Van Den Berg, H., Pribil, W., Cabaj, A., Gehringer, P., Sommer, R., and Duizer, E. (2004) Calicivirus inactivation by nonionizing (253.7-nanometer-wavelength [UV]) and ionizing (gamma) radiation. *Applied and Environmental Microbiology* **70**, 5089-5093

169. Alvarez, M. E., Aguilar, M., Fountain, A., Gonzalez, N., Rascon, O., and Saenz, D. (2000) Inactivation of MS-2 phage and poliovirus in groundwater. *Canadian Journal of Microbiology* **46**, 159-165

170. Gordon, C., and Toze, S. (2003) Influence of groundwater characteristics on the survival of enteric viruses. *Journal of Applied Microbiology* **95**, 536-544

171. Hodgson, C. J., Perkins, J., and Labadz, J. C. (2003) Evaluation of biotracers to monitor effluent retention time in constructed wetlands. *Letters in Applied Microbiology* **36**, 362-371

172. Nasser, A. M., Glozman, R., and Nitzan, Y. (2002) Contribution of microbial activity to virus reduction in saturated soil. *Water Research* **36**, 2589-2595

173. Selas, B., Lakel, A., Andres, Y., and Le Cloirec, P. (2003) Wastewater reuse in on-site wastewater treatment: bacteria and virus movement in unsaturated flow through sand filter. *Water science and technology : a journal of the International Association on Water Pollution Research* **47**, 59-64

174. Belgrader, P., Benett, W., Hadley, D., Long, G., Mariella, R., Jr., Milanovich, F., Nasarabadi, S., Nelson, W., Richards, J., and Stratton, P. (1998) Rapid pathogen detection using a microchip PCR array instrument. *Clinical Chemistry* **44**, 2191-2194

175. Cargile, B. J., McLuckey, S. A., and Stephenson, J. L., Jr. (2001) Identification of bacteriophage MS2 coat protein from E. coli lysates via ion trap collisional activation of intact protein ions. *Analytical Chemistry* **73**, 1277-1285

176. Kuzmanovic, D. A., Elashvili, I., Wick, C., O'Connell, C., and Krueger, S. (2003) Bacteriophage MS2: molecular weight and spatial distribution of the protein and RNA components by small-angle neutron scattering and virus counting. *Structure (London, England : 1993)* **11**, 1339-1348

177. Thomas, J. H., Kim, S. K., Hesketh, P. J., Halsall, H. B., and Heineman, W. R. (2004) Bead-based electrochemical immunoassay for bacteriophage MS2. *Analytical Chemistry* **76**, 2700-2707

178. Xiang, F., Anderson, G. A., Veenstra, T. D., Lipton, M. S., and Smith, R. D. (2000) Characterization of microorganisms and biomarker development from global ESI-MS/MS analyses of cell lysates. *Analytical Chemistry* **72**, 2475-2481

179. Kropinski, A. M., Mazzocco, A., Waddell, T. E., Lingohr, E., and Johnson, R. P. (2009) Enumeration of bacteriophages by double agar overlay plaque assay. *Methods in Molecular Biology (Clifton, N.J.)* **501**, 69-76

180. Stavis, R. L., and August, J. T. (1970) The biochemistry of RNA bacteriophage replication. *Annual Review of Biochemistry* **39**, 527-560

181. Branston, S., Stanley, E., Keshavarz-Moore, E., and Ward, J. (2012) Precipitation of filamentous bacteriophages for their selective recovery in primary purification. *Biotechnology Progress* **28**, 129-136

182. T. Maniatis, E. F. F. a. J. S. (1982) Molecular cloning: a laboratory manual. (Inglis, J. ed., Fourth Edition, Cold Spring Harbor, NY

183. Nash, M. A., Waitumbi, J. N., Hoffman, A. S., Yager, P., and Stayton, P. S. (2012) Multiplexed enrichment and detection of malarial biomarkers using a stimuli-responsive iron oxide and gold nanoparticle reagent system. *ACS nano* **6**, 6776-6785

184. Schneider, C. A., Rasband, W. S., and Eliceiri, K. W. (2012) NIH Image to ImageJ: 25 years of image analysis. *Nature Methods* **9**, 671-675

185. Lowman, H. B., Bass, S. H., Simpson, N., and Wells, J. A. (1991) Selecting high-affinity binding proteins by monovalent phage display. *Biochemistry* **30**, 10832-10838

186. Lowman, H. B., and Wells, J. A. (1993) Affinity maturation of human growth hormone by monovalent phage display. *Journal of Molecular Biology* **234**, 564-578

187. Walsh, G. (2010) Biopharmaceutical benchmarks 2010. *Nat Biotech* **28**, 917-924

188. Marichal-Gallardo, P. A., and Alvarez, M. M. (2012) State-of-the-art in downstream processing of monoclonal antibodies: process trends in design and validation. *Biotechnology Progress* **28**, 899-916

189. Xie, J., Aguilar, M.-I., and Hearn, M. T. W. (1995) Studies on the adsorption capacities of proteins with a tentacle-type ion exchanger and their relationship to the stoichiometric retention parameter Zc. *Journal of Chromatography A* **711**, 43-52

190. Heeboll-Nielsen, A., Dalkiaer, M., Hubbuch, J. J., and Thomas, O. R. (2004) Superparamagnetic adsorbents for high-gradient magnetic fishing of lectins out of legume extracts. *Biotechnology and Bioengineering* **87**, 311-323

191. Ethève, J., Déjardin, P., and Boissière, M. (2003) Adsorption of lysozyme on a hemodialysis sulfonated polyacrylonitrile membrane, with and without preadsorbed poly(ethyleneimine) on the external faces. *Colloids and Surfaces B: Biointerfaces* **28**, 285-293

192. Cramer, S. M., and Holstein, M. A. (2011) Downstream bioprocessing: recent advances and future promise. *Current Opinion in Chemical Engineering* **1**, 27-37

193. Klar, T. A., Jakobs, S., Dyba, M., Egner, A., and Hell, S. W. (2000) Fluorescence microscopy with diffraction resolution barrier broken by stimulated emission. *Proceedings of the National Academy of Sciences of the United States of America* **97**, 8206-8210

194. Moerner, W. E. (2007) New directions in single-molecule imaging and analysis. *Proceedings of the National Academy of Sciences of the United States of America* **104**, 12596-12602

195. Gustafsson, M. G. (2005) Nonlinear structured-illumination microscopy: wide-field fluorescence imaging with theoretically unlimited resolution. *Proceedings of the National Academy of Sciences of the United States of America* **102**, 13081-13086

196. Westphal, V., Rizzoli, S. O., Lauterbach, M. A., Kamin, D., Jahn, R., and Hell, S. W. (2008) Video-rate far-field optical nanoscopy dissects synaptic vesicle movement. *Science (New York, N.Y.)* **320**, 246-249

197. Rust, M. J., Bates, M., and Zhuang, X. (2006) Sub-diffraction-limit imaging by stochastic optical reconstruction microscopy (STORM). *Nature Methods* **3**, 793-795

198. Betzig, E., Patterson, G. H., Sougrat, R., Lindwasser, O. W., Olenych, S., Bonifacino, J. S., Davidson, M. W., Lippincott-Schwartz, J., and Hess, H. F. (2006) Imaging intracellular fluorescent proteins at nanometer resolution. *Science (New York, N.Y.)* **313**, 1642-1645

199. Burnette, D. T., Sengupta, P., Dai, Y., Lippincott-Schwartz, J., and Kachar, B. (2011) Bleaching/blinking assisted localization microscopy for superresolution imaging using standard fluorescent molecules. *Proceedings of the National Academy of Sciences of the United States of America* **108**, 21081-21086

200. Sharonov, A., and Hochstrasser, R. M. (2006) Wide-field subdiffraction imaging by accumulated binding of diffusing probes. *Proceedings of the National Academy of Sciences of the United States of America* **103**, 18911-18916

201. Zhou, X., Andoy, N. M., Liu, G., Choudhary, E., Han, K. S., Shen, H., and Chen, P. (2012) Quantitative super-resolution imaging uncovers reactivity patterns on single nanocatalysts. *Nature Nanotechnology* **7**, 237-241

202. Jungmann, R., Steinhauer, C., Scheible, M., Kuzyk, A., Tinnefeld, P., and Simmel, F. C. (2010) Single-molecule kinetics and super-resolution microscopy by fluorescence imaging of transient binding on DNA origami. *Nano letters* **10**, 4756-4761

203. Wu, D., Liu, Z., Sun, C., and Zhang, X. (2008) Super-resolution imaging by random adsorbed molecule probes. *Nano letters* **8**, 1159-1162

204. Walder, R., Nelson, N., and Schwartz, D. K. (2011) Super-resolution surface mapping using the trajectories of molecular probes. *Nature Communications* **2**, 515

205. Skaug, M. J., and Schwartz, D. K. (2012) Using the dynamics of fluorescent cations to probe and map charged surfaces. *Soft Matter* **8**, 12017-12024

206. Kastantin, M., Keller, T. F., Jandt, K. D., and Schwartz, D. K. (2012) Single-Molecule Tracking of Fibrinogen Dynamics on Nanostructured Poly(ethylene) Films. *Advanced Functional Materials* **22**, 2617-2623

207. Xu, X. H., and Yeung, E. S. (1998) Long-range electrostatic trapping of single-protein molecules at a liquid-solid interface. *Science (New York, N.Y.)* **281**, 1650-1653

208. Cuppett, C. M., Doneski, L. J., and Wirth, M. J. (2000) Irreversible Adsorption of Lysozyme to Polishing Marks on Silica. *Langmuir* **16**, 7279-7284

209. Ludes, M. D., and Wirth, M. J. (2002) Single-molecule resolution and fluorescence imaging of mixed-mode sorption of a dye at the interface of C18 and acetonitrile/water. *Analytical Chemistry* **74**, 386-393

210. Wirth, M. J., and Legg, M. A. (2007) Single-molecule probing of adsorption and diffusion on silica surfaces. *Annual Review of Physical Chemistry* **58**, 489-510

211. Cooper, J. T., and Harris, J. M. (2014) Imaging Fluorescence-Correlation Spectroscopy for Measuring Fast Surface Diffusion at Liquid/Solid Interfaces. *Analytical Chemistry*

212. Zhong, Z., Lowry, M., Wang, G., and Geng, L. (2005) Probing strong adsorption of solute onto C18-silica gel by fluorescence correlation imaging and single-molecule spectroscopy under RPLC conditions. *Analytical Chemistry* **77**, 2303-2310

213. Fang, N., Zhang, H., Li, J., Li, H. W., and Yeung, E. S. (2007) Mobility-based wall adsorption isotherms for comparing capillary electrophoresis with single-molecule observations. *Analytical Chemistry* **79**, 6047-6054

214. Skaug, M. J., Mabry, J., and Schwartz, D. K. (2013) Intermittent molecular hopping at the solid-liquid interface. *Physical Review Letters* **110**, 256101

215. Myers, G. A., Gacek, D. A., Peterson, E. M., Fox, C. B., and Harris, J. M. (2012) Microscopic rates of peptide-phospholipid bilayer interactions from single-molecule residence times. *Journal of the American Chemical Society* **134**, 19652-19660

216. Kisley, L., Chen, J., Mansur, A. P., Shuang, B., Kourentzi, K., Poongavanam, M.-V., Chen, W.-H., Dhamane, S., Willson, R. C., and Landes, C. F. (2014) Unified superresolution experiments and stochastic theory provide mechanistic insight into protein ion-exchange adsorptive separations. *Proceedings of the National Academy of Sciences* **111**, 2075-2080

217. Daniels, C. R., Kisley, L., Kim, H., Chen, W. H., Poongavanam, M. V., Reznik, C., Kourentzi, K., Willson, R. C., and Landes, C. F. (2012) Fluorescence correlation spectroscopy study of protein transport and dynamic interactions with clustered-charge peptide adsorbents. *Journal of Molecular Recognition : JMR* **25**, 435-442

218. Afanassiev, V., Hanemann, V., and Wolfl, S. (2000) Preparation of DNA and protein micro arrays on glass slides coated with an agarose film. *Nucleic Acids Research* **28**, E66

219. Cuatrecasas, P. (1970) Protein purification by affinity chromatography. Derivatizations of agarose and polyacrylamide beads. *The Journal of Biological Chemistry* **245**, 3059-3065

220. Asish Xavier, K., and Willson, R. C. Association and Dissociation Kinetics of Anti-Hen Egg Lysozyme Monoclonal Antibodies HyHEL-5 and HyHEL-10. *Biophysical Journal* **74**, 2036-2045

221. Kisley, L., Chang, W. S., Cooper, D., Mansur, A. P., and Landes, C. F. (2013) Extending single molecule fluorescence observation time by amplitude-modulated excitation. *Methods and Applications in Fluorescence* **1**, 037001-037001

222. Chandra, N., Brew, K., and Acharya, K. R. (1998) Structural Evidence for the Presence of a Secondary Calcium Binding Site in Human α-Lactalbumin. *Biochemistry* **37**, 4767-4772

223. Wirth, M. J., Fairbank, R. W., and Fatunmbi, H. O. (1997) Mixed self-assembled monolayers in chemical separations. *Science (New York, N.Y.)* **275**, 44-47

224. Giddings, J. C. (1965) *Dynamics of Chromatography*, CRC, Boca Raton, FL

225. Giddings, J. C., and Eyring, H. (1955) A Molecular Dynamic Theory of Chromatography. *The Journal of Physical Chemistry* **59**, 416-421

226. McQuarrie, D. A. (1963) On the Stochastic Theory of Chromatography. *The Journal of Chemical Physics* **38**, 437-445

227. Pernodet, N., Maaloum, M., and Tinland, B. (1997) Pore size of agarose gels by atomic force microscopy. *ELECTROPHORESIS* **18**, 55-58

228. Martin, A. J., and Synge, R. L. (1941) A new form of chromatogram employing two liquid phases: A theory of chromatography. 2. Application to the micro-determination of the higher monoamino-acids in proteins. *The Biochemical Journal* **35**, 1358-1368